Carinthia University of Applied Sciences

Spatial Information Management

The University of New Mexico

Department of Geography and Environmental Studies

MARSHALL PLAN REPORT

Development of a multi-temporal phenological 3D model of vine

Submitted in partial fulfilment of the requirements of the academic degree

Master of Science in Engineering

Author: Schneider Thomas Andreas, BSc.

Registration number: 1710362002

Supervisors: FH-Prof. Mag. Dr. Gernot Paulus, MSc. MAS

FH-Prof. Dr.-Ing. Karl-Heinrich Anders

Christopher D. Lippitt, PhD, CMS-RS

Villach, September 2019

Statutory declaration

I hereby declare that:

- the Master thesis has been written by myself without any external unauthorized help and that it has not been submitted to any institution to achieve an academic grading.
- I have not used sources or means without citing them in the text and any thoughts from others or literal quotations are clearly marked.
- the electrical submitted Master thesis is identical to the hard copy.
- one copy of the Master thesis is deposited and made available in the CUAS library (§ 8 Austrian Copyright Law [UrhG])
- I understand that this academic work is subject to a plagiarism check.

Villach, 11.09.2019 Thomas Schneider

Thomas Andreas Schneider

Abstract

This thesis is concerned with the development of a multi-temporal phenological 3D model of vine. In viticulture, the estimation of yield has an important role as it helps vineyard managers to predict the beginning of the next growth stage of vines and to improve their vineyard management related decision making. To enable accurate prediction of a vineyard's yield, it is necessary to track the phenological stages of vines and corresponding parameters throughout a whole season. Traditional phenotypical data collection and yield estimation methods are based on direct visual and manual in-field data collection by viticulture experts. Such approaches are very time-consuming and rely on strategic selection of representative vines for each block in a vineyard. Hence, the goal of this research project is the development of a multi-temporal phenological 3D model of vine and a critical assessment which phenological stages of vine can be modelled by multi-scale photogrammetric methods in order to provide reliable key parameters for yield prediction. The applied approach will support vineyard managers to better estimate the amount of yield throughout the phenological stages of vines in their vineyards.

Keywords

Grapevine, precision viticulture, vineyard, vine phenology, key phenological stages of vine, yield, photogrammetry, 3D modelling

Acknowledgements

I would like to thank my two supervisors FH-Prof. Mag. Dr. Gernot Paulus, MSc. MAS, FH-Prof. Dr.-Ing. Karl-Heinrich Anders from the Carinthia University of Applied Sciences and my supervisor Christopher D. Lippitt, PhD, CMS-RS from the University of New Mexico for all their advice and inputs they gave me throughout the joint work on the project and their patience they had with me.

Furthermore, I would also like to thank Ing. Ulf Erich Scherling for on the one hand, providing me with the necessary equipment such as a camera and the knowledge how to use the equipment and on the other hand, for continuously helping me to acquire the necessary data for the implementation of developed approach.

I would also like to thank Sean Thomas O'Neill, MSc. from the University of New Mexico, who helped me to set up my workplace at the UNM and solved many technical issues. Without his help many technical implementations during my stay at the UNM would not have been possible.

I am also very grateful to the Marshall Plan Program and the International Relation Office of the Carinthia University of Applied Sciences for giving me the opportunity to visit the University of New Mexico in the United States of America in the course of my master's thesis, to gain new experience and to work on part of my master's thesis there with Mr. Chris Lippitt as my supervisor.

Table of Contents

List of figures

List of tables

List of abbreviations

%	Percent
3D	Three dimensional
BBCH	Biologische Bundesanstalt für Land- und Forstwirtschaft, Bundessortenamt und Chemische Industrie
Caps	Calyptra
CC	CloudCompare
CV	Average number of clusters per vine
CW	Average cluster weight
DEM	Digital elevation model
DSM	Digital surface model
E-L	Eichhorn-Lorenz
GCP	Ground Control Points
GIS	Geographic Information System
GNSS	Global Navigation Satellite System
GPS	Global Positioning System
GSD	Ground Sample Distance
IMU	Inertial Measurement Unit
MVS	Multi-view-stereo
PD	Planting density
PV	Number of producing vines per spatial area
px	Pixels
RMSE	Root-Mean-Square-Error
RTK	Real Time Kinematic
SFM	Structure-from-motion
SFM-MVS	Structure-from-motion multi-view-stereo
TIN	Triangulated irregular network
UAS	Unmanned Aerial System
UAV	Unmanned Aerial Vehicle

1. Introduction

1.1 Motivation

The cultivation of vines and the production of wine plays an important role in the lives of many people and especially in the food industry. According to studies, approximately 28.4 million liters of wine were produced in 2015 which is an increase of 3.5% of wine production from 2014 (Wine Institute, 2019). In addition, the importance of vines for humans can be demonstrated by its long association with mankind. The history of humans and vine can be traced back to ancient times (Poupin et al., 2011) and is just as important today as it was then. Since the production of wine and thus a high quantitative and qualitative cultivation of vines plays an important role, it is necessary for vine growers to find efficient means to guarantee the most effective vine-growing possible. Consequently, in order to track the vines growth and to enable efficient viticulture, it is necessary for vineyard managers to record phenological data of their vines on a weekly basis (Westover, 2018). The knowledge of the parameters of their vines helps them to correctly time vineyard management practices or to predict the beginning of key phenological stages of vines. However, traditional methods, which are usually performed manually, are time-consuming and may be subject to human error. Technologies developed through precision viticulture such as sensor-based data acquisition systems and automated processes to estimate yield based on the recorded data can help vine growers to make their decision making processes more efficient and to execute practices in such a way to improve their vines health and growth.

Thus, this master thesis is concerned with the modelling a phenological stages of vine and to derive reliable parameters for yield estimation from created 3D models by using multiscale photogrammetric methods. In general, the aim is the development of a multi-temporal phenological 3D model of vine for the digital representation of key phenological stages of vine. Three objectives arise from the goal. The first objective focuses on the iterative implementation of 3D models at laboratory scale and field vineyard scale. The second objective is concerned with assessment and validation of the multi-temporal phenological 3D model results. Last but not least, the third objective is devoted to deriving and estimating yield-relevant parameters from the 3D models. The knowledge about the estimation of yield can be used to develop a yield prediction concept.

A multi-temporal phenological 3D model of vine and its extractable knowledge can provide useful information for vine growers and vineyard managers. It can help them plan and execute their vineyard management practices more efficiently and at the "right" times. The gained knowledge from the yield estimation can also be beneficial. It can be useful for wineries because, among other things, they can better predict how much expected crop they will have to manufacture into wine.

1.2 Research Questions

The main goal of this research project is the development of a multi-temporal phenological 3D model of vine using multiscale photogrammetric methods. “Multiscale” in this context refers to an integrated approach of combining ground-based and Unmanned Aerial Vehicle (UAV)-based photogrammetric data. The following research questions arise from the main goal of this research project:

1. To which extent is it possible to digitally model the individual phenological stages of vine using multiscale photogrammetric methods?
2. How accurate can key morphological characteristics in a vineyard be modelled over various scales with this novel approach?
3. How accurate can morphological changes of vine parameters be modelled and used as key input for yield prediction?

1.3 Approach

The goal of this master thesis is achieved through multiple phases. At first, an extensive literature and web-based research is conducted. The literature review is concerned with two major topics: the key term definition and the state-of-the art Research. In more detail, the key term definition focuses on the description of project relevant terms such as precision viticulture, phenology of vine and yield. The state-of-the art research deals with the examination and understanding of state-of-the art approaches which are used to collect phenotypical data from vines and to estimate the yield in a vineyard. Topics that are in particular covered by this chapter are traditional viticulture data collection, recent developments in viticulture data collection, state-of-the art phenological vine data collection and the utilization of unmanned aerial systems (UAS) in precision viticulture. The knowledge obtained from the literature review is on the one hand used to create a phenological characteristics matrix of vines in their key phenological stages and is also incorporated into the practical implementation of the master's thesis. Secondly, the methodology focuses on the definition of project relevant technologies which are applied to capture phenotypical data and the planning and elaboration of a conceptual workflow for the development of a multi-temporal phenological 3D model of vine.

The third phase of the research project is concerned with the implementation and is divided into two phases: a laboratory study and a field study. The field study is further divided into the quantitative comparison of nadir and oblique view imagery and the 3D modelling of and change detection of phenology of vine. The laboratory study focuses on the acquisition of phenological data from grape

bunches with close range photogrammetric methods in laboratory conditions and the development of 3D grape models based on the recorded data. Then, features such as the berry diameter are taken from the 3D grape models and a statistical analysis is executed to obtain yield relevant parameters. The quantitative comparison of nadir and oblique view imagery is carried out in three steps. At first, a multiscale data acquisition process is performed to obtain ground reference data and low-altitude aerial image data. Then, a data modelling step is executed to generate several 3D models from the acquired data. Finally, a quantitative comparison is conducted to evaluate the effects of nadir and oblique view imagery on the created 3D models.

The 3D modelling of and change detection of phenology of vine is accomplished with an iterative multi-step process. The process is executed for several key phenological stage of vine. Each process consists on a phenotypical data collection from vines by using multiscale in-field photogrammetric measurements, a data modelling step where phenological 3D models of vine are created and the following validation of the 3D model results. The final phase of the project is concerned with the evaluation of the project results. The results are examined in detail, critically reflected and analyzed for problems and possible solutions for improved results.

1.4 Expected Results

The main goal of the master thesis and related research questions give rise to the following expected results:

- State-of-the art literature review and best practice overview on vine phenology and yield prediction
- Requirement analysis and conceptual workflow for the development of a multi-temporal 3D model of key phenological stages of vine
- Iterative implementation of 3D models at laboratory scale and field vineyard scale with multiscale photogrammetric methods
- Assessment and validation of multi-temporal phenological 3D model results (laboratory and field)

1.5 Target Audience

Target audience of the research project are vine growers and vineyard managers. With the usage of the multi-temporal phenological 3D model and the contained vine specific information, they will have the opportunity to better monitor the phenological stages of vines in their vineyard. Furthermore, the obtained knowledge from the project can help them to prepare specific vineyard

management practices. Another profiteer can be wineries. The information about the estimate yield of a vineyard can support them in preparing their harvest scheduling or barrel and tank management.

1.6 Thesis Structure

This thesis is structured as followed. The first chapter provides an introduction into the thesis topic, defines the research questions and approach needed to reach the project's goal, the expected results and possible profiteers of the implemented approach. The literature review offers an insight into project relevant terms and recently developed state-of-the art approaches to collect and process data from vines. The methodology gives an overview about the theoretical background of applied data collection approaches and the workflow of the project. The fourth chapter "Project Implementation" covers the implementation of the laboratory study, a quantitative comparison of nadir and oblique view imagery and the 3D modelling of and change detection of phenology of vine. The evaluation focuses on a critical reflection of the implemented results. Following a conclusion summarizes the topics dealt with and the results obtained. The last chapter of the master thesis "Future Work" deals with an outlook into the future work and which additional technologies can be integrated and improvements can be made into a potential following project.

2. Literature Review

The initial phase of this master thesis is concerned with a literature- and web based research. The literature research is one of the core parts of every scientific project. It is utilized to conduct a research for topics which are relevant for the project's goal and to get familiar and understand definitions of terminologies and processes in those topics. Since the overall goal of this master thesis is the development of a multi-temporal phenological 3D model of vine the two pertinent main subjects the literature research is focused on are viticulture and geographic information systems (GIS). Consequently, the literature review of this research project describes issue-related terms and classifications of the topics viticulture and GIS in detail and gives an overview on how those two subjects are connected. Therefore, the research is separated into two major parts: the 2.1 Key Term Definition and a 2.2 State-of-the Art Research. In the sub-chapter 2.1 Key Term Definition subject-relevant and commonly used terms in this thesis are being described in detail. The 2.2 State-of-the Art Research is conducted to gather information and acquire knowledge about traditional data collection methods used by viticulture experts, recent developments in viticulture data collection and similar projects and approaches focused on phenological data collection from vines.

2.1 Key Term Definition

As the scientific fields of viticulture and GIS are very wide-ranging subjects, a key term research has to be carried out in order to identify, describe and understand terms of high relevance for this master thesis. Thus, a key term review is conducted to gather knowledge about important terminologies for the research project. The acquired information from key term review is summarized in the chapter 2.1 Key Term Definition. It gives a detailed overview about those key terms, classifications and methods which are frequently used in the work and are of high importance to be understood to reach the main goal of the research project. Since the master thesis is concerned with the topics phenological stages of vine, GIS and estimation of yield, the important terminologies are: precision viticulture, phenology, key phenological stages of vine, yield and yield prediction.

2.1.1 Precision Viticulture

Agriculture is one of the oldest businesses of human history and has been conducted since ancient times. It has been and still is one of the most mentioned and dealt with topics in food and beverage industry, commerce and scientific researches. Especially viticulture plays a big role in this subject. The term viticulture is described as the cultivation and harvesting of domestic grapevine. The wild vine is a very old plant and scientific surveys indicate that those vines exist since 65 million years. However,

also the history between the grapevine and humans is a very old one and goes back to ancient human civilizations. Scientific studies suggest that the history of grapevine domestication by humans started at about 6000 BC in the area where the Mesopotamian tribes lived between the southern Black sea and Mesopotamia (Poupin et al., 2011). Furthermore, throughout the historical domestication of grapevine the plant experienced various changes in its structure by interbreeding different grapevine breeds with each other. Those modifications should develop grapevines with better resistances against unfavorable climatic conditions and pests than previous plant generations and additionally improve the wine quality which is produced from the grapes of the new modified grapevine. Other historical phenotypic mutations of grapevines because of those methods are changes in cluster and berry size, the absence of seeds and the transformation from a dioecious plant into a domestic hermaphrodite plant with male (anther) and female (pistil) reproductive organs (Poupin et al., 2011).

Throughout the history of viticulture, scientists and viticulture experts always strive to find new methods which can be applied to on the one hand make viticulture management more efficient and on the other hand increase the quality of a vine's balance. The rapid technical progress in the modern ages of the 20th and 21st century provided and still gives experts many possibilities to develop new technologies and methods to control, manage and improve the quality of grapevine and wine. Therefore, the scientific technique of precision viticulture was born and it has an important role in the design and development of novel approaches for grapevine enhancement. Precision viticulture is part of the scientific field precision agriculture. In connection with viticulture, precision agriculture can be described as all means in viticulture which are dealing with the characterization of spatial variation in the production of crops. Technologies created by means of precision agriculture are applied to increase efficiency of viticulture management by estimating crop yield more accurately and reducing the necessity to use fertilizers (Dey, Mummert and Sukthankar, 2012).

More specifically, precision viticulture is described as the utilization of geospatial technologies and similar devices, tools and technologies which harness spatial location to collect, store, manipulate, analyze and visualize environmental data from vineyards. The application of those instruments and associated approaches give vine growers and viticulture experts the opportunity to collect data from their vineyards in real-time with accurate position information (Goldammer, 2015). Such data can then be exploited by the experts to achieve knowledge about the current situation and parameters in the vineyard. The obtained knowledge can be used to improve vineyard management related decision making. In the last few decades with the rapid rise of new technologies and the improvement of existing ones, the deployment of geospatial technologies by means of precision viticulture in vineyards has also seen a swift rise. Their application is continuously rising because they

give vine growers a wide range of benefits. The foremost advantage is the improvement of viticulture management which comes with other positive consequences. The improvement includes not only the enhancement of management techniques but also the ability to improve the decision making when to apply such a technique. On the one hand, this leads to an increase in yield efficiency and on the other hand to an enhancement of yield quality and security. Other results of an improved viticulture management are for example reduced need of operating resources and an enhanced balance between the usage of chemicals and the quality of the soil and groundwater around a vine (translated from Maniak, 2004). Consequentially, information acquired by combining global positioning system (GPS) sensors and GIS in vineyards through precision viticulture helps viticulture experts to better organize and manage vineyards, to improve a vine's balance and gain an improved wine quality.

2.1.2 Phenology

Since phenology is one of the core subjects this research project is concerned with, it is necessary to understand its definition and how it can be classified. Therefore, this chapter focuses on the description of the term phenology, on highlighting how the phenology of vines can be classified and describing the individual phenological stages of vine in detail. Additionally, it emphasizes why it is important to obtain information about the specific phenological stages of vine and why tracking their vegetative growth can be of great value for viticulture. The term phenology first appeared 1849 when physicist and astronomer Adolphe Quetelet described it as "observations of periodical phenomena of the animal and vegetable kingdom". A few years later starting with 1853, the term also occurred in works of Charles Morren, who is often seen as the founder of this term (Demarée and Rutishauser, 2011; Harlfinger, Koch and Scheifinger, 2002). In general, phenology is defined as the science which focuses on the research of the natural changes and development of organisms and their relationship with seasonal variations in climatic parameters (Centinari, 2018 b; Westover, 2018; Hellmann, 2003). However, there is no exact explanation of phenology and it may vary from source to source. A more detailed explanation of phenology is given by Harlfinger, Koch and Scheifinger (2002). In their book "Klimahandbuch der Österreichischen Bodenschätzung Klimatographie Teil 2" they describe phenology as the science which „deals with periodic developmental phenomena and their temporal dependence on plants and animals over the course of a year". They highlight that this science not only includes pure observation but also "attempts to explain the laws of periodic growth and also investigates the relationships between biological rhythms and environmental influences, in particular weather and climate conditions". Furthermore, phenology is also concerned with "the identification of interactions between vegetation development and various environmental factors,

with particular emphasis on temperature in temperate and higher latitudes" (translated from Harlfinger, Koch and Scheifinger, 2002).

2.1.2.1 Phenology Classification Systems

A feature that most definitions of phenology include is the constant natural growth of an organism over a specific time period. In aspect of viticulture, this phenological feature can be described as the vegetative change and development of vines over the course of a specific timespan, which is often defined as a year. Therefore, collecting data about the vegetative growth of a vine throughout a year is very valuable for vine growers. They can use such information to estimate when the next phenological stage of a vine is going to begin and when to execute specific vineyard management techniques like pruning grapes. However, a problem that arsis when trying to measure the natural development of a plant is that every plant has its own natural growth and it is a constantly ongoing process. Following, it can be difficult to separate the growth process into exact stationary phases. Furthermore, the exact number of phenological stages to record depend on the objectives of the vine growers (Westover, 2018).

A unified classification system which separates the phenology of a plant and specifically grapevines into distinct phenological stages can bring several advantages for viticulture experts. One the one hand, it simplifies the exchange of new knowledge and the work on collaborative projects regarding phenological stages of vines. On the other hand, knowing the characteristics of a specific phenological stage of vines is an advantage for field works such as agricultural practices, agricultural meteorology, agricultural insurances and applied botanical sciences (translated from Hack et al., 2001). All those rely on phenological information because they utilize this knowledge about phenological stages for different application to enhance the vines and wine quality. Additionally, vineyard related practices such as the management of canopy, nutrients, diseases and insects are carried out in certain phenological stages. Hence, it is vital for vine growers to collect data about the appearance of the individual growth stages of vines to for example be able to predict the beginning of the next stage (Centinari, 2018 b). Furthermore, recording a precise number of phenological stages of plants depends on the objective of the grower (Westover, 2018). Therefore, various scales and classification criteria for phenological stages of plants provide systems how to classify the growth process of a plant.

There exist several different classifications which divide the phenology of plants into a specific number of stages. One of the most used phenology classifications for plants is the classification created by the institutions Biologische Bundesanstalt für Land- und Forstwirtschaft, Bundessortenamt and Chemische Industrie (BBCH). Those worked together to design the so-called

BBCH-scale. The BBCH-scale is a classification used for unified coding of the phenological stages of mono- and dicotyledonous plants. As explained by Hack et al. (2001), unique and easily identifiable morphological characteristics were used to describe the individual phenological stages of plants. Furthermore, stages with similar characteristics were given the same code. In general, the BBCH-scale separates the whole vegetative growth cycle into 10 major stadiums which are numbered from 0 to 9. These major stages are (listed in chronological order): sprouting, leaf development, formation of side sprouts, shoot development, development of vegetative plant parts (harvest crop), appearance of the flower predisposition, flowering, fruit development, fruit and seed ripeness and dying or dormancy of the plant. However, the BBCH-scale further partitions each major stage into 10 micro stages that are also numbered from 0 to 9. Following, the combination of the macro and micro stage coding result in a classification system with 100 stages ranging from 00 to 99 (Hack et al., 2001).

A phenology classification used in Austria which is specified for phenological stages of vines is explained by Harlfinger, Koch and Scheifinger (2002). This system separates the seasonal vegetative growth of vines into 7 stages. The first stage is called seeding and describes the seeding of several fields. The second stage “rising” is characterized by plants that grew 1 centimeter out of the soil. In the third stage named bud break the first green leaf tips can be seen on at least 3 buds on the vine. The fourth stage called sprouting is characterized by the appearance of the first fully grown leafs on at least 3 spots on the vine. In the fifth stage “beginning of flowering” the first flowers can be seen on at least three spots of the plant. In the sixth stage termed véraison (translated as ripening or ripening period) the first ripe berries can be observed on some bunches. The seventh and final stage of the classification is characterized by the complete ripeness of the majority of fruit on vine (Harlfinger, Koch and Scheifinger, 2002, p.158-160).

Another often used and referred phenology classification system is the Modified Eichhorn-Lorenz (E-L) system. The Modified Eichhorn-Lorenz system serves as a classification and coding system specified for grapevines. The original E-L system was developed by Dr. K. W. Eichhorn and Dr. D. H. Lorenz in 1977 and is one of the most complete systems which separates the natural seasonal growth of vines into different stages. In 1995 the E-L system was changed for the first time by B. G. Coombe. In 2004 the altered E-L system was revised and modified again by Coombe and P. Dry and thus became the now well-known Modified Eichhorn-Lorenz system (Westover, 2018). The reason for modifying the original E-L system several times, is the fact that the visual characteristics in the early stages of bud growth varies among the grapevine types (Centinari, 2018 b). In detail, the Modified E-L system divides the annual natural growth of grapevines into 47 distinct vegetative stadiums, each assigned with a specific E-L number. Additionally, the Modified E-L system highlights eight of these

stages as key phenological stages. The following enumeration lists those 8 major growth stages in age based order starting with the youngest: bud burst, shoots reaching 10 cm, flowering begins, flowering, setting, berries pea-size, véraison and harvest (Westover, 2018). Figure 1 gives a detailed visual insight into the vegetative growth of vines and how it is classified by the Modified E-L system. The following subchapters examine each of these key phenological stages in detail.

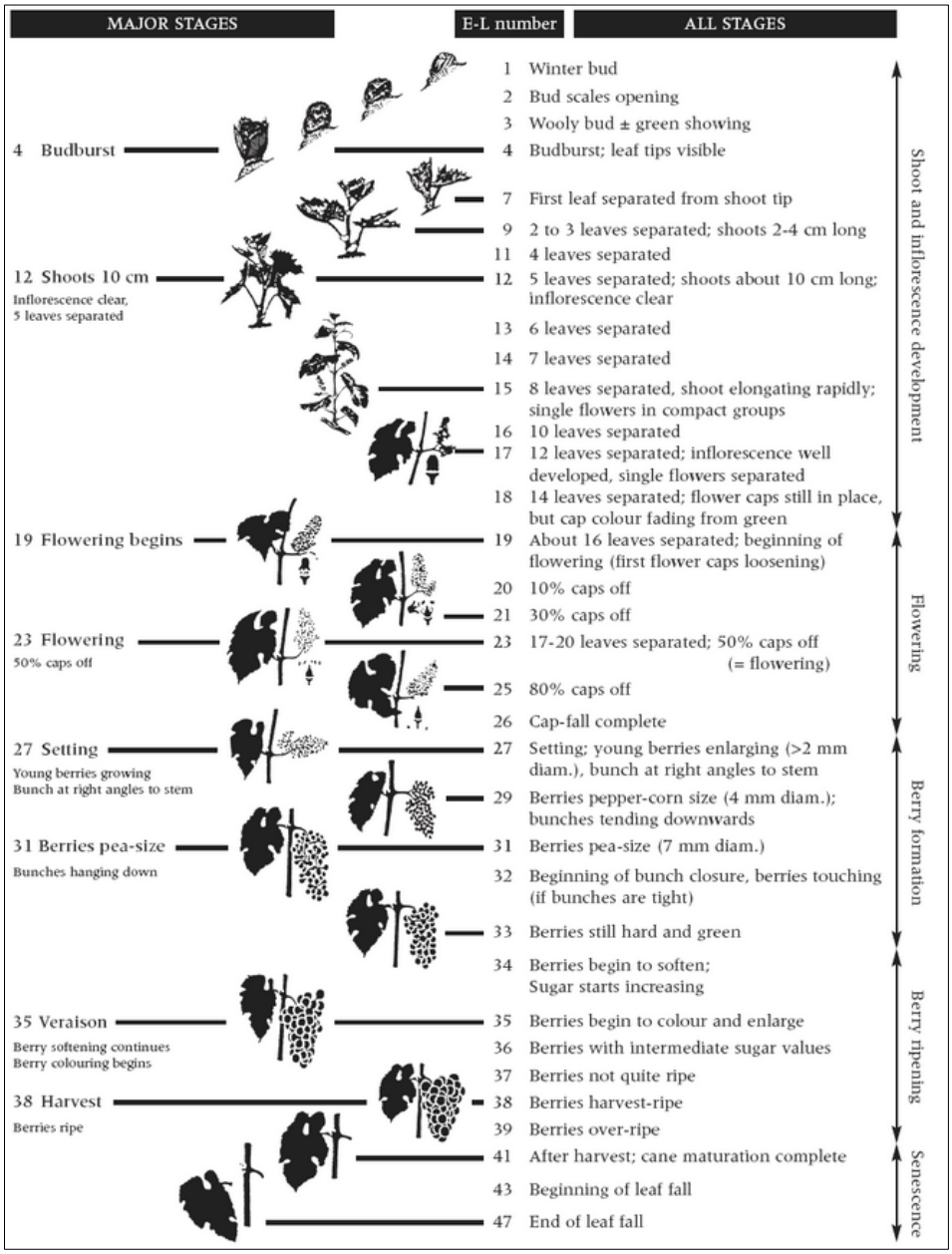

Figure 1: Modified E-L system - phenological stages of grapevine (Westover, 2018)

Before going in detail about these key stages in the following chapters, a few facts regarding the phenological stages of grapevines need to be mentioned. The key changes in natural growth of grapevines throughout a year are happening in the 8 stages which the Modified E-L system highlights as major stages. The end of a phenological stadium is the start of the next stage in the growth cycle. An important fact to mention is that the beginning and the duration of a phenological stage are

varying between grapevine types and are also underlying variations within those vine sorts. These variations are caused by grape variety, the differences in local climates and changes during and in between seasonal weather. Nonetheless, the general order of these phenological stages stays the same. Furthermore, it is well-known that some of the stadiums can overlap with others for certain periods of time (Goldammer, 2015; Hellmann, 2003).

2.1.2.2 Budburst

The first phenological stage which is pointed out as a key stage by the Modified E-L system is the so-called Budburst. Sometimes this stadium is also referred to as bud break (Centinari, 2018 b). In the Modified E-L system it is associated with the E-L number 4 and described as the event when buds burst open and following making the leaf tips visible (Westover, 2018). Figure 2 depicts a bud on a grapevine during budburst. At this stage, the dormant buds comprise 10 to 12 primordia and one to two cluster primordia. These primordia are the rudiments of the tendrils and flower clusters, which represent the inflorescences of vines (Hellman, 2003). The budburst usually begins in spring when the average daily temperature reaches about 10°C. If this condition is fulfilled, the beforehand dormant winter buds of the vines start to grow (Goldammer, 2015; Hellman, 2003). The timing when budburst begins not only depends on the temperature but also on the amount of buds that were left on a vine after pruning in winter. With pruning techniques, vine growers can regulate the amount of buds that remain and thus controlling the yield of the following season. Leaving too few ("overpruning") or too many buds ("underpruning") on a vine can have different consequences. In case of overpruning, fewer buds will remain, the shoot growth will be more vigorous and the yield of the next season may be lower than anticipated. If too many buds stay on a vine, more but weaker shoots will grow from those buds and the yield of the next year may be higher than expected. Moreover, budburst is negatively affected by other internal and external factors too. Negative grapevine-own influences on budburst are a low carbohydrate storage in vines or frost injuries. External factors which have a negative effect on budburst are cold and wet soils, drought resulting in too dry soils, a degree of chilling causing frost injuries on the vines and badly managed irrigation in the preceding season (Goldammer, 2015). With budburst the shoots begin to grow but at the beginning their growth rate is relatively slow. After a brief period of time a rapid growth phase known as "grand period of growth" which lasts until fruit set is entered by the vine (Hellman, 2003).

Figure 2: Bud burst on a vine

2.1.2.3 Shoots 10 cm

The second key phenological stage in the vegetative growth cycle of grapevine is called “Shoots 10 cm”. This stage is assigned the E-L number 12 and as the name implies, one characteristic of the stage is the specific length of the shoot. Figure 3 shows an illustration of a vine while its shoots are 10 centimeters (cm) long. Other properties of this phenological stage are that the inflorescence is clear and that 5 separated leaves can be seen on the vine (Westover, 2018). Another important feature of this stadium is the shoot growth. As mentioned before, shoot growth starts with budburst but initially it is quite slow. With the separation of the first leaves the shoot growth accelerates and it enters the “grand period of growth” during which the growth is rapid. A primary part of this shoot growth period is accompanied by the flowering process. The shoot growing slows down after flowering is finished and when the fruit setting starts. Usually the growth of the shoots stops after the beginning of the ripening process of the first grapes (Goldammer, 2015). A fact which should be considered by vine growers during this key phenological stage, is the timing of shoot thinning. Shoot thinning is the process of transforming the randomly grown green shoots into an ordered canopy structure. The thinning usually is performed when the shoots are between 10 and 25 cm long (Smith and Centinari, 2017). It is done to maintain non-damaged shoots on the grapevine in case of a late spring frost (Smith and Centinari, 2017) and to improve the balance between shoot growth and fruit crop which results in a better vine balance and fruit quality (Ames et al., 2016).

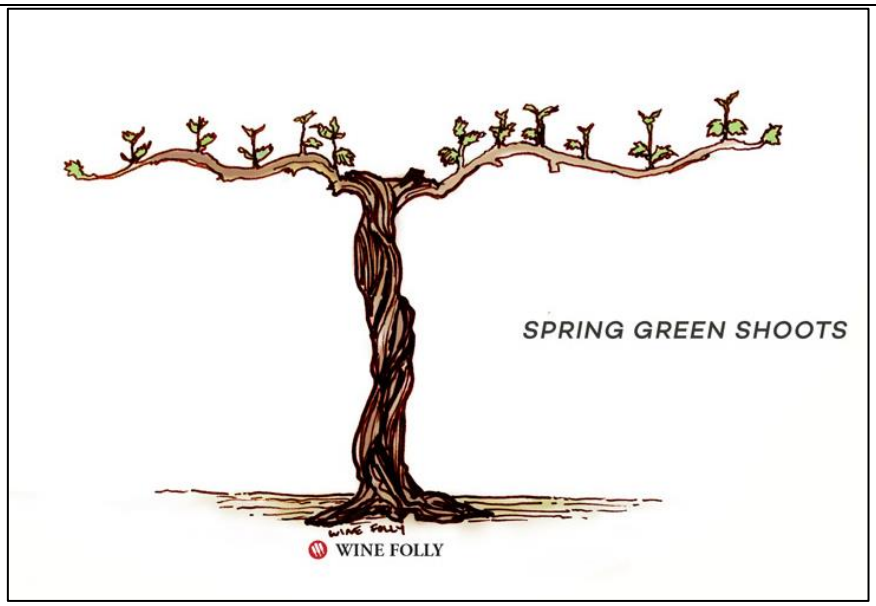

Figure 3: 10 cm long shoots (Wine Folly, 2016)

2.1.2.4 Flowering Begins

Before the third key phenological stage is explained, an important event called flower cluster initiation needs to be explained to understand how the flower clusters on shoots of grapevines grow. During the flower cluster initiation, the cluster primordia of the buds grow to become flower clusters which are the inflorescences of grapevines. As explained in chapter 2.1.2.2 Budburst, the dormant buds are comprised among other components of 10 to 12 primordia and 1 to 2 cluster primordia. For the primordia to develop into a flower cluster, three steps are necessary to happen inside the dormant winter bud before their budburst in spring. At first, uncommitted primordia grow within the buds. These primordia are undetermined at the beginning of their growth because they can grow into a flower cluster or a tendril. Secondly, the primordia become committed to either develop into a flower cluster or a tendril. Whether a primordia "decides" to become a flower cluster or not depends on environmental parameters and growing conditions (Goldammer, 2015; Hellman, 2003). Considering environmental conditions, the amount of sunlight exposure and temperature are crucial factors for primordia to become a flower cluster or a tendril. The higher the exposure of buds to sunlight, the larger is the size and number of primordia inside the bud growing to flower clusters. The growing conditions and thus development into a flower cluster or tendril can be somewhat controlled by viticulture experts with growing techniques such as pruning or shoot thinning. Growing management during this phase is important for vine growers, because the primordia which become a flower cluster represent the fruit potential of the grapevine. After a primordia's commitment is decided, the third phase begins, which starts just after budburst in the next spring. In this last phase of flower cluster initiation, the actual growth of primordia to a flower cluster takes place (Hellman,

2003). Usually, a shoot grows between 1 to 3 flower clusters (Goldammer, 2018). The primordia on the opposite side of the flower cluster primordia develop to tendrils (Hellman, 2015). When those committed primordia finished growing, the next phenological stage named “flowering begins” starts. It is the third key phenological stage which is highlighted by the Modified E-L system. Other synonyms which are used for this stadium are beginning of bloom or flowering initiation. In the Modified E-L classification this phenological stage is indexed with the E-L number 19. The main visual features of this phenological stage are that about 16 leaves are separated and the first flower calyptra (caps) are loosening from the flowers (Westover, 2018). The caps are a green plant structure which are part of the flower before bloom (Hellman, 2015). They are comprised of five petals and are located at the tip of a flower. Before the caps fall off the flower, they prohibit the flower from opening and protect the reproductive organs lying inside the flower. When the flowering of a vine starts, the caps of flowers being to detach at their base and to fall away (Poupin et al., 2011). In general, the flowering begins about six weeks after budburst and starts at the uppermost flower clusters. When the flowers exactly initiate the blooming depends on weather conditions and the grapevines breed (Goldammer, 2018). Suitable climatic conditions for a flower to lose its caps and to start flowering are short exposures to high temperatures and a high light intensity. One essential fact that must be considered is that grapevines need two successive growing seasons to be able to start blooming in the following season (Poupin et al., 2011; Carmona et al., 2007). Figure 4 shows an image of how a flower cluster on a vine looks like during this key phenological stage. In the displayed image all caps are still on the flowers.

Figure 4: Grapevine cluster during beginning of flowering

2.1.2.5 Flowering

The fourth key phenological stage which is pointed out by the Modified E-L system is called flowering. This stage is associated with the E-L number 23 and has two main visual features by which it can be recognized. On the one hand, 17 to 20 leaves are separated on a vine during this vegetative phase. On the other hand, about 50% of flower caps have fallen off of most flowers clusters (Westover, 2018). Usually, it is expected that flowering starts about six to eight weeks after budburst has occurred (Goldammer, 2015; Christensen, 2000). However, this is not always the case since the time when flowering occurs is subject to external factors such as weather conditions and varieties in features of vine breeds (Goldammer, 2015). For example, a very important factor regarding the timing of bloom is light exposure (Carmona et al., 2007; Hellman, 2003). The more light a flower is exposed to, the earlier the cap of a flower falls off and the process of flowering begins. Following, the higher a flower cluster is located on a shoot and the higher a flowers is positioned on a flower cluster, the earlier it starts blooming. Therefore, flowering occurs first on the uppermost shoots. Furthermore, due to those differences to light exposure the key phenological stages of flowering begins (E-L 19) and flowering (E-L 23) might overlap between vines.

When the cap of a flower falls of, its process of flowering begins. This is a visual cue for viticulture experts that the phenological stage of flowering has started. After the cap has detached from a flower, it begins to open and its reproductive organs are revealed. Most cultivated grape breeds are hermaphroditic flowers and have two different reproductive organs (Christensen, 2000). These organs are the pistil (female organ) and the anther (male organ). Usually a flower consists of one pistil, which is located at the inner base of a flower, and five stamens whereas an anther lies on the tip of each stamen. The pistil is composed of tissues and the ovary. During flowering, the ovaries of the flowers can be fertilized by the sperm inside the pollen from the anthers (Hellman, 2015). Fertilization is completed when the sperm reaches the eggs located inside the ovary and has fertilized them (Christensen, 2000). In general, this process of flowering continues for one to three weeks (Goldammer, 2018) and optimal temperatures for bloom are 29°C to 35°C (Christensen, 2000). Once flowering is finished and a flower is pollinated, it starts to develop into a berry (Poupin et al., 2011). In detail, the tissues and the ovary of the pistil of the flower develop to become the berries and the ovule grow to seeds (Hellman, 2015). Consequently, the berry growth and the next phenological stage starts. Figure 5 give a visual impression of the flower cluster of a vine during flowering. The white parts flowers in the image are the stamens with the anthers on top of them.

Figure 5: Grapevine cluster during flowering

2.1.2.6 Setting - Fruit set

As described at the end of the previous chapter 2.1.2.5 Flowering, the next key phenological stage starts when the flowers form into berries (Goldammer, 2015). This key phenological stage is named "Setting" by the Modified E-L system but is also often referred as "Fruit set" in literature. This stage is indexed with the E-L number 27. The description of the vegetative stage by the Modified E-L system reveals two main visual characteristics by which fruit set can be identified. On the one hand, the young berries are enlarged during the phenological stage and have a diameter of about 2 millimeters (mm). Another visual feature of the stage is that the bunch are aligned at the right angles to the stem (Westover, 2018).

Before going into detail about the berry growth process which is an important feature of the phenological stage of setting, the "technique" of fruit set itself needs to be explained since not all flowers of a vine are able to become berries during this stage. Fruit set is a sort of "self-thinning" technique of the vine. It is an important measure of the vine to adjust its crop in such a way that all available resources of the plant are effectively used but the survivability of the plant is not at risk. Therefore, the plant gets rid of some flowers or small berries which have already been developed and the remaining ones become fleshy berries (Centinari, 2015). This measure of the plant shedding parts of its crop after full bloom is called berry shatter (Christensen, 2000). This percentage (%) of flowers that form berries is a quantitative value for vine growers to check if the fruit set of their vines

is normal or below-average. Normal fruit set is commonly described with 30% to 50% of flowers growing to berries. If less than 30% berries develop, it is considered a poor fruit set. However, these fruit set thresholds are vastly different and depending on the grape variety (Centinari, 2015). Weather conditions are another factor influencing the percentage of fruit set (Hellman, 2015). Cold temperatures below 18°C, hot climatic conditions with temperatures above 37°C, rainy weather and high humidity have a negative effect on the flowers and result in fewer berries being developed. While fruit set, when the initial shape and structure of a berry is developed, the berries diameter reach from 1.6 mm to 3.2 mm (Christensen, 2000).

Once a vine finished regulating its crop, the fertilized flowers begin to grow into berries. Firstly, the initial berry structure is developed. Every flower grows into a very small initial berry composed of a thin skin, flesh and seeds which develop from the ovule (Stafne and Martinson, 2012). Following the berry initiation, the growth process begins. The berry growth from berry initiation to a ripe berry is separated into three phases: a rapid growth phase, a short period of slow growth and a final rapid growth stage. At the beginning, the berries enter a stage of rapid growth called “Rapid Growth Phase”, which is part of the key phenological stage “Setting” in the Modified E-L classification system. This berry growth phase can be recognized by two visual key features. On the one hand, it can be identified by the rapid growth of berries. This rapid growth is noticeable in the change of size of the berries. The diameter of the berries can double in size and reach 4 mm to 6 mm (Goldammer, 2015). The size of a berry is influenced among other things by the number of seeds in the berry. Since there is a maximum number of four ovules in a flower, a berry contains no more than 4 seeds. Furthermore, the rapid development of the berry size during the rapid growth phase is also affected by the environmental situation. For example, cold and wet weather conditions have a negative effect on fruit set, resulting in possibly fewer and or smaller berries (Hellman, 2015). The ideal temperature interval for rapid cell division and enlargement and thus berry growth is 20°C to 25°C. Another important parameter affecting berry size development are the light conditions. The amount of light exposure is an essential factor, especially during this rapid growth phase at the beginning of the berry growth process. If a berry in this phase is subject to heavy shade, it will be significantly smaller than a berry exposed to light (Christensen, 2000). Vineyard management practices and water management can also be applied to regulate the berry size (Hellman, 2015). On the other hand, this growth phase can be recognized by the appearance of the berries. During the rapid growth phase the berries have a dark green color and are firm (Goldammer, 2015). This phase is also very important for wineries, as the berries begin to accumulate acidity (Stafne and Martinson, 2012). The rapid berry growth phase commonly lasts between three to four weeks (Christensen, 2000; Hellman, 2003). Figure 6 illustrates how a bunch of vine can look like during this key phenological stage.

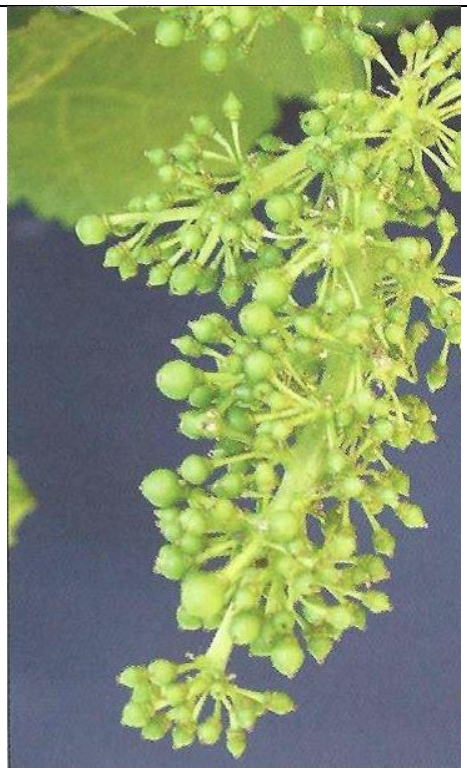

Figure 6: Grapevine cluster during setting (Iland et al., 2011)

2.1.2.7 Berries pea-size - Lag Phase

When the berries have finished their rapid growth through cell division and cell enlargement the next berry growth stage begins. It is the second growth stage and also a key phenological stage classified by the Modified E-L system. It is called “Berries pea-size” in the Modified E-L system (Westover, 2018) and often referred as “Lag Phase” In literature (Goldammer, 2015). It is associated with the E-L number 31 and characterized in the classification with two visual features. It can be identified by the size of the berries, which are about 7 mm in diameter during the stage. Another visual cue of this key phenological stage are the bunches. Instead of being positioned in a right angle to the stems they are hanging down, due to the increase of total weight of the berries on the bunches (Westover, 2018). During this phase the berry growth slows significantly down, after the rapid berry growth in the first phase. At the beginning of the lag phase, the growth of the shoots slows down further and at some point during the phenological stage shoot growth completely stops. Furthermore, while the lag phase, the berries start to lose and become less firm. When the end of the lag phase approaches and the beginning of the next key phenological stage is about to start, a critical visual change can be observed. Through losing chlorophyll (Christensen, 2000), the berries begin to change their color from a green or dark green to their grape variety typical color. Thus, it is a reliable indicator when the next key phenological stage starts. Generally, the berries pea-size stage lasts about 14 to 40 days

(Goldammer, 2015). The duration of the lag phase varies depending of the climatic situation during the phenological stage (Christensen, 2000). An image of a grape cluster during the berry pea-size stage is shown in Figure 7.

Figure 7: Berries during lag phase (Odneal, 2018)

2.1.2.8 Véraison – Fruit Ripening

Following the slow berry growth in the Berries pea-size stage, the berries enter the final growth phase which is another phase of accelerated berry growth. Until the harvest, the berries size doubles (Goldammer, 2015). This phenological stage is the seventh key phenological stage in the Modified E-L system and mainly called véraison, although it can also be found by the name of "Fruit Ripening" in literature. It is indexed with the E-L number 35 and its main characteristics described by the Modified E-L system are the change of color and the enlargement of the berries (Westover, 2018). The berry color change comes with the loss of chlorophyll and the accumulation of phenolic compounds. These phenolic compounds are responsible for the typical color of a vine variety. This visual transformation is a sign that the fruit maturation of a berry begins. The process of ripening can be determined not only by the color change of the berries, but also by a change in consistency of the berries. Throughout the ripening process in véraison, the berries start to soften and begin to mature irregularly among and within a grape cluster. Usually, berries located at the upper part of a bunch besides to the stem, start to ripen first and faster (Goldammer, 2015). The potential size and weight of the berries are depending on the number of cells, the cell volume and concentration of sugars in the berry. The time when the ripening process of the berries begins depends on several factors. It is

affected be the grape variety, the climatic conditions during berry growth and the crop amount. The amount of time how long it takes berries from fruit set till véraison to start ripening is measured in degree-days. Generally, the number of degree-days for a berry to start maturing is different between grape breeds and also influence by temperatures. Cold weather conditions and hot temperatures above 40°C while berry growth delay the start of berry ripening. To ensure optimal berry ripening in a bunch, it should have about 18 leaves. This key phenological stage typically lasts for about six to eight weeks (Christensen, 2000). At the end and after véraison the berry start to accumulate sugar compounds. These concentrations of sugars are influenced by the hanging time of the bunch, the crop load, canopy size, diseases and water availability. These factors can also be influenced by vine growers to some extent and thus they can regulate the sugar content in the grapes (Stafne and Martinson, 2012). Figure 8 displays grape clusters during véraison. The picture shows very well how unevenly the berries ripen in a bunch during this key phenological stage.

Figure 8: Grapevine cluster during véraison

2.1.2.9 Harvest

The final key phenological stage of a growing season is called “Harvest” and associated with the E-L number 38. Its main characteristics is that all berries have ripened, reached their potential size, adopted their breed typical berry color and thus can be harvested (Westover, 2018). The color change is the visual key feature how the beginning of the Harvest stage can be identified by direct

visual observation. The completed ripeness of the berry can be specified by measuring the sugar and acidity concentration, the pH-value or the flavor. Furthermore, by surveying these berry factors, the fruit quality of a berry can be determined (Goldammer, 2015). Although the Harvest stage is usually the time when ripe berries are harvested, if they remain on their bunch, they continue to ripen since ripening is a lasting process and the remaining berries are still supplied with nutrients from the vine. Therefore, if berries are not immediately harvested when they show signs of complete ripeness, they will further ripen and accumulate more sugar and other compounds. Thus, the harvest time of berries depends on their intended use and the desired ripeness parameters by the vine grower. Finally, the ripeness of berries and their fruit quality are no fixed values but determined by the individual preferences of the vine grower and viticulture experts (Hellman, 2003). Figure 9 illustrates a harvest ripe bunch of a vine where all berries have completed ripening and taken their variety typical color.

Figure 9: Harvest-ripe grapevine cluster

The images in Table 1 and Table 11 give a visual overview of all key phenological stages in chronological order. Table 11 can be found in Appendix A: Phenological Characteristics Matrix. Table 11 must be highlighted specifically since it is a characteristic matrix of the key phenological stages of vine which has been created on basis of the information obtained from the literature research. The 9 rows of the matrix depict the header of the columns and the eight key phenological stages. The 7 columns of the matrix are representing specific parameters and characteristics of each key phenological stage. Colum 1 and 2 contain a numeration and the Modified E-L numbers of each key stage. Column 3 shows the names of the phenological stages and column 4 the corresponding pictures. Column 5 displays the approximate appearance and duration of the vegetative stages.

Column 6 contains the phenotypical characteristics and column 7 the references to the information given in the characteristics matrix. The characteristics shown in Table 11 can be used as requirements for the identification of the vines in those stages with technical measurements such as photogrammetry.

Table 1: Images of key phenological stages of vine

1

Bud burst (E-L 4)

2

Shoots 10cm long (E-L 12)

3

Flowering Begins (E-L 19)

4

Flowering (E-L 23)

5

Setting (E-L 27)

6

Berry pea-size (E-L 31)

7

Véraison (E-L 35)

8

Harvest (E-L 38)

Nowadays, farmers and scientists engaged in agricultural research are searching for methods and procedures to improve the understanding of local differences of vegetative parameters in a field. The scientific field precision agriculture, and in specific precision viticulture, survey and develop concepts to enhance viticulture management practices which are applied to collect data from variability of spatial and temporal vine parameters (translated from Maniak, 2004). Consequently, the data from the characteristics matrix and the collection of such data is important information for vine growers and viticulture experts since they can use those to make several improvements in their vineyards. One the one hand, the collection of information about phenological stages helps viticulture experts to improve their decision making in their vineyard over a whole growing season. In this context, the key phenological stages and corresponding characteristics are used as benchmarks for vine growers to execute vineyard practices like canopy management, monitoring of the vineyard nutrients and pest and disease control. Furthermore, the collection of the latest phenotypical parameters of vines helps vine growers to deploy these vineyard practices based on the current growth stage of their vines. This results in an improved efficiency of vineyard management, reduces labor costs and enhanced vine health. On the other hand, tracking phenological parameters of vines also helps viticulture experts to predict the time when the next key phenological stage will start. This information about the timing of phenological stages can help vine growers to estimate when the "sweet spot" of a growth stage occurs and to apply vineyard practices at that point of time to improve a vine's balance (Westover, 2018). Moreover, not only vine growers have an advantage from knowledge about phenotypical data but also wine production profits from it. The knowledge about every process and change in vine growth throughout a season is important to utilize vineyard management practices in such way to get vines with ideal characteristics and therefore to improve the quality of the produced wine. Last but not least, the tracking and collection of phenotypical data of vines is useful to estimate a vineyard's yield (Goldammer, 2015).

2.1.3 Yield

Another very important term in viticulture is yield. This chapter is concerned with explaining the definition of yield and why it is important to know about the yield of a vineyard. Furthermore, the topic yield prediction is also discussed. Yield is the amount or weight of fruit over a given spatial area and can be for example be measured in tons of grapes over a vine block or surface unit. In specific applications it may also be referred as the amount of fruit on a single vine (Moyer and Komm, 2015). On the one hand, the knowledge about the current yield of vineyard helps vine growers to check if the yearly yield and quality goals are going to be reached. Since the amount of berries on vines and the yield in a vineyard are closely tied together, the knowledge about these data helps viticulture

experts to apply vineyard practices in such a way to improve a vines quality and therefore to reach the yield and quality goals. In addition, yield prediction is a vital exercise for every vine grower. The estimation of yield is necessary for example to know when to utilize specific vineyard practices or when a vine grower needs to prepare for harvesting (Nuske et al., 2011).

In general, the estimation of yield from a vineyard is described as a process of predicting as precisely as possible the quantity of crop that is going to be harvested from a vineyard (Goldammer, 2015). Peter May recognized in the 1970s that not only yield estimation during harvest is necessary, but also that yield prediction in the key phenological stages is valuable. He identified that there are fixed times during annual vine growth, which are the key phenological stages, when the potential of yield was fixed and supported the prediction of yield by assessing the vine components at the key phenological stages. Moreover, in order to verify the performance of a yield estimation method and to obtain an accurate yield prediction result, measurements should not only be carried out in the individual key phenological stages as suggested by Peter May, but also be assessed over many vineyard block and throughout many seasons (Dunn, 2010).

Yield prediction is an essential operation for every vineyard grower (Nuske et al., 2011). The obtained information from the estimation of yield of a vineyard throughout the phenological stages of the vines bears several advantages for vine growers. Yield prediction helps them to enhance their vines balance by improving their decision making regarding the application of vineyard related practices (Moyer and Komm, 2015). Information about yield gives those experts the opportunity to find the correct timing when and how to apply these vineyard management practices and thus to optimize the vines growth (Nuske et al., 2011) and fruit quality (Nuske et al., 2014). An improved vine growth and fruit quality guarantees that desired fruit composition values are met and that the potential size of crop is reached (Goldammer, 2015). The knowledge of yield from key phenological stages also helps vine growers to plan and prepare several vineyard operations in advance. For example, it supports them in preparing harvest relevant operations (Nuske et al., 2014) such as planning logistics for harvest (Dey, Mummert and Sukthankar, 2012). Other vineyard operations that can be prepared based on yield data are the shipping of crop, the storing of crop and the selling of harvested crop on the market (Nuske et al., 2014).

In addition, product manufacturers such as winery or juice factories also gain some advantages from the knowledge about yield prediction results. On the one hand, those information are important for a winery since they need to know in advance how many grapes they are expected to manufacture in a vintage. Hence, this knowledge of yield has an influence on the logistics of a winery. The adaptation of logistical operations are for example harvest scheduling or utilizing tank or barrel space in the winery (Goldammer, 2015). If a rapid influx of fruit in a vineyard occurs, it is critical information for

winery managers because they need to prepare their winery for this specific situation. Furthermore, yield prediction is also of relevance for juice facilities to assess if additional juice concentration from other sources needs to be acquired to maintain the quality of their product (Moyer and Komm, 2015).

As mentioned beforehand, Peter May already recognized in the 1970s that yield prediction can be performed in various times throughout the key phenological stages of vine. However, it cannot only be applied at different times during a growing season but also be utilized in different manners depending on the individual preferences of the viticulture experts. In general, yield estimation approaches and formulae are including the four factors planting density (PD), number of producing vines per spatial area (PV), average number of clusters per vine (CV) and average cluster weight (CW). PD can be specified as the number of vines per spatial unit (Moyer and Komm, 2015). However, these four factors are also often summarized in yield prediction calculations as the variables: number of clusters per vine, number of berries per vine and cluster weight (Goldammer, 2015; Nuske et al., 2014). Due to the variances in yield in a vineyard, the variance of these three variables are often used for yield estimation. Following, a commonly used method based on these three components calculates the total yield by using the following formula:

$$Yield = (0.6 * variance\ in\ number\ of\ cluster) + (0.3 * variance\ in\ number\ of\ berries\ per\ cluster) + (0.1 * variance\ in\ berry\ weight)$$

(Nuske et al., 2011). Another approach to estimate the current yield of a vineyard is to combine these factors with the knowledge of previous yield results and weather patterns. Traditionally, these yield prediction variables are collected manually by viticulture experts in the field (Nuske et al., 2014).

2.2 State-of-the Art Research

The state-of-the art research is the second chapter of the literature review. Since one of the main parts of the master thesis is concerned with the development of a multi-temporal phenological 3D model and the related phenotypical data acquisition, it is advantageous to have information about already existing similar approaches. Hence, the state-of-the art research is conducted to obtain information about several phenotypical vine data collection methods and yield prediction processes, which are already used in viticulture. Therefore, the following sub-chapters of the state-of-the art research focus on the topics:

- Traditional viticulture data collection
- Recent developments in viticulture data collection
- State-of-the art phenological vine data collection

- UAS in precision viticulture

The acquired knowledge about specific aspects of these approaches, such as used data, applied software or workflows, help to better understand the process of data collection from vines or vineyard yield prediction and support the development of a data collection and processing method which is implemented in this research project.

2.2.1 Traditional Viticulture Data Collection

This sub-chapter focuses on the description of traditional data collection methods of vine which are used in viticulture and why it is necessary to develop new approaches to overcome challenges and difficulties of these traditional processes. Overall, several different methods and factors are used to collect phenotypical data from vines and to estimate the yield of a vineyard. The utilized approaches and factors depend on the viticulture expert's preferences and the applied yield prediction methods. A feature which is common for all traditional approaches is that they are non-sensor-based data collection methods which are conventionally used by viticulture experts to acquire data about vine parameters and a vineyard's yield. Since those are non-sensor-based processes, they rely on direct visual or manual in-field measurements (Moyer and Komm, 2015). These in-field measurements are often direct manual sampling techniques utilized to obtain information about phenotypical data which can then be used to calculate specific vine relevant factors. Due to time-constraints, only a selected amount of vines can be sampled. Following, the manual sampling is executed based on the selection of vines from the vineyard. However, before starting to apply a manual sampling technique to gather phenotypical information, it is beneficial to have information about the variability of a vineyard. Data about a vineyard's variability helps to select vines from a vineyard in such a way that they are representative for the whole vineyard. Factors which have an influence on the vineyard's variability and thus on the selection of representative vines are for example the distribution of different vine breeds in the vineyard, the vineyard's soil characteristics, its topography or the vines age. Furthermore, it is often suggested to select several vines from every block in a vineyard, to choose the vines in a random fashion and to avoid taking samples from unusual vines or vines lying at the beginning or end of the row. The number of samples to collect is affected by the size of vineyard and by the level of variation between vines. Usually, the larger a sample size is, the more accurate are the calculated results such as the vineyard's yield (Centinari, 2018 a). However, a larger sample size also increases the time needed to finish the sampling of phenotypical data. All these factors have an influence on how the phenological data is manually collected in a vineyard. Consequentially, the utilized traditional sampling techniques can greatly vary depending on the vine growers preferences,

the available information about a vineyard's local variabilities and parameters influencing the vines balance (Centinari, 2018 a).

Once a sampling process is finished and the collected phenological data is stored, it can be used to compare it with previous data and to apply necessary vineyard practices to improve the vines balance. In addition, this data can be exploited to calculate the vineyard's yield with a traditional yield estimation method. Two traditional yield estimation methods, which are commonly deployed to calculate a vineyard's yield, are: the in-season cluster counting and the dormant winter bud dissection (Moyer and Komm, 2015).

The in-season cluster counting can be further divided into two similar methods which are used to calculate yield: the traditional, historical cluster harvest weight method or the lag phase (weighting) method. The traditional, historical cluster harvest weight method uses the formula

$$PY = \frac{PV * CV * CW(\text{harvest})}{w}$$

to estimate yield. The variable PY is the resulting yield value and usually given in tons per hectare (ha) in the metric system and in tons per acre in the imperial system. A special variable in this formula is CW(harvest). A historical final harvest weight value from a previous season must be stated for this variable to guarantee an accurate yield value. The w variable is a standard weight variable. If values with units from the imperial system are used w needs to be replaced by 2000 (pounds per tons). If the stated values have metric units the weight values has to be replaced by 1000 (kilogram per (US) tons). An advantage of this yield prediction method is that it can be applied anytime during the growing season (Moyer and Komm, 2015). Therefore, this traditional method is often used early in the season to estimate yield (Goldammer, 2015). However, it is relying on historical data from previous seasons (Moyer and Komm, 2015).

The other method of the in-season cluster counting to calculate yield, is the lag phase (weighting) method. The big difference between this and the traditional, historical cluster harvest weight method is that the lag phase method can only be reliably used with data from the lag phase which is the sixth key phenological stage of vines (E-L 31). This method uses the formula

$$PY = \frac{PC * CV * CWlag * HM}{w}$$

to calculate a vineyard's yield. The estimated yield is described by the variable PY. Two important variables are CW_{lag} and HM. CW_{lag} needs to be replaced by the average cluster weight during lag phase of the vines. This value needs to be measured from sample vines while they are in their berries pea-size stage of their growth process. HM is a harvest multiplier value that is used to adapt the lag phase cluster weights (CW_{lag}) to an estimated cluster weight. For HM the value 2.0 is usually used (Moyer and Komm, 2015). The multiplier 2.0 is stated for HM because it is generally expected that

the berry weight doubles from the Berries pea-size stage to the Harvest stage. A difficulty which comes with the usage of this method is to predict when the lag phase begins so that everything needed for this yield estimation approach can be prepared in advance (Goldammer, 2015).

The third method that can be utilized to estimate yield is the dormant winter bud dissection. This method relies on removing a selected number of compound buds from vines during winter while they are in their dormant phase. While the vines are in a dormant stage, their buds are still compound and in an overwintering state. As part of the dormant winter bud dissection, the collected compounds buds have to be dissected. Therefore, the outer buds scales are carefully removed from the buds. Then, the buds structure and especially their developing cluster primordia are analyzed and counted using a hand lens or microscope. This dissection of the buds and the analysis of the cluster primordia give information about the potential amount of cluster per shoots for the upcoming season. To guarantee a high accuracy for these three yield estimation methods it is required to apply them consistently in several consecutive years (Moyer and Komm, 2015).

Although these traditional approaches give viticulture experts the flexibility to use data from vines they selected themselves, they bear some major challenges. On the one hand, the manual surveying of data from selected vines in a vineyard is a demanding task. It involves hard in-field work to gather data from vines of each vine block and to set up a strategic plan for sampling representative vines (Moye and Komm, 2015). The sampled data is then used to extrapolate it to the whole vineyard. However, the number of selected vines from which data are collected does not usually coincide with the variability of the vineyard and therefore cannot guarantee accurate yield prediction and makes yield estimation spatially coarse. Yet, acquired data from a larger sample size is more time-consuming and expensive, and manually examining all the vines in a vineyard is simply too time-consuming. Those features make traditional data collection and yield estimation methods very time intensive and expensive (Nuske et al., 2014). Moreover, manual data collection approaches such as the dormant winter bud dissection commonly include destructive sampling (Dey, Mummert and Sukthankar, 2012). Another limiting factor of these traditional methods is that an interpretation of the surveyed vines is necessary (Westover, 2018). Hence, the manual measurement of data can be prone to human failures through incorrect interpretation or subjective evaluation (Rose et al., 2016). Furthermore, yield estimation methods such as the lag phase (weighting) approach or dormant winter buds dissection can only be conducted once a year during specific seasons or phenological stages of vines (Moyer and Komm, 2015). In summary, these information reveal that traditional data collection and yield estimation practices of vineyards have some challenges to overcome such as time-intensive and expansive labor or inaccurate or destructive data sampling (Nuske et al., 2011).

2.2.2 Recent Developments in Viticulture Data Collection

Since traditional data collection and yield estimation methods have several disadvantages, viticulture experts and scientists are researching methods which can be applied without having to deal with the problems from manual in-field approaches. As one task of vineyard managers is to survey phenological data of vines on a weekly basis, it is suggested by Westover (2018) to develop a camera or scanning device which automatically collects phenological data every week. The recording of data in a weekly rhythm is necessary to avoid gaps in the phenological datasets. Sensor-based data acquisition would, among other things, avoid sources of error such as the subjective human interpretation (Westover, 2018). Consequently, in the recent years, vineyard managers and researcher have set their focus on sensor-based approaches to overcome the challenges of traditional methods. Quite newly developed sensor-based approaches such as those proposed by Nuske et al. (2011), Nuske et al. (2014) and Rose et al. (2016) could help to create such an automated data collection device or system. An automated data collection system on basis of sensor-based approaches would reduce data acquisition time, make yield estimations more accurate and reduce labor costs (Rose et al., 2016). Furthermore, it could collection the data from vines in a non-destructive way whilst covering a greater spatial area at once (Dey, Mummert and Sukthankar, 2012). It also provides the possibility to not only execute phenological data collection and yield estimation several times in a growing season, but to also deploy it in a weekly rhythm or even several times a week if necessary.

2.2.3 State-of-the Art Phenological Vine Data Collection

This sub-chapter in concerned with the topic of state-of-the art approaches which are applied for phenological data collection of vine. At first, it is explained why the usage of sensor-based methods for the data acquisition from vines is reasonable. In addition, several of these sensor-based systems are introduced. A detailed advantage and disadvantage analysis can be found at the end of this subchapter. The knowledge about their functionality can be supportive for the implementation of the multi-temporal phenological 3D model of vine of this master thesis. Overall, the research and understanding of those topics is of relevance for this research project because the to-be-implemented approach is also based on sensor-based data collection.

Sensor-based data collection approaches, which for example use photogrammetric processes to record the data, have specific advantages compared to traditional methods. On the one hand, the data acquisition can be done with low cost sensors (Dey, Mummert and Sukthankar, 2012) and in less than a day. On the other hand, fine grained structures like grapes in their initial stages can also be surveyed with those methods assuming that the accuracy of the deployed sensor permits this.

Furthermore, color information is often included with the recorded data (Dey, Mummert and Sukthankar, 2012). In particular multi-view stereo photogrammetric approaches, such as the novel multi-camera system proposed in this research project, are well suited for those data acquisition tasks. An application of those systems provides following benefits:

- A high adaptability, especially if they are mounted on to mobile platforms like UAVs
- They are budget friendly
- They produce high detail point clouds, which can be used to generated 3D models from the surveyed vineyard or vines
- They diminish the effect of occlusion

(Rose et al., 2016). Sensor-based systems can be mounted on to different platforms and thus enable the recording of data over a bigger spatial area than traditional methods. These platforms are for example ground-based systems such as vehicles driving along a track or aerial platforms like satellites, planes, UAVs or balloons. Sensor-based technologies which have already been utilized to collect data from vines or to estimate yield in vineyards are trellis tension monitors, multispectral sensors or visible-light image processing (Nuske et al., 2014).

A system which has been successfully applied in the collection of phenotypical data of vine and to estimate yield in a vineyard is introduced in the work of Nuske et al. (2014). In their paper, they present a “sideways-facing camera” which is mounted onto a “vineyard utility vehicle”. By means of the vehicle, they are able to drive along a track between the vine rows and collect data of single vines with the camera. The generated images of the vines from the selected vine rows are then processed in a three step approach to estimate the yield in the surveyed area. In the first step of their data processing approach they use a set of images with manually marked locations of grapes to train an algorithm which should find “grape keypoints”. In the second phase, the trained algorithm is applied on all images to identify keypoints of grapes and to extract features at those locations. Those are then classified as grape or non-grape. In the final step, the generated data is combined with harvest or in-season samples to estimate the total yield of the area. Through this process they are able to detect berries and to extract information such as texture, color and shape of the berries from the images and to estimate the yield based on the recorded data (Nuske et al., 2014). With their approach they feature a method how phenotypical data can be collected from vines and manipulated in such a way to estimate the yield of the investigated area.

Another application on how sensor-based systems can be used to capture phenological data is presented in the work of Rose et al. (2016). In their paper, they introduce a “track-driven vehicle” that includes a camera system, real-time-kinematic GPS and hardware for vehicle steering, data storage and image acquisition. They use a four step process to detect and count the grapes on the

vines in their test area. At first, they utilize their surveying system to acquire georeferenced RGB images from the vines via the PHENOBot and then process the images with the Pix4DManager software to create 3D point clouds. In the following preprocessing step, they apply algorithms to remove outliers from the point cloud and to smooth it. Then a point cloud classification is deployed to extract color and geometry data from the point cloud and use it to train a classification model. Consequently, the trained classification model is utilized to identify points belonging to grape bunches in the 3D point clouds. In the final phase, they execute an algorithm to acquire information such as quantity of grape clusters and the berry diameter (Rose et al., 2016). They showed that the collection of phenotypical data of vines through optical systems is achievable. It can also be assumed that their generated data, like the number of detected grape clusters and the berry diameter, is usable to calculate the yield of the test area.

Each of the mentioned sensor-based systems in combination with different platforms have various advantages and disadvantages. An advantage of most sensor-based methods over traditional approaches is that they are not only cost effective because they can be used with low-cost sensors, but can also be deployed time-efficiently. Once the selected sensors for recording data are attached to existing machinery such as ground vehicles or UAVs and calibrated, they can be easily integrated into daily vineyard management (Goldammer, 2015). A benefit of ground-based monitoring systems to collect phenotypical data is the avoidance of background noise caused by mixed pixels including soil, grass and vine canopy information (Goldammer, 2015). Another advantage of sensor-system mounted onto aerial vehicles is that they are more flexibly usable and a greater spatial area can be covered in a shorter amount of time.

However, the application of remote-sensing methods which use cameras containing sensors to capture data also have some drawbacks. A disadvantage of deploying remote sensing approaches to collect phenotypical data is their issue with vertical trellising which they are hardly able to detect. Furthermore, remote sensing methods are usually limited to measuring electromagnetic waves reflected or emitted by objects and thus are relying on the spectral characteristics of the survey objects. Another downside is their sensitivity towards atmospheric influences. For example, atmospheric conditions such as cloudy or windy weather or a high humidity rate have a negative influence on the data capturing with sensor-based methods (Goldammer, 2015). Moreover, the processing of multi-spectral images to estimate yield is restricted to vineyards with uniformity requirements (Nuske et al., 2014).

2.2.4 UAS in Precision Viticulture

This chapter focuses on the benefits of using unmanned aerial vehicles in vineyards to collect phenological data from vines, as their usage plays an important role in this research project. Nowadays, two UAV frametypes are applied in vineyards. Fixed wing UAVs are deployed due to their simpler aerodynamic characteristics and their ability to stay longer in the air and to fly at higher speeds. The usage of multi-rotor UAVs has an advantage and a disadvantage. On the one hand, they can vertically take-off and land at nearly every location and also hover in flight. Their drawback is the short flight duration because of their high mechanical complexity and short battery power. Furthermore, UAVs are a cost efficient option to capture data from vineyards. The utilization of low-cost UAVs is cost effective compared to other aerial platforms like satellites or manned planes. They can also be deployed every day and even during cloudy weather which are unsuitable conditions for applying planes or satellites. A further advantage is that they can be operated with advanced autopilot systems. This enables autonomous data recording whereby the drone follows a planned flight route of GPS coordinates. The application of UAVs allow to see and survey the whole study vineyard in a short period of time when they are maneuvered to a high altitude. However, the vineyard coverage also depends on the size of the vineyard. In connection with GIS, the use of UAVs gives viticulture experts the opportunity to identify problems in vineyards based on the data which is recorded by the drone and then processed and visualized in the GIS. Once such a system is set up, it can be used by those experts to solve the identified problems as quickly as possible. As a result, vine growers can flexibly deal with pest or disease infestations on plants, react to nutrient shortages or to supply plants that are affected by drought damage (Goldammer, 2015).

However, the deployment of UAVs also has some limitations. One of the disadvantages is the often non-existent reaction of UAVs in unfavorable situations such as an abrupt change in weather or sudden appearance of objects. Although UAVs with detect-and-avoid systems are already in use, this does not usually apply to low-cost models. In case of an unexpected event like the sudden emerge of an object in front of an UAV during a flight over a vineyard, the drone pilot will most likely be not able to take quick countermeasures, especially if the UAV is beyond line-of-sight. Consequently, those UAVs are limited to be used in line-of-sight. Furthermore, a trained drone-pilot is needed to be able to exploit the full flight potential of drones (Eisenbeiss, 2009).

3. Methodology

The methodology consists of four parts and deals with theoretical definitions and descriptions of the technologies and equipment used to collect, process and validate the data and with the explanation of the conceptual model and workflow. The first subchapter gives an insight into photogrammetry and certain types of photogrammetry which are relevant for recording phenological data of grapevines. The second section is concerned with describing the applied technologies and methods which are utilized to collect image- and ground reference data and to process the recorded data. The methods used to validate the generated results are described in subchapter 3.3 Validation. The fourth chapter 3.4 Conceptual Model and Workflow provides a detailed overview of all major steps of this master thesis.

3.1 Theoretical Overview of Photogrammetry

Photogrammetry plays a central role in the master thesis, as it is used for surveying and the related data acquisition of the study area. In general, it is an important and frequently used scientific method for recording phenomena on the earth's surface. It has a particularly high priority and use rate in some engineering disciplines such as Geoinformation and in specific Remote Sensing. The term originates from the Greek words “phot”, “gramma” and “metrian” (Schenk, 2005). A direct translation of these words would be light drawing measurement. An accurate scientific description of the term is very difficult to find as there is no uniform scientifically accepted definition of the word “photogrammetry”. Nonetheless, Schenk (2005) offers a detailed description of the term in his work "Introduction to Photogrammetry". Photogrammetry is defined in his work as „the science of obtaining reliable information about the properties of surfaces and objects without physical contact with the objects, and of measuring and interpreting this information" (Schenk, 2005).
The frequent use of photogrammetric methods in these scientific fields results from the advantages they offer when the appropriate equipment is available. Photogrammetry is able to cover areas quickly and thus, enables the rapid measurement of study areas. Equipment for the execution of photogrammetric methods can be easily purchased and also allow easy access to information from the air. Thus, the cost of deployment for photogrammetry is low. With the help of photogrammetry very high resolution images can be acquired. These offer the possibility to create high-resolution 3D models which, among other things, can be used for the inspection of building damage (Purdue University, 2018). A disadvantage of photogrammetry is its dependence on waves of the electromagnetic spectrum. Since photogrammetric methods measure the reflected and emitted electromagnetic radiation from phenomena on the earth’s surface, unfavorable light conditions or

weather conditions can have a more or less strong influence on the recorded data (Goldammer, 2015).

There are various means how photogrammetry can be classified. However, for this research project close range photogrammetry, nadir photogrammetry and oblique view photogrammetry are of particular interest as they are used in the project's data acquisition approaches. These are briefly highlighted in the follow sub-chapters.

3.1.1 Close Range Photogrammetry

One type of photogrammetry is close range photogrammetry. In general, close range photogrammetry is defined as the usage of photogrammetric methods to capture terrestrial images of objects up to 300 meters away from the photogrammetric device (Wolf, Dewitt and Wilkinson, 2014). Close range photogrammetry has a wide area of usage. It can be applied to capture and analyze data of sea structures such as deep-sea oil rigs or to inspect other human-made constructions like bridges. Another deployment of close range photogrammetric methods are the surveying of landscapes or the sea. This can be used, for example, to examine coastal sections or sections of the sea for pinnacles (Gillies, 2015). In the case of this research project, close-range photogrammetry is used to generate high-resolution images of the study vineyard. High-resolution data enables the creation of high-density 3D point clouds of vines in which individual vine structures such as berries, leaves or stems can be identified.

3.1.2 Nadir Photogrammetry

Nadir photogrammetry is a special type of photogrammetry that is quite often used for remote sensing systems. It is a type of aerial photogrammetry with the unique characteristic that the utilized optical system is aligned at the right angle to the earth's surface. Thus, the distance to the observed object is exactly the distance between the earth's surface and the lens of the applied objective (Philpot and Philipson, 2012). The name of this image acquisition method is derived from the word nadir. The term originates from the Arabic language and can be translated as "opposite". It is called the opposite because the nadir point represents exactly the point on the opposite position of the zenith. The zenith is defined as the location lying vertically above the observer (Merriam-Webster, 2019). Nadir photogrammetry is a widely used image processing technique. It finds its application in areas such as the investigation of buildings to for example derive specific parameters like height, area or volume from them (Vacca, Dessì and Sacco, 2017) or in combination with oblique imagery to reconstruct a quarries topography (Rossi et al., 2017).

3.1.3 Oblique View Photogrammetry

Oblique view photogrammetry is another type of photogrammetry and it sees its rise of use in the recent years (Rossi et al., 2017). It can also be found in literature or on the web by the synonyms “Oblique Airborne Photogrammetry” or “Oblique Aerial Imagery”. As the name implies, oblique view photogrammetry is concerned with capturing imagery of terrestrial phenomena from an oblique perspective of the lens. The direction and the angle in which the examined phenomenon is viewed can be varied at will. Oblique view photogrammetry is used for many different practices. It is deployed for road land updating, parcel boundary determination or monitoring of mass events to name a few examples (Remondino and Gerke, 2015). Due to its rise of application in the recent years, it is also more often combined with nadir photogrammetry. Their combination is summarized by the term “multi-view photogrammetry”. It is especially useful to obtain images from multiple different directions and angles onto an object and thus give the opportunity to create high-detail 3D models such as the structure of a quarry (Rossi et al., 2017).

3.2 Applied Technologies and Methods

This chapter deals with the technologies and methods used in the research project. The utilized UAV and its components, the multi-camera system and the applied processes and methods for data modelling are described.

3.2.1 Unmanned Aerial System

The unmanned aerial system used to record the airborne image data consists of a UAV and a multi-camera system mounted on it. The utilized UAV is a modified Leica AX20. The detailed technical characteristics of the UAV are: its dimensions are 1.67 x 1.52 x 0.76 m (propellers, frame arms and GPS mount unfolded), it weighs 9.1 kg, has a maximum payload capacity of 6 kg, it can reach a flight speed up to 64.8 km/h (18 m/s), and a vertical flying accuracy of 0.5 m and a horizontal flight accuracy of 1.5m along the predefined route (Leica, 2018).
It consists of several hardware components which enable a precise flight and data acquisition. The hardware of this UAV consists of a hexacopter frame with six frame arms and six propellers, an autopilot system, wireless communication equipment, a handheld tablet and payload. The hexacopter frame is the housing that contains other hardware components such as the autopilot system, batteries and communication ports. The six propellers are located on the outside of the six frame arms, which run away from the main part of the housing. The name "Hexacopter" also comes

from these propellers and they are used for the propulsion. The autopilot system is one of the core parts of the UAV for an autonomous flight operation. It is composed of a board computer, a global navigation satellite system (GNSS) receiver, an inertial measurement unit (IMU), barometric altimeter, airspeed indicator and flying control software. The GNSS receiver is based on the Leica SmartCheck and Leica RTKplus GNSS technology to determine the location of the UAV. This component uses GNSS and Real Time Kinematic (RTK) technology to calculate the exact x- and y-coordinates of the UAV's position. The barometric altimeter determines the z-coordinate which is the current flight height above sea level of the drone. The IMU determines the spatial position of the UAV in space. It constantly records the three angles roll, pitch and yaw. Roll defines the UAV's tilt along its x-axis, pitch the tilt along its y-axis and yaw the rotational change of the vertical axis of the mounted optical system (Philpot and Philipson, 2012). Furthermore, the autopilot system is able to identify the flight speed with the build-in airspeed indicator. All these autopilot system components enable the UAV to constantly calculate its spatial position and thus by comparing it to a predefined route to autonomously fly along a predefined flight plan, which is stored in the board computer. The wireless communication system is an AR20 remote control. It enables control and communication with the UAV up to 5 km distance from the operator. The handheld tablet is an AC20 tablet with multi-touch display. It used to monitor the current flight position of the UAV and to take control of the drone in emergency situations. (Leica, 2018)

3.2.2 Multi-Camera System

Besides the UAV, the multi-camera system is another essential part for the data acquisition process to generate the low-altitude aerial images. The multi-camera system is a novel in-house constructed pentacam. It is used as the payload of the UAV during the flight missions and is composed of two major parts: five Sony ILCE-QX1 cameras and a multi-axis housing in which the cameras are mounted. This camera configuration is called Maltese cross configuration (Remondino and Gerke, 2015), since one nadir and four tilted cameras are used. Relevant technical specifications of the Sony ILCE-QX1 camera are: it has 20.1 megapixels, an APS-C type sensor with a width of 23.2mm and height of 15.4mm, a lens focal length of 35mm and a focal length multiplier of 1.5. The resolution of large images is 5456 x 3631 pixels (Sony, 2019). Part A) of Figure 10 illustrates the structure of the pentacam housing in form of a sketch. It displays the Maltese cross configuration in form of a cross-shaped cassis illustrated as thick black line and the five cameras which are fixed in the housing in red color. The camera in the middle of the housing is the nadir camera (N), which is facing the ground at a 90-degree angle (bird's eye view). The other outward facing cameras are the front (F), aft (A), starboard (S) and port (P) oblique cameras. Once the pentacam is mounted on the UAV and a flight

mission is started, the cameras will trigger and create an image every two seconds. Consequently, each single trigger event can be assigned five images. Each of those images from a trigger event covers a specific area on the ground, called footprint. Part B) of Figure 10 shows five footprints of a single trigger event from a flight mission. The yellow colored polygon in the middle is the actual ground which is covered by an image of the nadir camera. The other polygons are the footprints of the respective oblique cameras. Another example of footprints from an image dataset recorded by the pentacam is displayed in Figure 11. In detail, Figure 11 illustrates footprints of images from a pentacam image dataset, which overlap with a small test area in the center of the vineyard. Such a map can be used to examine the area coverage of the images of the individual cameras, to compare them and if necessary to adjust the pentacam setup for the next flight mission.

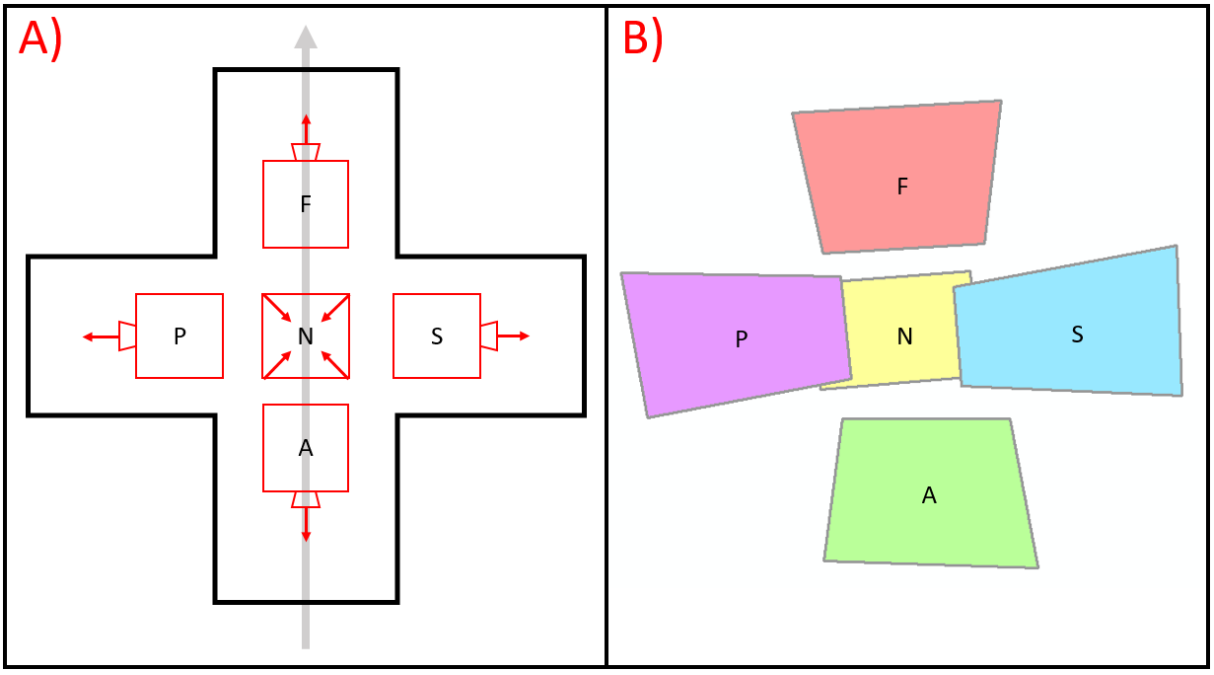

Figure 10. Sketch of the pentacam and image footprints from a single trigger event

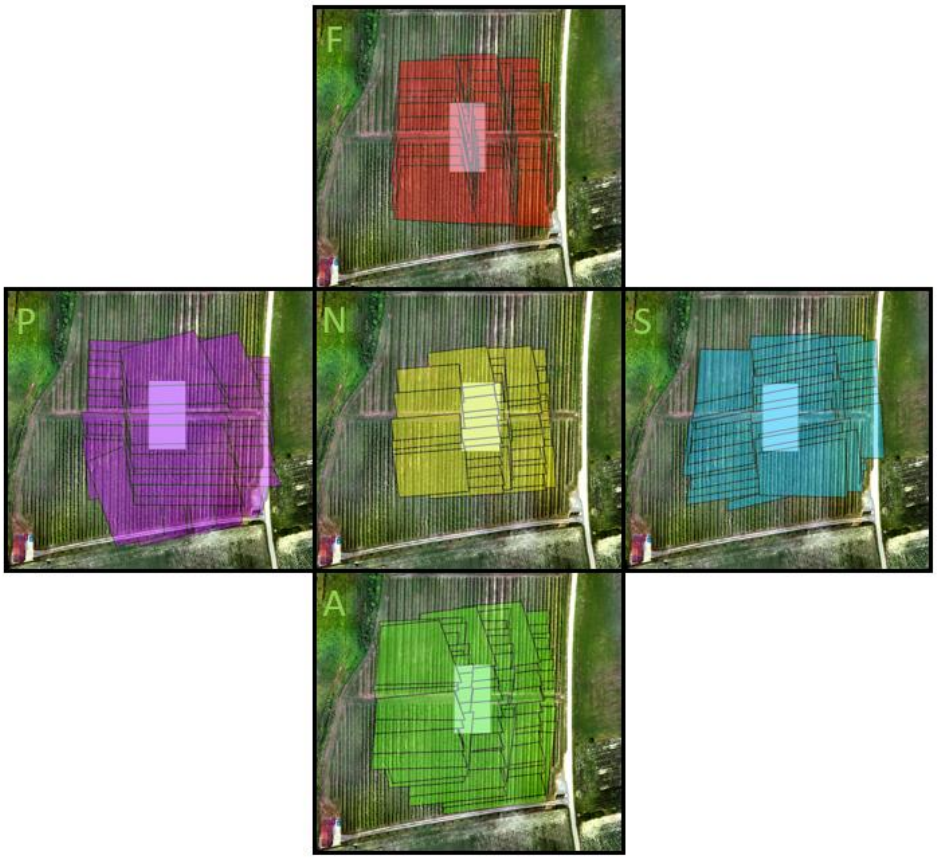

Figure 11: Footprints of images intersecting with a test area in the study vineyard

3.2.3 Applied Technologies and Methods

This chapter is concerned with the general description of the most important methods and algorithms for 3D modeling used in this research project. The 3D modelling of vines in this thesis are based on the automated 3D scene reconstruction. This form of 3D modelling is a common method for the analysis of three-dimensional structures on the earth's surface. Today such 3D models are used for a wide range of applications. Among others, they are used for the analysis of geomorphological processes such as erosion and mass movement (James and Robson, 2012), damage assessment of buildings (Murtiyoso et al., 2014) or the investigation of quarries (Rossi et al., 2017). In order to create high-resolution 3D models of objects or scenes in the study area, such as vines or the vineyard, this project uses automated 3D scene reconstruction based on structure-from-motion multi-view stereo (SFM-MVS) techniques. Structure-from-motion (SFM) techniques enable the estimation of the camera's position and internal orientation and the generation of 3D scene structures in form of point clouds by identifying features in overlapping images taken from multiple viewpoints (Lee, Huang and Lin, 2012; Zhang et al., 2016). Multi-view stereo (MVS) methods facilitate the refinement and improvement of these point clouds (Gómez-Gutiérrez et al., 2014) and the reconstruction of a 3D digital mesh (James and Robson, 2012; Morgenroth and Gomez, 2014).

The applied automated 3D scene reconstruction with SFM-MVS techniques is a complex photogrammetric workflow consisting of many processes (Zhang et al., 2016). Commonly used methods in this procedure are image matching based on features detection in overlapping images using SFM techniques, georeferencing and scaling of the model, estimating and refining camera model parameters using bundle adjustment, refining the point cloud using MVS algorithms and generating high quality 3D models based on the refined point cloud (Zhang et al., 2016; Gómez-Gutiérrez et al., 2014; Lee, Huang and Lin, 2012; Zhang, Xiong and Hao, 2011).

One of the first steps of 3D scene reconstruction is the so-called image matching process. It is an essential process for solving problems in computer vision. Furthermore, it is also a requirement for subsequent steps such as bundle adjustment or creation of the 3D models. This method uses SFM-MVS techniques to determine the image overlap and relative rotation angle between neighboring images, to match all images, and to extract feature points to create a point cloud. In the matching step, two images are compared with each other and each feature in one image is compared with all features located within a Euclidean radius between feature vectors around that feature in the other image. Then, the feature points are extracted from the images to create a first point cloud. A refinement algorithm is applied to refine the point cloud in such a way that it only includes feature points showing the strongest interest value (Zhang, Xiong and Hao, 2011). This results in a point cloud consisting of millions of tie points from the overlapping images (Zhang et al., 2016).

The created point cloud often requires a subsequent georeferencing and scaling step using ground control points (GCP). It is a necessary process as the point cloud created by the SFM-MVS techniques in image matching are aspatial. Thus, it has no “absolute geographic position or scale”. One possibility to georeference and scale the point cloud is to add ground control points with known coordinates to the matched images (Morgenroth and Gomez, 2014). For this purpose, the coordinates of the GCPs are often measured in an in-situ survey and then determined on the corresponding matched images using markers.

Another frequently applied process of 3D scene reconstruction is the optimization of camera parameters and tie points coordinates. Since the utilized digital cameras are often non-metric, their internal parameters such as the interior orientation alter as time goes on. As a result, unavoidable deviations occur between the camera parameters estimated by the program and those of the data acquisition process. Since these camera parameters are also used to match the images and to generate the tie point cloud, the deviation also affects the coordinates of the matched points. Thus, an optimization process such as bundle adjustment is necessary (Zhang, Xiong and Hao, 2011). Bundle adjustment is a method which iteratively adapts the orientation and position parameters of the cameras (Mouragnon et al., 2006). The method uses the tie points and the GCPs which are

referenced on the matched images. The known overlap values based on the tie points can be used to estimate their original position and coordinates. Using the optimized tie point positions and reassessing the camera orientation can lead to improved estimated camera orientation parameters (Zhang, Xiong and Hao, 2011).

In a further step, a dense point cloud and a 3D model (Agisoft Metashape User Manual, 2019; USGS National UAS Project Office, 2017) can be generated by applying SFM-MVS techniques. The dense point cloud is created on basis of the tie point cloud (Zhang et al., 2016). Thus, tie point information are used by SFM-MVS techniques such as dense image matching and forward intersection (Zhang, Xiong and Hao, 2011) to generate a dense point cloud. Furthermore, SFM-MVS techniques can also be utilized to recreate a 3D model. The 3D model can be reconstructed in several forms. For example, it can be reconstructed in the form of a digital surface model (DSM) (Zhang, Xiong and Hao, 2011) or a triangulated irregular network (TIN) mesh (Zhang et al., 2016). A final step of the 3D scene reconstruction can be the closing of holes in the 3D model (Lee, Huang and Lin, 2012) by applying an interpolation algorithm.

3.3 Validation

This section deals with the explanation of the validation processes in which the results of the laboratory and field study are examined and validated. For this purpose, a validation step is performed with the generated data after the respective implementation processes in these studies. Various methods and tools such as statistical calculations or the ModelBuilder of the ArcGIS software are used for this purpose.

The first validation process is performed with the acquired data from the laboratory study. In this procedure, the digitally measured data from the dense point clouds and 3D models are compared with the manually measured data in a statistical analysis. In detail, the obtained information is utilized in the statistical analysis to calculate parameters of the grapes such as mean length and width, average and total weight or volume and to record them in a table. This table is then applied to compare the statistical values of the manual and digital measurements of the red and green grapes. The analysis is performed, among other things, to identify specific patterns and to analyze whether the values of the manually and digitally calculated volume of grapes are similar. A more detailed explanation of the validation process of the laboratory study is given in chapter 4.1.4 Statistical Analysis and Validation.

In the validation processes of the field study, the generated models such as dense point clouds and DSMs are compared. Among other things, the geometric accuracy and computational complexity of the models, local differences between the models and possible patterns such as phenological

changes of the vines are investigated and validated. The geometric accuracy of the reconstructed models is determined in a validation process by means of measured vertical and horizontal geometric accuracies. These are calculated with mean Root-Mean-Square-Error (RMSE) values of ground control points referenced in the models. The RMSE values are identified using the error values of the GCPs displayed in the reference pane in Metashape Pro. In addition, the GCP information saved in the reports generated by the "Export Reports" tool of Agisoft Metashape Pro are also utilized. The mean RMSE values of GCPs in x- and y-direction are used to estimate the vertical geometric accuracy of a model. The horizontal geometric accuracy is determined on basis of the average RMSE values in z-direction.

Furthermore, the computational complexity of the generated models is also investigated. For this purpose, the computing time of each step of the 3D modelling processes are recorded. Based on these processing times, the total computation time of a 3D scene reconstruction process is also determined. These values are then recorded in a table and the computational complexity of the individual models is compared with each other. A more detailed description of the validation process of the geometric accuracy and the computational complexity is given in chapter 4.2.3.4 Geometric Accuracy and Computational Complexity Measurements.

In another validation procedure, local differences between the reconstructed digital models are determined. A model created with the ArcGIS ModelBuilder is applied to calculate height difference datasets showing local height differences. The digital surface models, which are generated from the airborne image datasets, serve as input data. In the model, two DSMs are compared with each other at a time. In three steps, these DSMs are first cut to the shape of the vineyard, then brought to a uniform cell size and finally the older dataset is subtracted from the younger dataset. Thus, it is guaranteed that only areas of the vineyard are represented in the final map and that a height increase over time is represented as a positive value and a height loss as a negative value. As a result, a height difference map is generated in which the local height differences between the two input DSMs are displayed. The information obtained from the validation procedures, such as positive height differences between two height models at the locations of the vine rows, can be used, among other things, to draw conclusions about specific patterns in the vineyard like phenological changes of the vines.

3.4 Conceptual Model and Workflow

This chapter gives an overview of the whole workflow of the research project. A sketch of the conceptual model and workflow is illustrated in Figure 12. Figure 12 reveals that the project's workflow is divided into six major phases. It starts with an extensive literature and web-based review.

Literature Review

The literature review is executed in two steps, one dealing with the research of project-relevant key terms and the other with the identification of the state-of-the art approaches concerned with phenological data collection of vine and yield estimation in the vineyard. On the one hand, the review are conducted to understand the key phenological stages of vine and to determine factors that have an influence on vines in these stages. On the other hand, it is executed to analyze the state-of-the art approaches and to understand how those utilize photogrammetric methods to measure vine parameters and changes in morphological characteristics in a vineyard.

Planning Phase

The second phase of the research project is engaged with using the obtained information of the literature review to create matrixes and plans which help to plan the structure of the further thesis development. In this phase, a phenological characteristics matrix is created based on the acquired data of the phenological parameters of vines in their respective key phenological stages. A requirement analysis is performed to have information about specific requirements which need to be met to acquire high-resolution images from vines. Furthermore, the acquired information are used to construct a conceptual workflow model for the development of the multi-temporal phenological 3D model.

Laboratory Study

The third phase of the research project is the laboratory study. It is the first phase of the project implementation procedure and it is concerned with the conceptualization and principal design of a 3D grape model and derivation of parameters from it for yield prediction based on close range photogrammetric methods. The purpose of the laboratory study is to test the methodological approach under laboratory conditions. The laboratory experiment is also useful to recognize which requirements are needed for a bigger scaled in-field research at vineyard scale. The necessary data for the laboratory research is acquired by taking multidirectional images from single grapes using a camera equipped with an embedded GNSS sensor and IMU. These recorded images are then used to

derive photogrammetrically a high-density 3D point cloud of the simulated grapes. 3D point cloud classification methods are applied to identify grapes and volume calculations are performed for validation. These experiments provide the basis for the design and implementation of the field research at vineyard scale.

Quantitative Comparison of Nadir and Oblique View Imagery

The second phase of the implementation process deals with the quantitative comparison of nadir and oblique view images and is conducted at the University of New Mexico (UNM). Firstly, a data collection process is executed in which a multi-rotor UAV with an attached multi-camera system are applied to survey the study vineyard. This data acquisition flight is used to generate a low-altitude aerial image dataset containing images of a nadir and four oblique cameras. Then, the obtained image data is used to create 11 models representing various combinations of the cameras. In a subsequent data modelling procedure, a high-density 3D point cloud and DSM is created for all 11 models. These results are subjected to a quantitative comparison.

3D Modelling of and Change Detection of Phenology of Vine

The third and final phase of the project implementation is concerned with iterative sensor-based in-field photogrammetric measurements and the following data modelling and data processing for various phenological stages of vine. At the beginning, flight planning is done to schedule the survey flights, examine the structure of the test area and weather conditions. Then the data collection is executed to acquire the necessary aerial image data which contains phenotypical information of vines in their key phenological stages from the test vineyard. Therefore, multi-directional oblique view photogrammetry is used to acquire airborne data on vineyard-scale by utilizing a multi-rotor UAS equipped with a novel multi-camera system from the air.

Next, an extensive data modelling process deals with the development of a multi-temporal phenological 3D model of vine and the deployment of photogrammetric methods to detect changes of phenology of vine in the generated 3D model. The applied data modelling workflow is conducted for several airborne image datasets containing information about the vines in different phenological stages. In this process, high-density 3D point clouds and DSMs of the vineyard are created from each dataset used. As a result, a multi-temporal 3D model of vine is obtained, which consists of several models showing the vines of the study vineyard in different phenological key stages. Then, photogrammetric methods are applied to detect changes in phenology of vine in the generated 3D point clouds and digital surface models.

Evaluation and Validation

The final phase of the research project deals with the evaluation and validation of the results. The validation of the results is achieved through the comparison of RMSE values and difference calculations between the generated DSMs. With the help of the resulting difference values, phenological changes in the vineyard can be identified. Finally, an evaluation process is executed to analyze and critically assess the created multi-temporal phenological 3D model and identified phenological change detection. Furthermore, the results are discussed with viticulture experts.

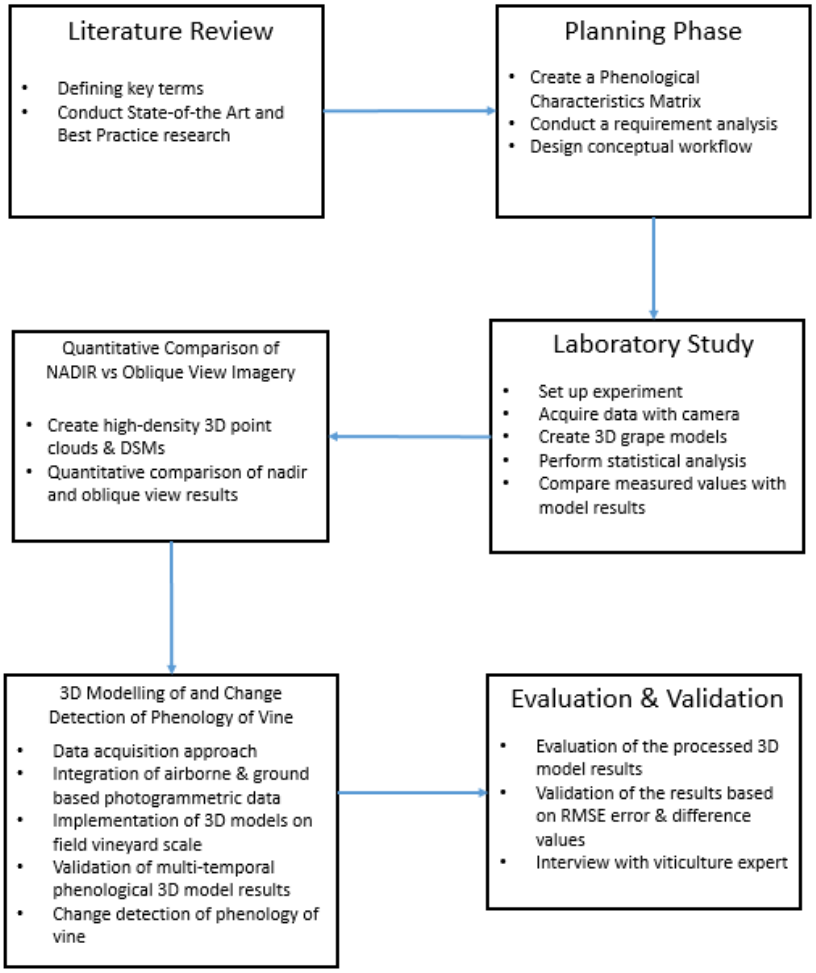

Figure 12: Conceptual workflow model

4. Project Implementation

The third phase of the research project is the implementation process. The implementation focuses on the generation of 3D models of scenes and objects of the study vineyard and the development of a multi-temporal phenological 3D model of vine. The implementation process is divided into two phases: a laboratory study and a field study. The laboratory study is discussed in the following chapter and the field study is explained in section 4.2 Field Study.

4.1 Laboratory Study

The laboratory study is the first part of the implementation phase of this research project. The laboratory experiment is concerned with the conceptualization and principal design of 3D grape models and the derivation of parameters from them for yield prediction based on close range photogrammetric methods. The laboratory study serves two purposes. On the one hand, it is executed to test how well empirical measurements can be transferred to model measurements. On the other hand, it is utilized to find out which setup and image resolution is needed to create high precision 3D models of grapes and how detailed the generated 3D high-density point clouds of grapes need to be to detect the shapes of grapes with a shape detection tool. Furthermore, the laboratory experiment is also useful to recognize which requirements are needed for a bigger scaled in-field research at vineyard scale.

In general, the laboratory study is separated into four parts: the laboratory setup, a data capture process, the multi-view 3D photogrammetric analysis and last but not least, a statistical analysis and validation procedure. The setup phase focuses on identifying requirements and preparing the equipment, which are needed to successfully execute the laboratory experiment and the construction of the experimental setup. The data capture phase deals on the one hand with the acquisition of multi-view image dataset and on the other hand with the manual measurement of grape parameters such as width, length and weight. The multi-view 3D photogrammetric analysis is concerned with the modelling of the captured image data to generate 3D models of the surveyed grapes. Finally, the quality of the created 3D models is analyzed and the manually and digitally measured values are statistically evaluated and compared. These experiments provide the basis for the design and implementation of the field research at vineyard scale.

4.1.1 Laboratory Setup

As explained in the introduction part of the laboratory study, the laboratory setup focuses on identifying the requirements for the deployment of the experiment and the actual setup of it. The experiment planning and setup consists mainly of smaller tasks, which need to be fulfilled to ensure that the laboratory study is carried out successfully. Therefore, at first all the necessary equipment is gathered. Things, which are needed for the experiment, are commercially available green and red grapes, a camera, a tripod, flasher, bars, strings, a scale, a caliper rule and a paper containing a table. The used camera is a Sony Alpha 7r3 with 42.4 megapixels, a sensor size of 35.9 times 24.0 and a pixel dimension of 7953 pixels (px) times 5304 px. The camera is also equipped with a GNSS sensor and an IMU to get the position and the angle of the images in which they are taken (Sony, 2018). Furthermore, for taking the images, a wide-angle lens is used and the focus length of the camera is set to 90mm and the aperture to 22. The scale is a commercially available exemplar and can measure the weight of the grapes up to one gram. The paper containing the table is needed to record the manually measurements which are done after the image acquisition.
Following the acquisition of all essential parts for the experiment, the experiment construction is setup. Therefore, a framework consisting of three bars is constructed. One bar is fixed onto the two others. Next, the grapes are attached with a piece of string and tape in the middle of the fixed bar. The grapes are attached in such a way that they can be rotated. Hence, it is only necessary to rotate the grapes and the camera does not have to be moved from the spot. Then, the camera is mounted onto a tripod in front of the grapes. The distance from the camera to the grapes is 1 meter. The final setup of the laboratory experiment is displayed in Figure 13 and Figure 14 whereas Figure 13 shows the construction from the back and Figure 14 shows it from the front.

Figure 13: Experiment setup viewed from back

Figure 14: Experiment setup viewed from ahead

4.1.2 Data Capture

Once the setup of the laboratory study is finished, the next phase can be started. It focuses on data capture and consists of two parts. At first, the image dataset needed for the multi-view 3D photogrammetric analysis is obtained by taking multidirectional images from single grapes using the Sony Alpha 7r3. After the image acquisition, the manual measurement of the grapes is executed to record parameters such as size and weight of the grapes which are used in the validation process.

4.1.2.1 Close Range Multi-Directional Image Capturing

The first task, after setting up the construction for the experiment, is the image capturing process. It is executed in two equally structured phases whereas the first focuses on the green grapes and the second phase is concerned with the red grapes. In both phases, close range photogrammetry is applied to take high-precision images from the grapes. Furthermore, photos from multiple direction are taken of the grapes since those are mounted onto the construction in such a way that they can be rotated. After taking a picture of the grapes from a specific position, they are rotated a bit and then the next image is captured. This is repeated until one whole rotation of the grapes is completed. After completing a whole rotation, the angle of the camera facing the grapes is changed. Then, the camera is either facing upwards or downwards onto the grapes. This is done to capture images from the grapes from different angles. Following, again images from a whole rotation of the grapes are taken. When a phase is completed, photos of the grapes from multiple angles and directions were made, without the necessity to move the vertical position of the camera to the grapes. An image of

the horizontal positions of the camera facing the grapes during the image acquisition is illustrated in Figure 15.

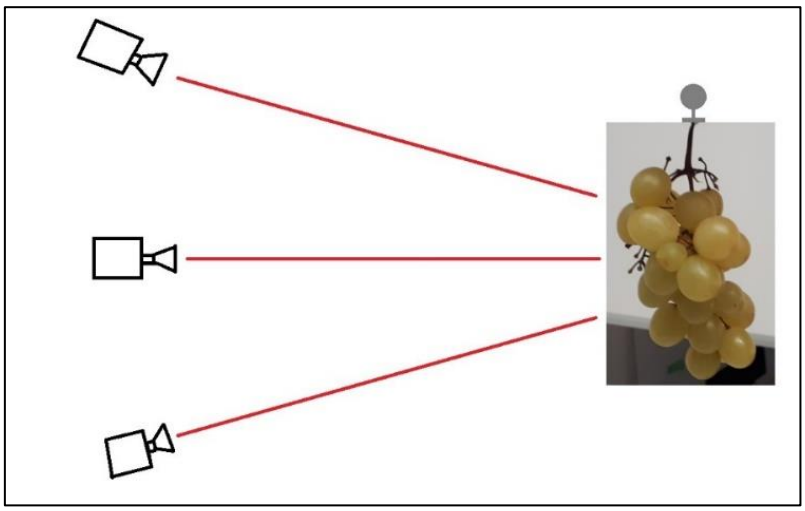

Figure 15: Different horizontal camera positions

4.1.2.2 Manual Measurements of Phenological Features

After finishing the image capturing process, the next measurement task starts. This phase of the laboratory study is concerned with the manual measurements of bunch and single grape features such as length, width and weight. Equipment, which is used for the manual measurements of those characteristics, are a caliper rule, a scale and a paper containing a chart. The setup of the manual measurements is displayed in Figure 16 and Figure 17. Figure 16 shows the setup of the green grape measurements and Figure 17 depicts the manual measurement of the red grapes.

Figure 16: Manual measurements of green grapes

Figure 17: Manual measurements of red grapes

Firstly, the total weight, length and width of the bunch with the stems is measured and noted. Following, the grapes are picked from the bunch, counted and the number of grapes of the green and red bunch are then recorded. After removing all grapes from the bunches, the total weight of the grapes without the stems is measured. Next, the length, width and weight of all single green and red grapes are quantified and noted. The length of a grape is recorded by measuring the line, which goes from the point where stem is connected with the grape to the opposite side of the grape. The measured length of a grape is usually longer than its width since grapes are often elliptical. Figure 18 displays an image how the length and width is defined. Once all manual measurements of the grapes are done, the next phase can be started.

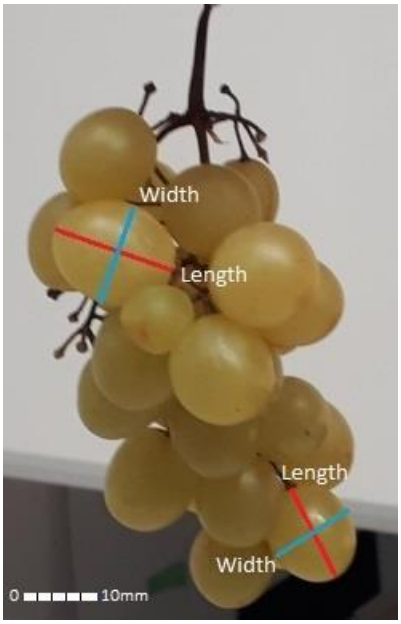

Figure 18: Length and width of grapes

4.1.3 Multi-View 3D Photogrammetric Analysis

In this phase, a multi-step process is performed to create 3D models of the grapes based on the captured multi-view image data and to acquire yield relevant data. The recorded images are used to derive photogrammetrically high-density 3D point clouds of the simulated grapes. Following, these point clouds are meshed to a 3D model of the grapes. Then, the RANSAC shape detection plugin of the program CloudCompare (CC) is applied to test how well single grapes can be identified from the generated 3D models. Finally, information about parameters are taken from these shapes to make a statistical analysis and to calculate the volume, which is needed for the validation of the measurements.

4.1.3.1 3D Model Creation

The next phase focuses on the creation of the digital 3D models of the green and red bunches. Firstly, the captured images need to be transferred from the internal storage of the camera onto a drive of a computer. When the grape photos are saved, the 3D model creation can be started. Therefor, the program Agisoft Photoscan Professional 1.4.3 (build 6529) is used (Agisoft, 2019 a). In a first step, the captured images need to be added to the workspace of the program. To do so, the option “Add Photos” in the tab “Workflow” is clicked and a selection window opens. Then, the saved images can be selected in the selection window and by pressing the button “OK”, they are loaded into the program. Optionally, the images can also be selected in the folder they are saved in and loaded into Agisoft Photoscan via the drag and drop function. The red rectangle displayed in Figure 19 highlights where the “Add Photos” option can be found in Agisoft Photoscan.

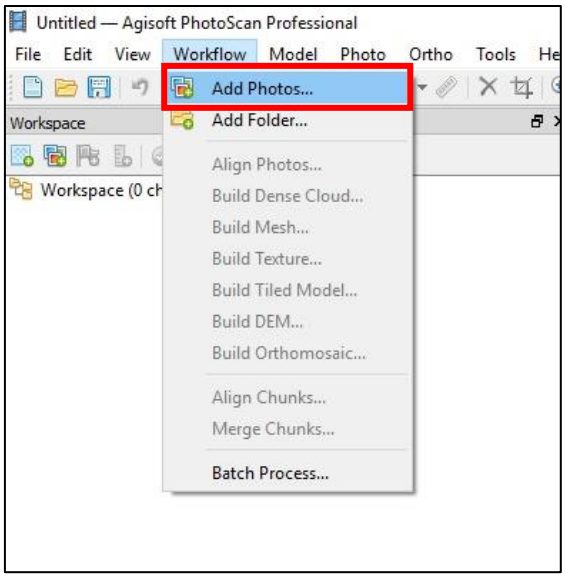

Figure 19: Adding images to Agisoft Photoscan

After the images finished loading into the program, the masking of the images is started. Creating a mask on an image is useful because it can make the resulting 3D model more precise. Masks on images restrict the program is such a way that is will only use unmasked parts of images for the calculation of point clouds and 3D models. To create a mask on an image several different options can be used. In case of this research project the option “Magic Wand” from the tab “Photo” is used. This tool makes masking on images with big homogenous pixels areas quite easy as it selects all neighboring pixels of an area with the same hue. The location where the tool is located and an example how masking can be done is shown in Figure 20. It needs to be mentioned that the 3D model creation has also been tested with unmasked images. Although those 3D models were also very precise, some of them were showing unnatural white streaks. Therefore, it was decided that the final 3D models will be created based on self-masked images.

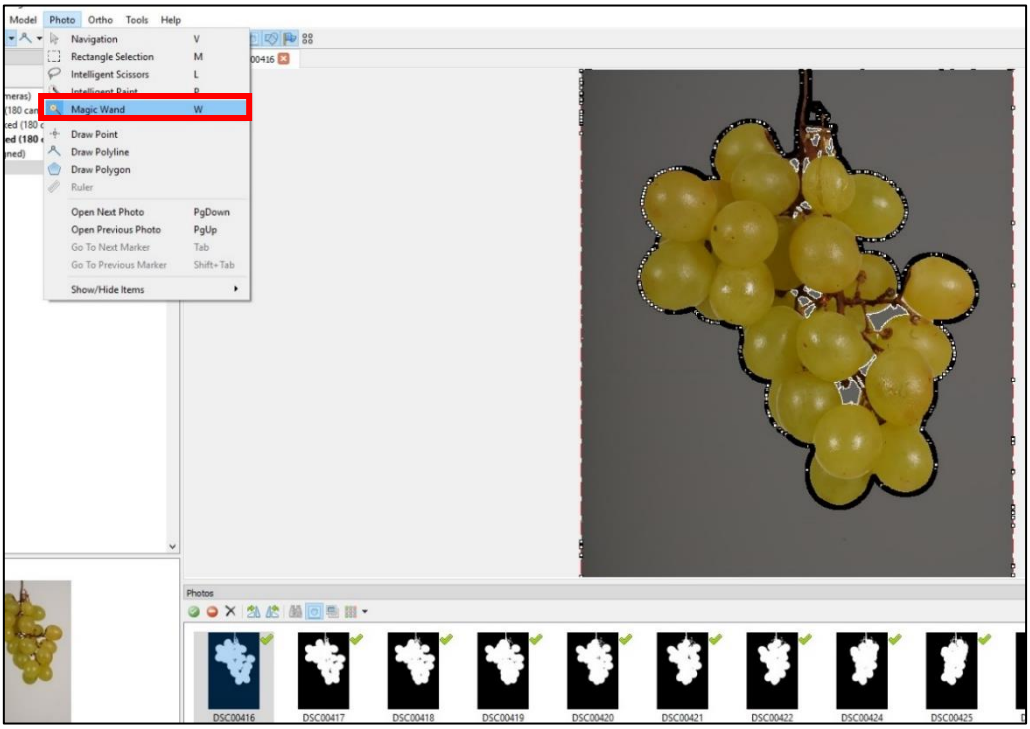

Figure 20: Image masking with “Magic Wand” tool

When all needed images are masked, they can be aligned. Therefor, the tool “Align Photos” from the tab “Workflow” is used. By clicking on the option “Align Photos”, a small window is opened where the accuracy of the calculation process can be chosen. Then, by pressing the “OK” button the calculation processes is started. After the program finished calculating, a sparse point cloud is added to the workspace. Figure 21 displays the settings, which were used for the creation of the final 3D model of this research project and an example how such a sparse point cloud of grapes can look like.

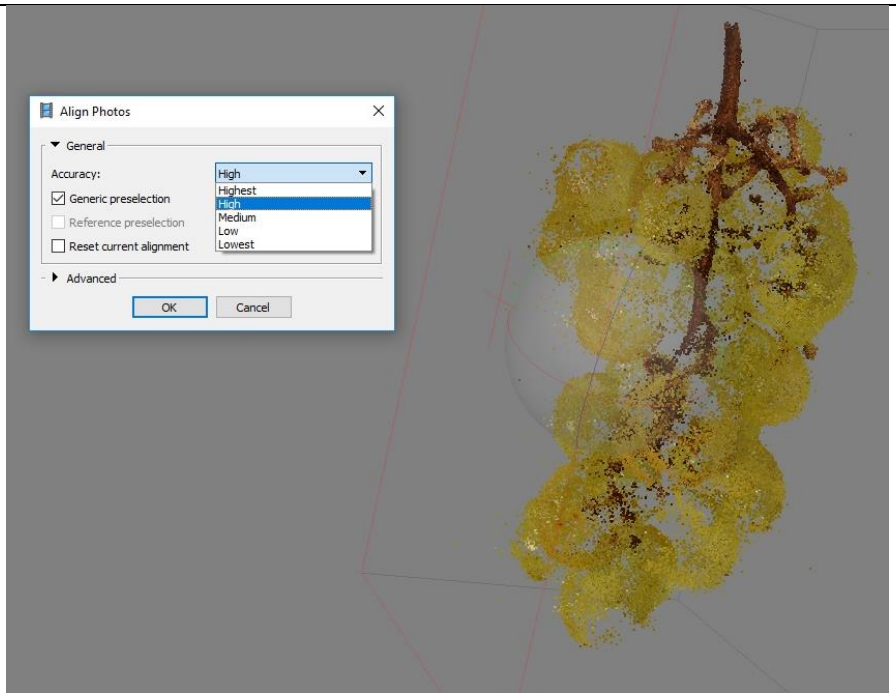

Figure 21: Settings of image alignment

The next step is concerned with the generation of a dense point cloud. To do so, the tool “Build Dense Cloud” is utilized. The link to this tool is located in the tab “Workflow” beneath “Align Photos”. When the option is clicked, the settings window of the tool appears. The chosen settings for the final 3D models and an example of a dense point cloud of the green grapes is shown in Figure 22.

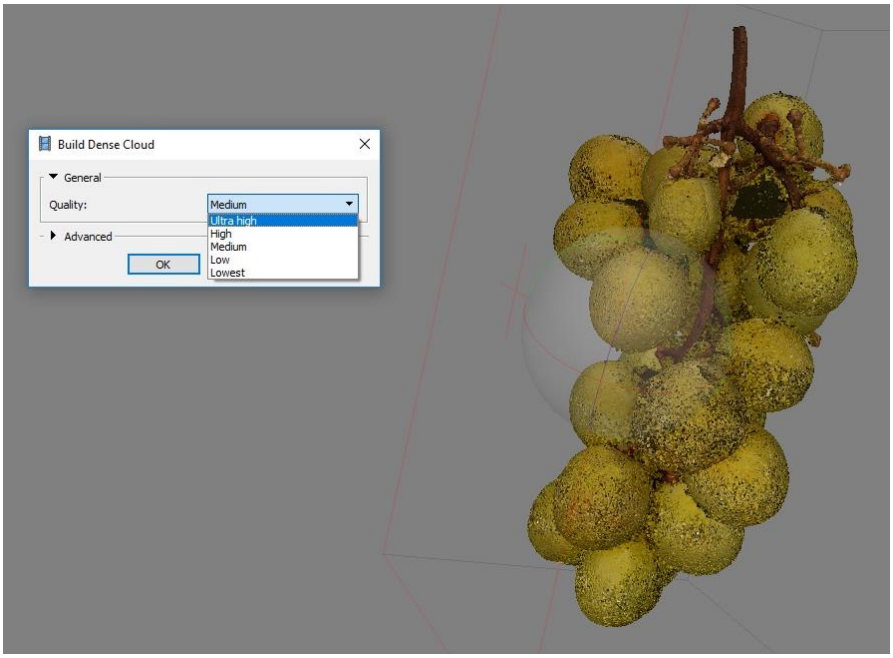

Figure 22: Building dense cloud from sparse point cloud

After the dense point cloud is created, the next tool can be executed. In this step the tool “Build Mesh” is applied to generate the mesh of the 3D model. The settings window of the tool can be accessed by clicking on the option “Build Mesh” in the “Workflow” tab. Figure 23 displays the selected setting and the mesh of the 3D green grape model.

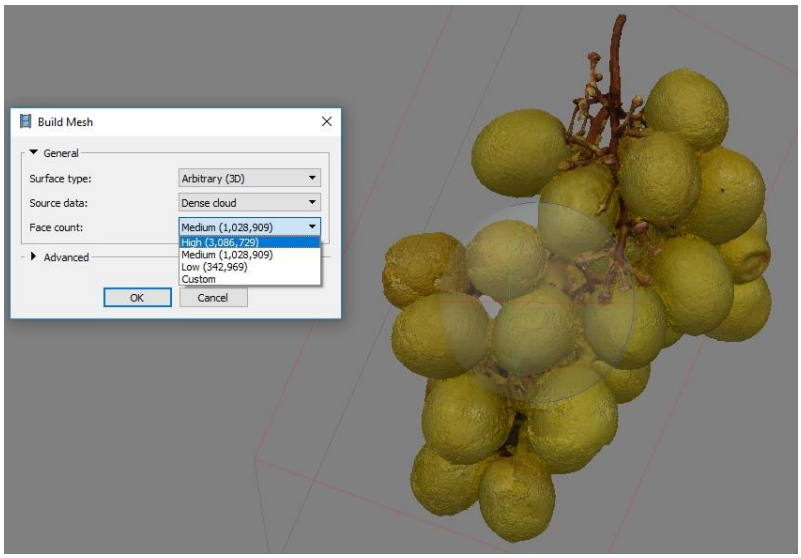

Figure 23: Creating mesh from dense point cloud

The next process focuses on adding a texture onto the previously created mesh. Therefor, the tool “Build Texture” is deployed, which can be found in the tab “Workflow”. When the link is clicked, the settings window of the tool opens. In the settings window, for blending mode the option “Generic” is selected from the dropdown box next to it and the default setting “Mosaic (default)” of blending mode is kept. Then the “OK” button is pressed and the program starts calculating. When the tool finished calculating, the textures are added onto the mesh of the 3D model. Figure 24 illustrates the settings which were chosen for the final 3D models and the result of the tool calculation.

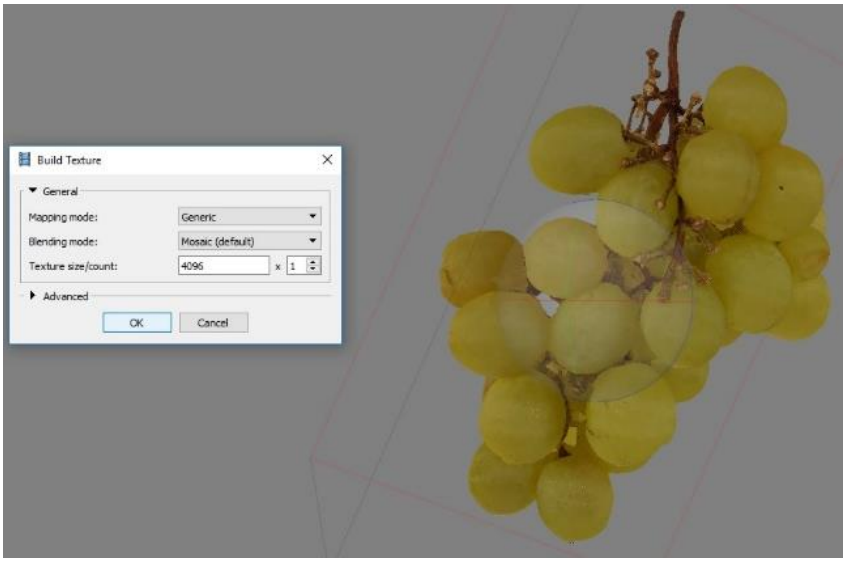

Figure 24: Settings of the texturing tool

Figure 25 shows the final 3D model of the surveyed green grapes. The 3D model of the red grapes is displayed in Figure 26. Overall, the generated 3D grapes models are very precise since among other things, the whole stems are shown in high detail and even small hairs can be seen on the modelled grapes. Additionally, even most of the small ends of the stems are precisely modelled although their diameter is in the single digit millimeter part. It should be noted that the creation of the 3D models of grapes underwent a lot of changes in choosing the right settings of the tools. In the end, the best settings for the created 3D grape models are a high accuracy for aligning the images, an ultra-high accuracy for building the dense point cloud and a high accuracy for building the mesh.

Figure 25: Final 3D model of the green grapes

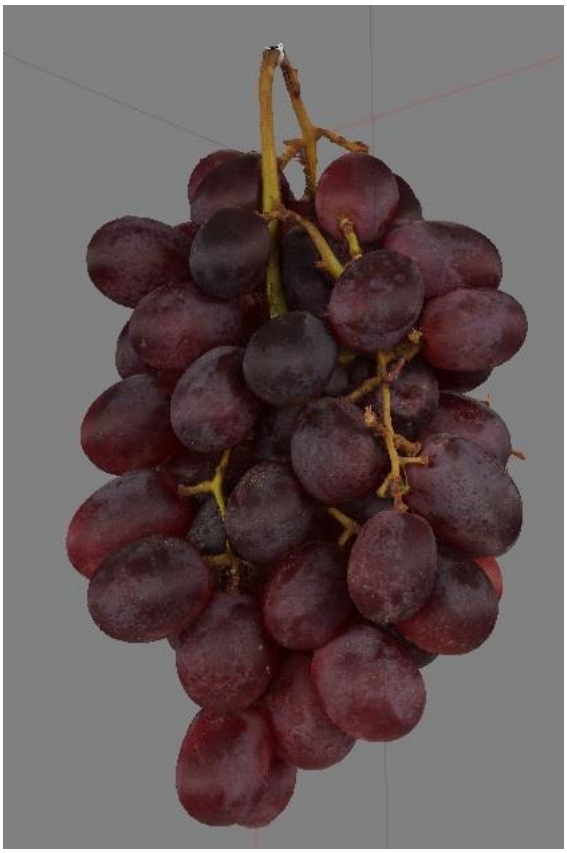

Figure 26: Final 3D model of the red grapes

4.1.3.2 Shape Detection in the 3D model

Since the final 3D models are finished, the next step can be started. It is concerned with the automatic identification of single structures such as single grapes on the created 3D grape models. Therefor, the RANSAC shape detection plugin of the program CloudCompare is applied on the final 3D models. However, before starting this process the 3D models first need to be exported from the software Agisoft Photoscan and imported into CC. To do so, the correct folder needs to be selected in

the workspace of Agisoft where the created 3D models are located and then the “Export Model” window opened. Figure 27 displays where the “Export Model” window can be found and opened. Once, the option “Export model” is clicked, a new window opens. In this window, the file in which the model is saved can be given a name and a fitting file type needs to be selected. In case of this research project the file type “wavefront OBJ” with the extension “.obj” is always used for transferring the 3D models between the programs Agisoft Photoscan and CC. Figure 28 gives an example how such a file can be named and where the file type is selected. After pressing the “OK” button, the “Export Model – Wavefront OBJ” window opens. There several settings such as the file type for the texture of the 3D model need to be selected. Figure 29 illustrates which settings were chosen for the 3D models of this master thesis. Then, by pressing the “OK” button, the 3D models are exported and saved in files.

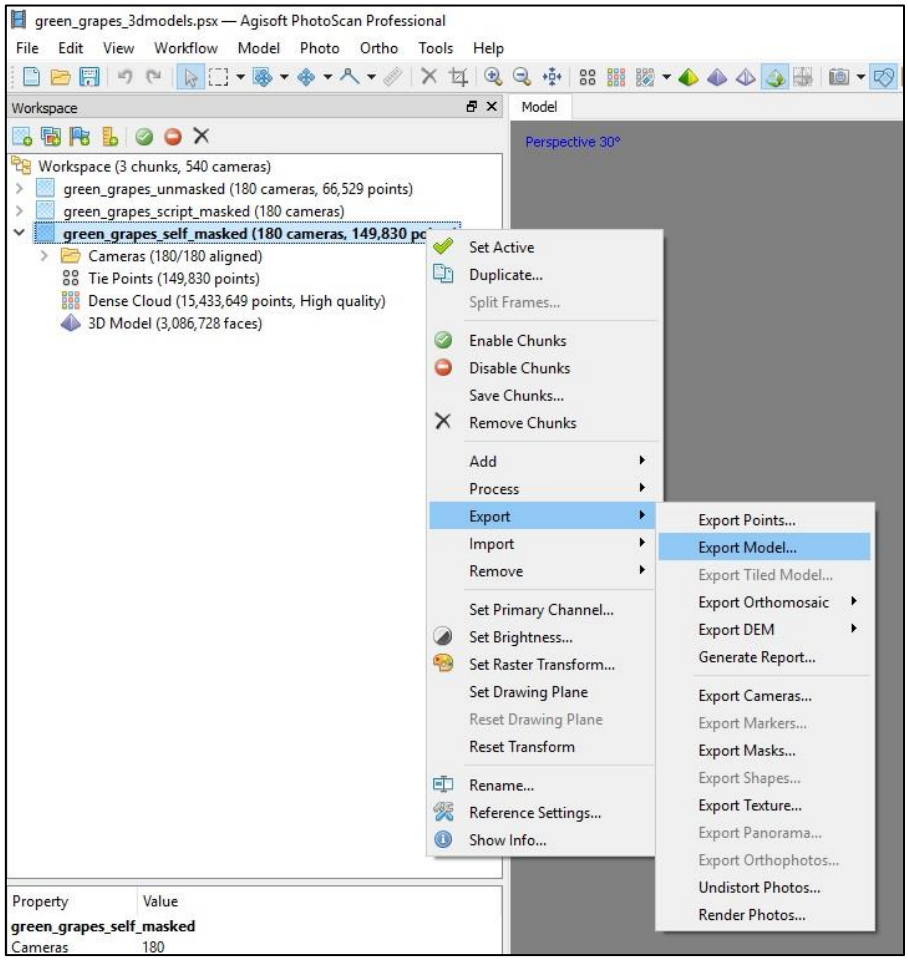

Figure 27: Opening the export model window

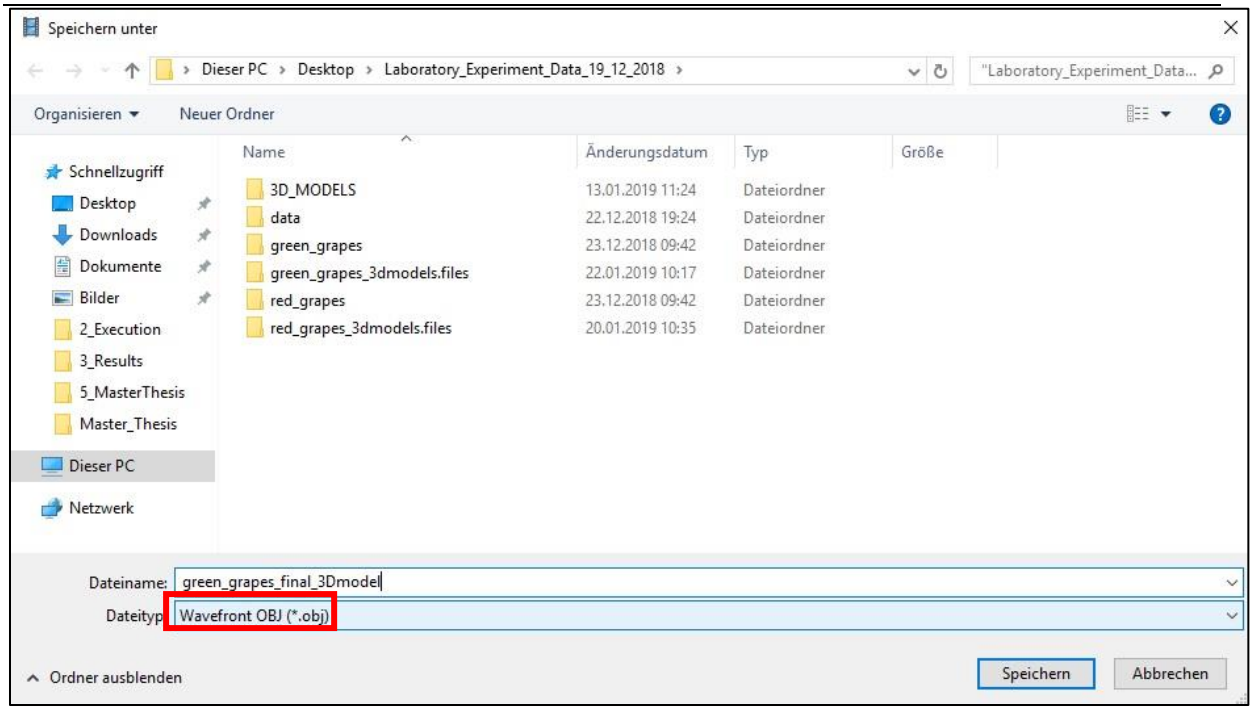

Figure 28: Naming the file and selecting a fitting file type

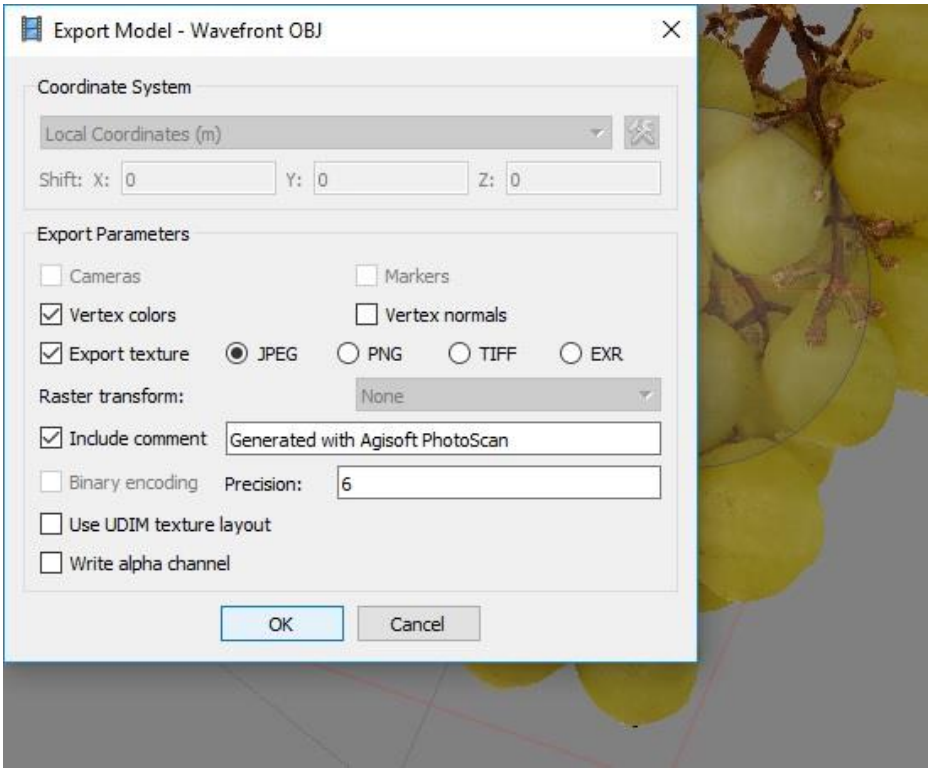

Figure 29: Exporting the 3D model as wavefront object (.obj)

Now the program CloudCompare can be opened and the exported 3D models imported into CC. In this research project, the CC version v2.10-alpha [64-bit] is used (CloudCompare, 2019). After opening CC, the window to import the 3D models can be accessed by clicking on the tab “File” and the option “Open”. Following, a window called “Open file(s)” appears. In this window, the correct type of the 3D model file needs to be selected. Then, the file of the 3D model with the appropriate file type has to be picked. After everything is correctly setup and the “Open” button is clicked, the 3D model is loaded into CC. Figure 30 shows how the final 3D models of this project are imported into CC.

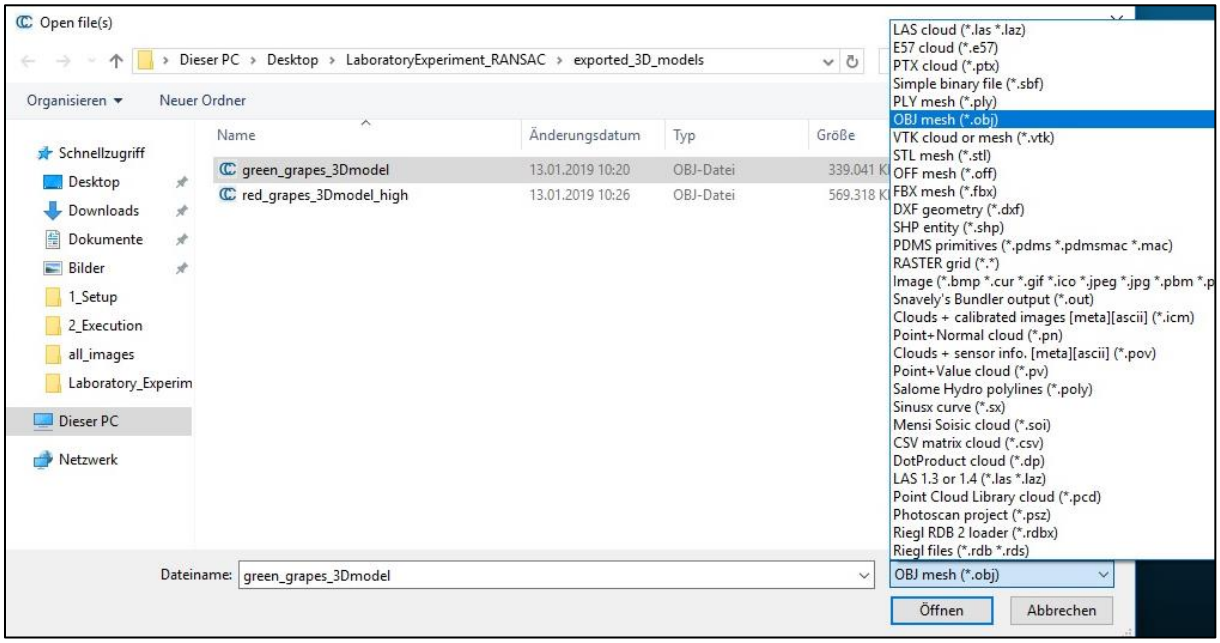

Figure 30: Importing the 3D model into CC

When the program has finished loading the 3D models, they are displayed on screen. However, before being able to use the shape detection tool, a sample point cloud needs to be created from the imported 3D grape models. Therefor, the tool “Sample Points” is applied. It can be accessed via the tab “Edit” in the menu “Mesh”. In the opened “Points Sampling on mesh” window the amount of points that should be sampled can be stated. After pressing the “OK” button a sample point cloud is created and added to the current working session. The point sampling settings for this research project are illustrated in Figure 31.

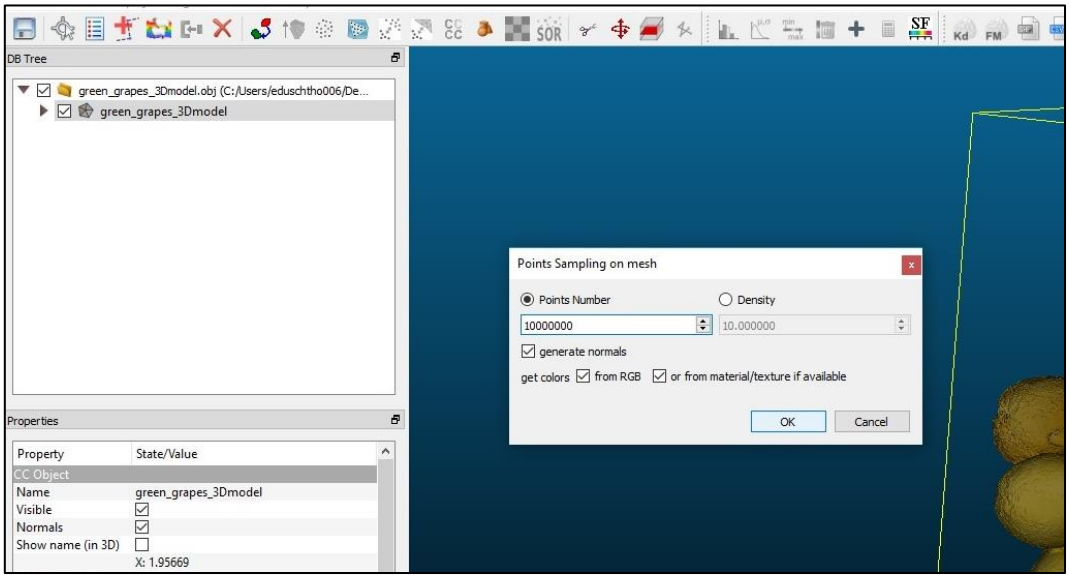

Figure 31: Sampling points from the 3D model

Once the sample point cloud is created and selected, the shape detection tool can be accessed and opened. The tool is called “RANSAC Shape Detection” and can be found in the tab “Plugins”. Figure 32 displays where the link to the tool is located. When the link is clicked, the “Ransac Shape Detection” window appears.

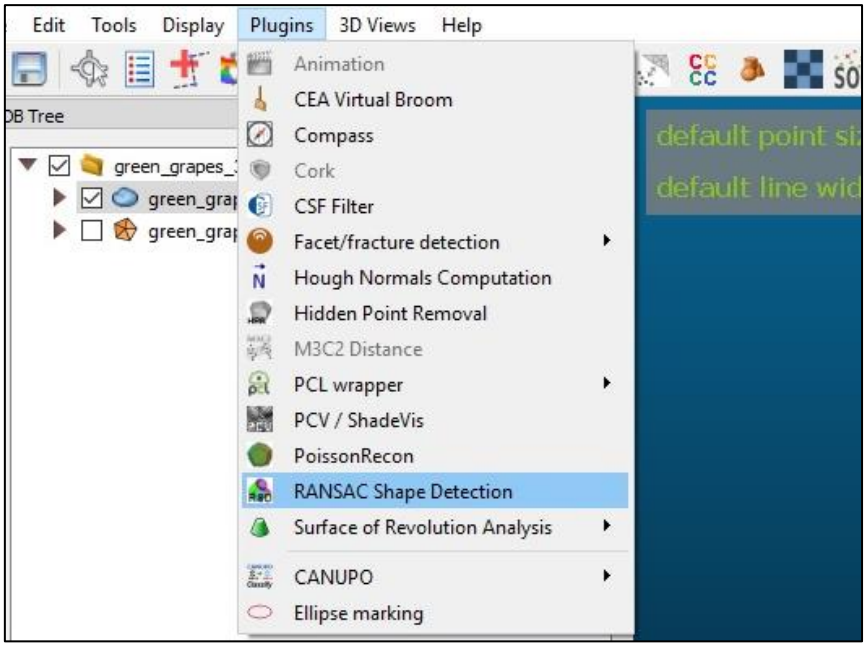

Figure 32: Opening the RANSAC plugin window

When the tool window is open, several settings can be adjusted. On the one hand, different shapes can be selected which the tool then uses to identify objects in the sample point cloud. It should be mentioned that the individual shapes are called “Primitives” in this tool. On the other hand, the

minimum number of support points per primitive can also be set. This setting gives the user the possibility to set a minimum point threshold for the shapes that should be detected by the tool. After testing out the tool several times, the most beneficial number of minimum support points for single grape shapes of this project is 100000 points per primitive. Figure 33 gives an overview of the settings which were used for identifying shapes on the sample point clouds of the grapes. By clicking on the "OK" button, the tool is executed and may take a while to calculate, identify and create the shapes. When the tool is finished calculating, the identified shapes are added to the working session as single shapes.

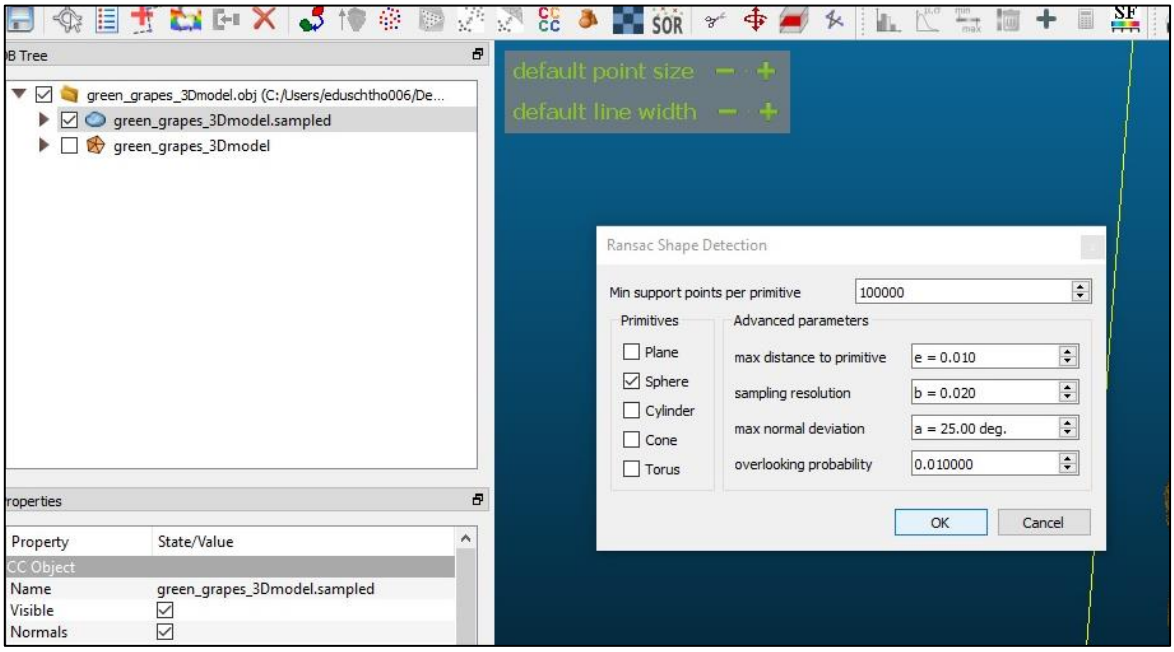

Figure 33: RANSAC shape detection settings

The results of the shape detection process of this laboratory study is displayed in Figure 34 and Figure 35. Figure 34 shows the detected shapes from the 3D model of the green grapes and Figure 35 illustrates the identified grapes from the red grape 3D model. As it can be seen in those two figures, the created shapes are colored in different hues, which is done by the software automatically. This circumstance makes it easier to recognize the individual identified shapes in the interface. Additionally, in the two figures the detected shapes are displayed above their corresponding 3D models to show how accurate the individual shapes were estimated by the RANSAC shape detection plugin. The red circle in Figure 34 for example shows that sometimes grapes are not correctly determined. Furthermore, the tool not only identifies and creates the shapes but also calculates specific parameters such as the radius for spherical shapes. Those information are used for the statistical analysis and validation of the grape measurements in the next step.

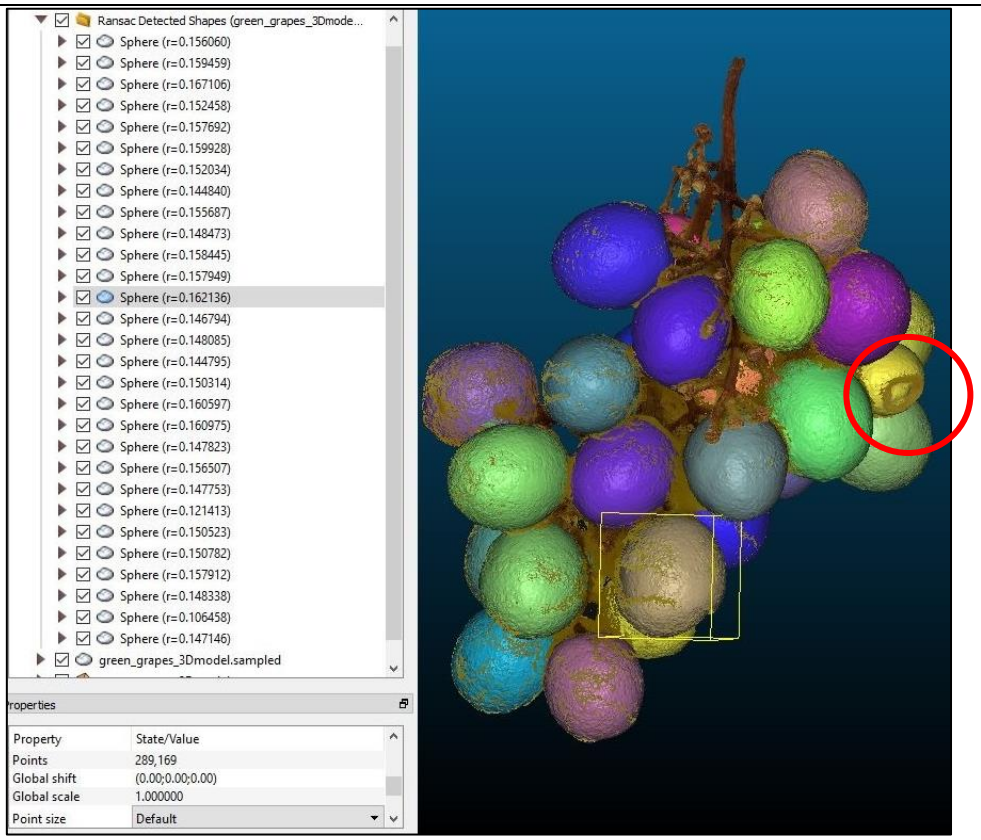

Figure 34: Detected green grapes with the RANSAC tool

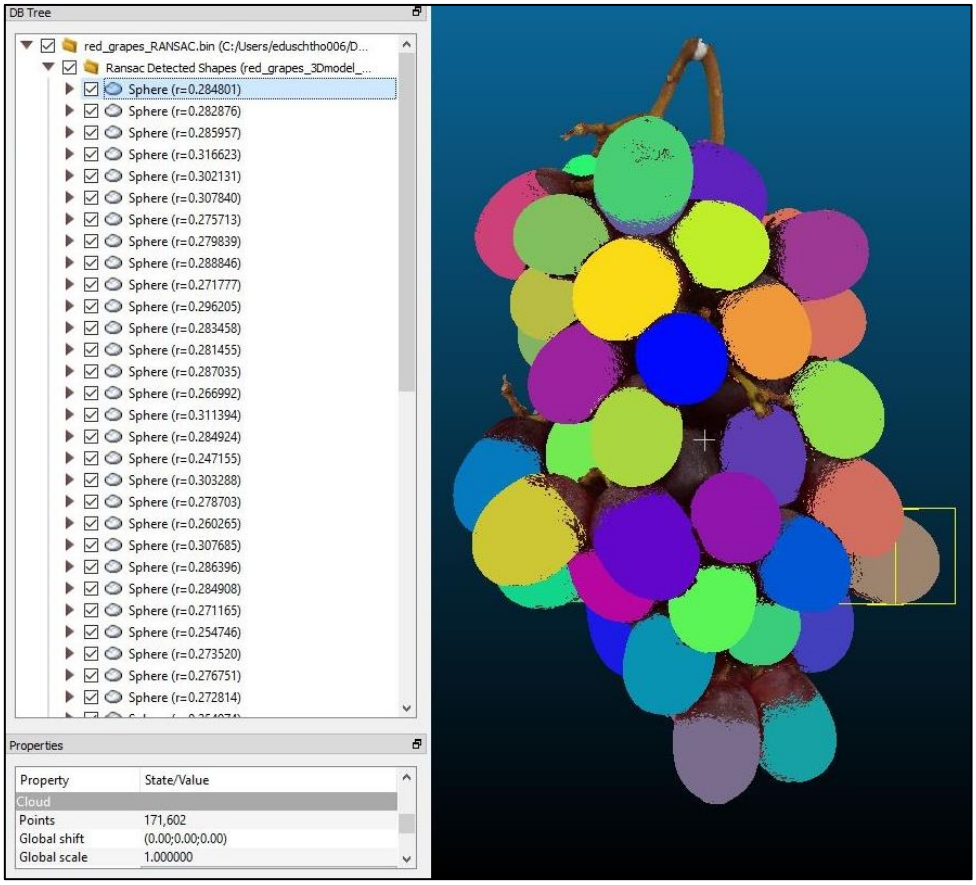

Figure 35: Detected red grapes with the RANSAC tool

4.1.4 Statistical Analysis and Validation

Since the data modelling process is finished and the necessary data is acquired from the real grapes and the 3D models, the statistical analysis and validation of the measurements can be started. At first, the data from the manual measurements are taken and features such as average length, mean width, length variance, width variance, total and mean weight, volume and average density of the grapes are calculated. To calculate the volume the formula

$$\mathrm{V} = \frac{4}{3} * \pi * \left(\frac{b}{2}\right)^2 * \left(\frac{a}{2}\right)$$

is used. The variable a is the length and b the width of a grape. The density is calculated based on the formula $\varrho = \frac{W}{V}$ whereas ϱ (Rho) is the density, W is the weight and V is the volume. The results of these calculations are illustrated in the second and third column of Table 2. By comparing the length and width values of the green and red grapes from Table 2, it is recognized that although the red grapes are on mean significantly longer than the green grapes, they are slightly thinner (0.34 mm). This can be attributed to the strongly elliptical shape of the red grapes. However, their overall bigger size is reflected in the weight and density of these grapes. The calculated values reveal that the average weight of the red grapes is 0.82 gram higher than those of the green grapes. On the other side, the variance results of all parameters of the red grapes are considerably higher than the variances of their green counterparts. Furthermore, the mean density of red grapes is slightly above the density of the green grapes.

To validate the results from the manual measurements, the same calculations are made with the results from the detected grapes. Before being able to calculate the parameters of the grape models, another additional value needs to be determined. As displayed in Figure 34 and Figure 35, CloudCompare also determines the radii of these identified grapes. However, these radii are dimensionless and therefore, a scaling factor needs to be calculated from the average radii of the real and grape models. Then, the radii of the modelled grapes are multiplied with the scaling factor to get the scaled radii. This procedure is necessary to make the to-be calculated parameters of the grape models comparable with the already determined parameters of their natural counterparts. Following, the scaled radii are used to calculate the mean length and width, the total and mean volume, total and average weight and the variances of those parameters of the modelled grapes. The resulting values are shown in the columns three and four of Table 2. The comparison of the measured and calculated parameters of the real and modelled grapes reveal that all 29 green grapes were detected by the RANSAC Shape Detection tool. The tool has also identified 55 from 62 red grapes with the sphere primitives although the red grapes have a strongly elliptical shape. The calculated volumes of the modelled grapes are marginal different from those of the real grapes.

Moreover, the determined weight values of the modelled grapes are also very similar to the empirically measured values. Another pattern which can be observed is that the variance of all model parameters are smaller than those of the real grapes. Especially, the variance values from the modelled red grapes are noticeably smaller than those of the real ones. This may be due to the fact that the RANSAC Shape Detection tool uses nearly perfect spheres to estimate the shape of the grapes and thus the resulting shapes of the modelled grapes are more rounded than the very elliptically shaped real red grapes. In summary, the 3D modelling process and the shape detection tool can be used very well to create highly accurate 3D models of grapes, detect individual grapes from them and to determine parameters such as their radii. Based on this, data such as volume or weight of the grapes can be calculated, which is important information for yield estimation of grapes.

Table 2: Measured and calculated phenological values by hand and from model

Category [unit]	Manual green grapes	Model green grapes	Manual red grapes	Model red grapes
Number of grapes [-]	29	29 (29)	62	55 (62)
Scaling Factor [-]	-	62.1006	-	32.534
Length - Mean [mm]	21.18	21.18	24.11	24.11
Width - Mean [mm]	18.75	18.75	18.41	18.41
Length - Variance [mm]	1.46	1.07	3.81	1.22
Width - Variance [mm]	1.04	0.94	2.06	0.93
Volume [mm³]	115444.02	115005.25	269494.7	239288.22 (269743.08)
Volume - Mean [mm³]	3980.83	3981.05	4346.69	4350.69
Volume - Variance [mm³]	639.16	556.33	1565.36	684.93
Weight [g]	138.00	137.48	346.00	307.22 (346.32)
Weight - Mean [g]	4.76	4.74	5.58	5.59
Weight - Variance [g]	0.76	0.67	2.01	0.88
Density - Mean [g/mm³]	0.001195	-	0.001284	-

Although most of the grapes where identified by the RANSAC Shape Detection tool, some problems occur due to the not perfect round form of the grapes. On the one hand, grapes that are deformed in some way are very difficult for the RANSAC plugin to correctly detect. An example is highlighted by the red striped circle in Figure 36. Despite this grape being detected in the final result, several tries with different settings were necessary for the tool to detect the grape. On the other hand, other partially circular forms are also quite difficult to recognize for the tool and can lead to unexpected results. The strongly elliptical form of the red grapes lead to some unexpected detection results. The yellow striped circle in Figure 37 shows that sometimes only one half of these grapes are correctly

estimated. Another inconsistency is highlighted by the red striped circle in Figure 37. The tool detected two shapes into the modelled grape.

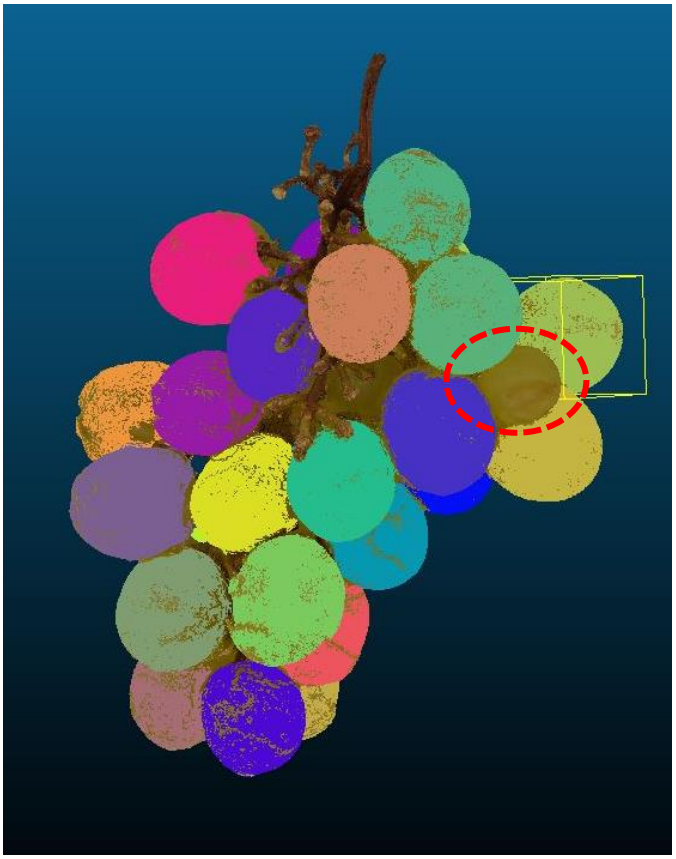

Figure 36: Difficulties with detecting deformed grapes

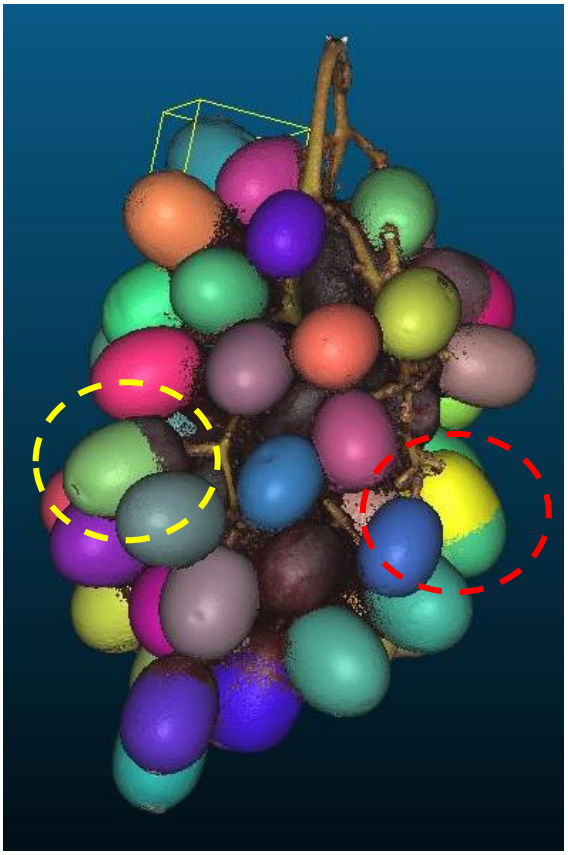

Figure 37: Difficulties with correctly identifying very elliptic grapes

4.2 Field Study

This chapter is concerned with the acquisition and processing of the recorded aerial image data in order to conduct a quantitative comparison of nadir and oblique images and to create a multi-temporal phenological 3D model of vine. First of all, subchapter 4.2.1 Study Area describes the location and structure of the study area. The recorded image data and ground reference data are explained in chapter 4.2.2 Data. In the subsequent chapters 4.2.3 Quantitative Comparison of Nadir and Oblique View Imagery und 4.2.4 3D Modelling of and Change Detection of Phenology of Vine the data modelling procedures based on the low-altitude aerial image data and ground reference data are explained. Chapter 4.2.3 Quantitative Comparison of Nadir and Oblique View Imagery describes the quantitative comparison of nadir and oblique images which is performed at the UNM. Section 4.2.4 3D Modelling of and Change Detection of Phenology of Vine deals with the 3D Modelling of vine and a change detection analysis of phenology of vine.

4.2.1 Study Area

The project's study area is a small vineyard called "Vinum Virunum" in St.Donat, Carinthia, Austria. Part B) and C) of Figure 38 give an overview of the location of the study vineyard. Part B) shows a map of Austria and its states. The red star in the image displays the location of the vineyard in the state "Carinthia". Part C) contains a map which depicts the municipality "St.Veit" with its districts. The red star in the map of part C) highlights the approximate position of the town "St.Donat" where the vineyard "Vinum Virunum" is located. The aerial image displayed in part A) of Figure 38 illustrates the actual appearance of the vineyard. The vineyard is approximately 515 meters above sea level, with the highest point at roughly 531 meters and the lowest point at 501 meters. The vineyard extends over an area of approximately 34600m². Furthermore, the aerial image also reveals the structure of the vineyard. Its structure can be divided into blocks and other smaller parts such as vine rows, inter-row spaces, individual vines and vine spacing. The vineyard "Vinum Virunum" consists of three uneven sized blocks, with the most southern block 1 occupying the largest area. Each block contains several vine rows. In this study vineyard the amount of vine rows per block greatly varies due to the slightly different shapes and sizes of the blocks. The area between the vine rows is called "inter-row space" and is approximately 2.5 meters in this vineyard. The vine rows are made up of the individual vine plants. The spaces between the vines in a vine row is called "vine spacing". On average, the vine spacing distance between the vine plants is 75 cm. However, since the vine plants in this vineyard were planted by hand, the vine spacing distance varies greatly from a range of 50 cm to 95 cm.

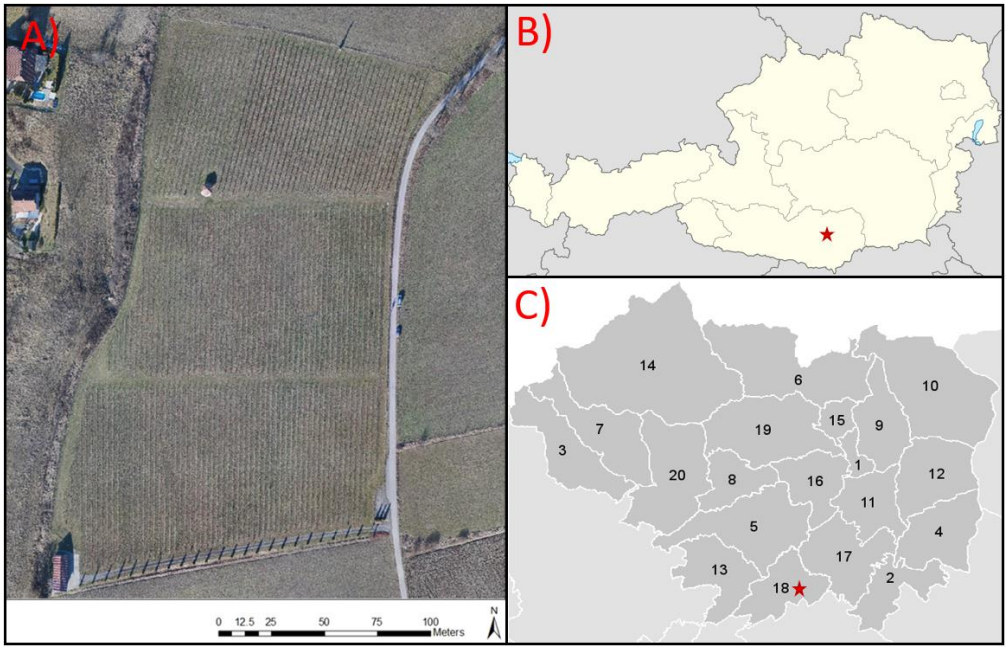

Figure 38: Image of the study vineyard "Vinum Virunum" and its location in Austria

4.2.2 Data

This chapter examines the datasets that were collected by means of data acquisition procedures and used for the data modelling in the subsequent implementation processes. The generated data are divided into two categories: airborne image data and ground reference data. They are explained in the following two subchapters.

4.2.2.1 Airborne Image Data

One part of the data collected are image datasets which are used for data modelling. In detail, these image datasets consist of low-altitude airborne image data, which are generated with a UAV and a novel in-house constructed multi-camera system. The utilized UAV is described in detail in chapter 3.2.1 Unmanned Aerial System and the multi-camera system is explained in chapter 3.2.2 Multi-Camera System. The five cameras of the multi-camera system are set in such way that they are triggered every two seconds during the data acquisition flight with the UAV and produce five aerial images. Following, at each trigger event, five airborne images of the scene below the UAV are taken from different angles. The resulting images are saved as .JPG files in five separate folders which correspond to the five individual cameras of the multi-camera system. The generated images are composed of 5456 x 3622 pixels (Sony, 2019) and have a ground sample distance (GSD) between 7 and 8mm per pixel. The data acquisition flights are carried out several times throughout a year in order to obtain airborne image datasets of the vines in their various phenological stages. This is a prerequisite to guarantee the creation of a multi-temporal phenological 3D model of vine based on multiple airborne image datasets of the vineyard at different times. An example of the recorded airborne images is shown in Figure 39. It shows five images of a trigger event which was made during a data acquisition flight in early July.

Figure 39: Airborne images of a single trigger event from the multi-camera system

4.2.2.2 Ground Reference Data

Additionally, ground reference data is also used in this research project. The ground reference data are objects, which are pre-installed in the vineyard. On the one hand, 16 white 10cm x 10cm sized marks and three brownish manholes can be found in the vineyard. 15 of these objects are regularly distributed at the edge of the vineyard and the remaining four are installed along an airline in the middle of the study area. They are used as ground control points for georeferencing and scaling the airborne images and 3D models and to assess their accuracy. The exact coordinates of these control points were collected using a total station. The accuracy of the determined coordinates of the GCPs is 0.005m. Figure 40 shows the study vineyard and the distribution of the 19 used GCPs. The green stars in the image depict GCPs which are used as control points and the red stars illustrate GCPs used as check points.

Figure 40: Image showing the GCPs as control points and check points

4.2.3 Quantitative Comparison of Nadir and Oblique View Imagery

The quantitative comparison of nadir and oblique view imagery is the second part of the projects implementations phase. Since this part of the project is based on the collaboration with the University of New Mexico, the comparison of the nadir and oblique images is performed at the UNM. With the increase of data collected by the UAS, there has been a renaissance of photogrammetric techniques for 3D measurement of scenes. Among other things, it was shown that the extremely accurate vertical and horizontal models can be generated by applying SFM-MVS techniques using high resolution image data with high overlap as input data. Furthermore, the additional use of oblique images, which increases redundancy and parallax, promises to further reduce geometric errors in 3D modelled scenes while improving the reconstruction and optical characterization of vertical surfaces.

Thus, this part of the research project in cooperation with the University of New Mexico is concerned with the evaluation of the tradeoff between the accuracy of the 3D scene reconstruction and computation complexity of the generated models. The goal is it to explore and answer the question what the cost and benefit of oblique view imagery in 3D scene reconstruction for low-altitude aerial photography is. In a multi-stage process, the low-altitude aerial nadir and oblique images are first recorded with a UAV system and an attached novel in-house constructed pentacam. Then, a SFM-MVS process is executed to generate 11 different 3D scene models from the image datasets of the five cameras. These 11 photogrammetric models represent combinations of the cameras. The models are then compared with a reference model in terms of the geometric accuracy of vertical and horizontal surfaces and their computational complexity as computation time. Based on calculated and observed measurement results, tables for the accuracy and computation time measurements are created and analyzed.

4.2.3.1 Data Acquisition

This section deals primarily with the detailed explanation of the data acquisition process to generate a low-altitude airborne image dataset and the collection of ground reference data for the quantitative comparison of nadir and oblique images. For this purpose, an UAS and a total station are utilized. The UAS used consists of the Leica Hexacopter UAV and the novel in-house constructed pentacam. The application of the UAV has several advantages for the generation of a low-altitude airborne image dataset. One of the main advantages of UAV usage is the ability to produce low-altitude images with very high ground resolution even under unfavorable conditions such as light wind or overcast sky. Another advantage is the ability to use UAVs to capture images with very high overlap and from multiple angles. The possibility to record lots of images with high end- and side-lap

from different viewing angles are especially advantageous for 3D scene reconstruction of objects. Compared to traditional photogrammetry, the high overlap rate of low-altitude images allows each ground point in the study area to be seen in multiple images, thus allowing programs to find many tie points in the images (Zhang, Xiong and Hao, 2011).

The data recording procedure is performed during noon on a cloudless day, so that there are no clouds and shadows that could have a negative influence of the image quality and that the sun's rays fall all perpendicular as possible to the ground. This initial situation should guarantee a safe flight for the UAV and as clear images as possible. Furthermore, the flight is setup to cover enough area around the vineyard to guarantee that every camera takes images of any part in the vineyard. At the beginning of the data collection process, the pentacam is attached to the drone and checked for possible errors. After the successful start of the UAV, it uses the built-in autopilot system to fly along a pre-defined route, which is saved in the board computer. The five pentacam cameras are setup up in such a way, that they trigger and create images every two seconds during the flight of the drone. In order to generate a low-altitude aerial image dataset for this implementation process, such a flight mission was conducted at the beginning of July. The technical and environmental details of this flight mission are as follows: The average flight altitude of the UAV during the data acquisition flight was about 66m. The GSD is about 7.69mm per pixel. The end- and side-lap ratio of images in and between flight strips is 80% and 70% respectively. 12 flight strips were completed by the UAV over the vineyard. The distance between two trigger events in a flight strip is about 7m. Figure 41 displays the 12 flight strips covering the vineyard, the locations were the images have been triggered along these flight strips and other calculated data acquisition relevant information such as the GSD or the number of images generated. The software Agisoft Metashape Pro is used to create the graphic of the flight mission and the corresponding calculated information shown in Figure 41 (Agisoft, 2019 b). Furthermore, a total station is used during the data acquisition process to collect the exact coordinates of the 19 GCPs which are installed in the vineyard. Figure 40 displays the locations of those 19 GCPs in the vineyard. The resulting ground reference dataset such as the recorded airborne image data are examined in more detail in following chapter 4.2.3.2 Recorded Data.

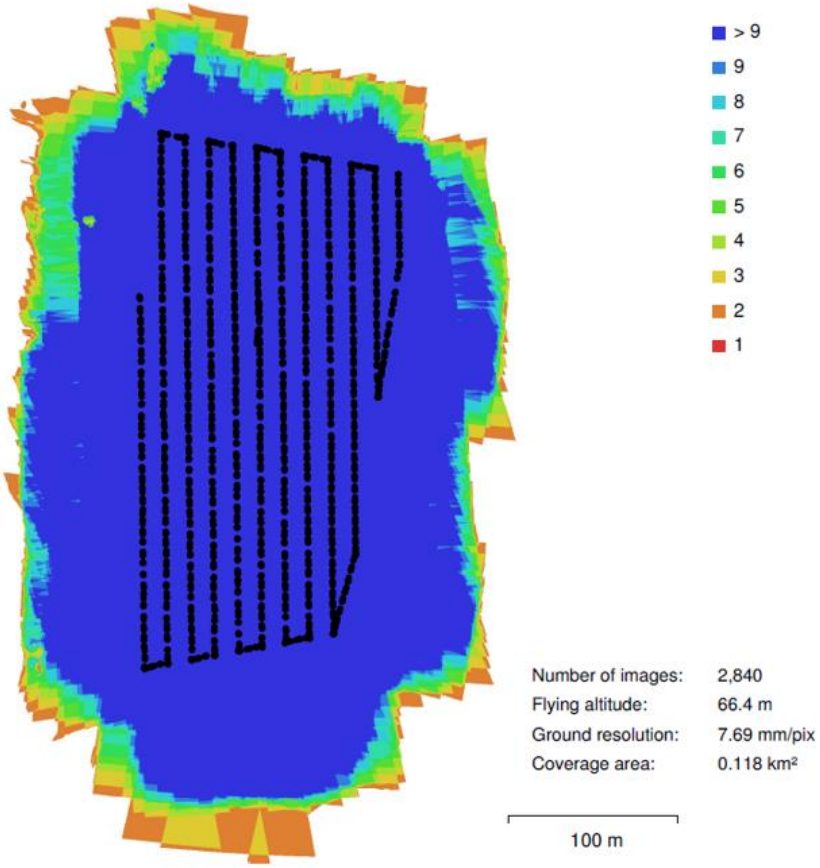

Figure 41: Flight strips, trigger event locations and image overlap of the used image dataset

4.2.3.2 Recorded Data

This chapter is concerned with the description of the data recorded during the data acquisition process, which are used to investigate the quantitative comparison of nadir and oblique images. In the following two sections, the generated low-altitude airborne image data and the collected ground reference data are described in more detail.

4.2.3.2.1 *Low-Altitude Airborne Image Data*

One part of the data recorded in the data collection mission is a low-altitude airborne image dataset. The image dataset is collected using the five pentacam cameras which are attached to the UAV during the flight mission. The generated images are stored as .JPG files in five folders whereas each folder represents a camera of the pentacam construction and contains 802 low-altitude aerial images. However, only images of the actual flight strips are used for data modelling. Therefore, all images taken during the take-off and landing phases of the UAV are not included in these processes. Thus, the number of images of the applied image dataset is 2840 as shown in Figure 41, which corresponds to 568 images per camera. All images are composed of 5456 x 3622 pixels (Sony, 2019)

and the GSD per pixel is 7.69mm. The image dataset covers an area of about 440m x 275m and roughly 120.000m². Hence, the image dataset covers a much larger area than the study vineyard. The additionally covered area can mainly be attributed to the images of the oblique cameras. Figure 42 illustrates a comparison between the area covered by the nadir camera images and the images of the starboard oblique camera. It shows that the oblique images of the starboard camera cover a larger area than the nadir images. The large area coverage of the oblique images is also reflected in the image overlap rates of the image dataset. The image overlap of the recorded low-altitude aerial image dataset can be observed in Figure 41. It reveals that each vineyard location is covered by at least 9 images. On the one hand, it can be attributed to the end- and sidelap ratio of 80% and 70% between images of flight strips. On the other hand, the image overlap rate can also be attributed to the large area, which is covered by the oblique images.

The image footprints displayed in Figure 42 are generated with two programs. Agisoft Metashape Professional 1.5.2 Build 7838 (64 bit) is used to create the polygon shapes of the image footprints (Agisoft, 2019 b). ArcGIS 10.6 is used to visualize those footprints (Esri, 2019).

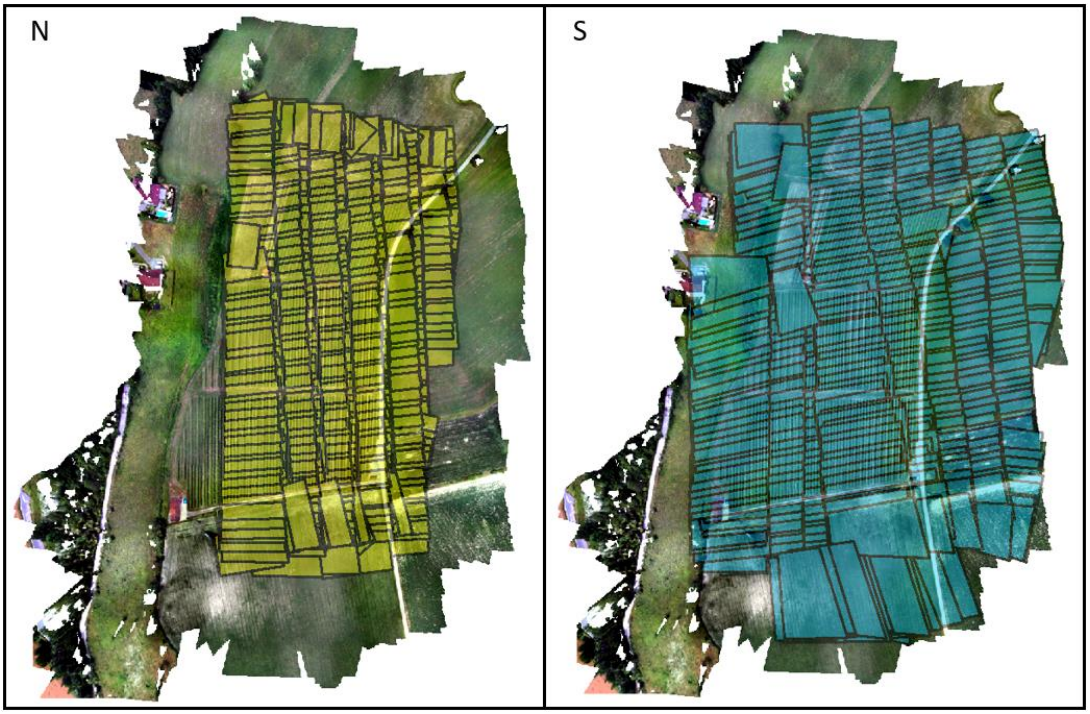

Figure 42: Ground coverage comparison of nadir and starboard oblique images

4.2.3.2.2 *Ground Reference Data*

The second part of the collected data is the ground reference dataset. This dataset contains ground reference data of pre-installed objects in the vineyard. The pre-installed objects are 16 white 10cm x 10cm sized marks and three brownish manholes. These objects and their collected location

information are used as GCPs for georeferencing and scaling the 3D models. 12 of the GCPs are used as control points and 7 as check points. 15 GCPs are distributed in a regular pattern at the edge of the vineyard. The other four can be found in the middle part of the vineyard. The exact positional information of the 19 GCPs is recorded with a total station. The position accuracy of the recorded coordinate information of the GCPs is 0.005m. The distribution and locations of pre-installed GCPs are illustrated in Figure 40. Furthermore, Figure 40 shows the 12 GCPs used as control points as green stars and the 5 check points as red stars.

4.2.3.3 Data Modelling

This chapter is concerned with the detailed explanation of the data modelling procedure of this implementation phase. The applied data modelling is a 3D scene reconstruction process which uses SFM-MVS techniques. 3D scene reconstruction is a multi-stage procedure which is applied to recreate high-resolution three-dimensional scenes from photogrammetric data. In this research project, the photogrammetric data are the low-altitude airborne images. They are used as input to generate photogrammetric models that represent real scenes from the study vineyard. The software Agisoft Metashape Professional 1.5.2 is used for this purpose (Agisoft, 2019 b).
The 3D scene reconstruction process is performed because it has specific advantages for the reconstruction of real scenes based on high resolution images. High resolution photogrammetric data can often show fine structures of real objects, as it is the case with man-made objects like statues and buildings or natural ones such as vine plants. 3D scene reconstruction allows the reconstruction of realistic 3D models in which these fine textured structures can be represented. These 3D models are used, among other things, for the three-dimensional representation of urban environments (Zhang, Xiong and Hao, 2011).
In this implementation phase, a six-step reconstruction procedure is used to create scenes of the study area in the form of photogrammetric models, which is based on the various functionalities and operations of the software used. The seven stages of this procedure are: 1) Pre-process preparation, 2) image alignment, 3) ground reference data integration, 4) camera and image alignment optimization, 5) dense cloud generation, 6) DSM generation and 7) orthomosaic computation.
The first step of the 3D scene reconstruction process involves importing the data into the software and preparing and managing the data and program environment before the actual calculation procedure is started. This is done in three steps. Firstly, the photogrammetric low-altitude aerial image data are imported into the program using either the ‘Add Photos’ operation or dragging and dropping the folder containing the images into the active program window (Agisoft Metashape User Manual, 2019). Once the software has finished loading the images, images from the starting and

landing phases of the UAV are manually removed. This guarantees that only images of the actual flight strips are used for modeling. Then, a suitable coordinate system is selected so that the internal coordinate system matches the coordinate system of the GCP coordinates.

In the second step, the images are matched in an image alignment process. Image matching is an essential requirement for 3D scene reconstruction because it extracts three-dimensional information from multiple images, which than can be used to construct 3D scenes (Zhang, Xiong and Hao, 2011). The image alignment process is started by using the option “Aligning Photos”. It is a four-step procedure which calculates the camera positions and image orientation of the individual images and creates a sparse point cloud. In the first phase, distinctive points are detected in the images. Then, pairs of these distinctive points which are found in multiple images are selected. Afterwards, the selected point pairs are matched to create tie points. The point cloud formed by the tie points is the sparse point cloud. Finally, the camera locations are estimated based on the tie points. Once the process is finished, the program displays the camera positions of all matched images and the sparse point cloud. (Agisoft Metashape User Manual, 2019; USGS National UAS Project Office, 2017)

The third step deals with the integration of the recorded ground reference data. It is done through placement of markers on the images. First, a prepared table containing the previously recorded coordinates of the GCPs is loaded into the program. Then, markers are placed on all images where the white GCPs can be seen. In order to guarantee a faster and more efficient placement of the markers, the “Refine Marker” function of the software is used. Once that is finished, the 12 GCPs shown in Figure 43 as yellow points are set as control points and the other seven GCPs as check points.

The fourth phase of the 3D scene reconstruction procedure is concerned with the optimization of the camera stations and the sparse point cloud. The optimization is done by executing the operation “Camera Optimization”. It is suggested to execute this operation only after the images and model have been georeferenced by placing markers on all images as explained in the third step. During the optimization process a “least square bundle adjustment” is applied (USGS National UAS Project Office, 2017). The bundle adjustment algorithm updates the estimated point coordinates of the sparse point cloud and determines camera parameters such as the internal and external camera orientations to adjust potential lens distortions. (Agisoft Metashape User Manual, 2019; USGS National UAS Project Office, 2017)

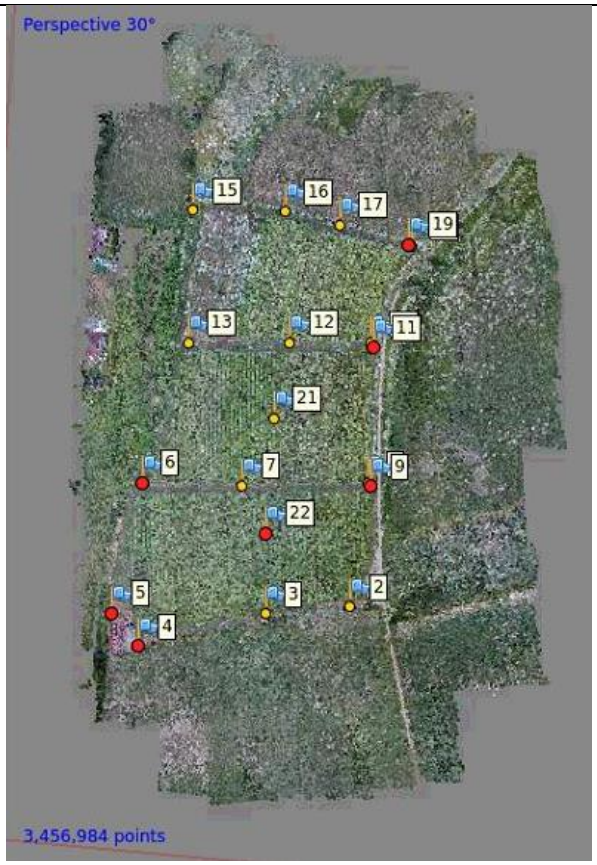

Figure 43: Visualization of tie point cloud with the 19 GCPs

In the fifth step of the 3D scene reconstruction, a dense point cloud is generated. It is run by executing the "Build Dense Cloud" option and is one of the most computationally intensive operations of the model generation. First, based on the estimated camera positions, depth maps are calculated for each image (Agisoft Metashape User Manual, 2019). Then, the depth information contained in the depth maps is combined to calculate the x-, y- and z-coordinates and color values of the points of the dense point cloud (USGS National UAS Project Office, 2017). During this process, various filter algorithms are also executed to remove possible outlier points (Agisoft Metashape User Manual, 2019). Depending on the number of images and the selected quality in the function window, millions or even billions of points can be calculated. This can take from several hours up to several weeks for one dense point cloud generation process. After this step, most of the vineyard's structure can already be observed in the point cloud.

In the sixth phase, a surface model in form of a DSM is generated. The created DSM is a raster containing height values of the vineyard. The DSMs will be compared with each other in a later procedure to investigate local height differences between the models. In case of this research project, the generation of the DSM is based on the dense point cloud data, as it generates the most accurate results (Agisoft Metashape User Manual, 2019). The process is started by first opening the

“Build DEM” window. Next, the coordinate system “MGI Austria GK Central” is selected and the “source data” option is set to “Dense Cloud”. Then, by pressing the “OK” button the computation process is started. Once the process is finished, the generated DSM can be visualized in Metashape by double clicking on the DSM in the respective chunk in the workspace pane.

The seventh and final processing phase of the SFM-MVS model generation is concerned with the generation of an orthomosaic. It is a high resolution imagery which is created based on specific source data such as a digital mesh or a DSM. Orthomosaic are often used in context of airborne photogrammetric data processing or to get a detailed view on a surveyed objects (Agisoft Metashape User Manual, 2019). In the case of this research project, the orthomosaic is calculated on the basis of the previously generated DSM. For this purpose the operation 'Build Orthomosaic' is started in Agisoft Metashape Professional. Then, the option “DEM” is selected as source data. After executing the tool, an orthomosaic is created. One of the orthomosaics created is shown in Figure 44.

Figure 44: Generated orthomosaic showing the whole vineyard

This entire data modeling workflow is performed 11 times to create 11 photogrammetric models based on various combinations of the five pentacam cameras. The camera combinations used for each model are shown in column 2 of Table 4. For each of these models a dense point cloud, a DSM and an orthomosaic are generated. Then, the model containing images from all cameras is selected as reference model and it is compared with all other models in a quantitative comparison process.

4.2.3.4 Geometric Accuracy and Computational Complexity Measurements

In order to conduct a quantitative comparison of nadir and oblique view images based on the 11 generated photogrammetric models and to evaluate the tradeoff between the accuracy and computational complexity of these models, several measurements and statistical calculations are performed. These measurements are divided into two parts. On the one hand, the geometric accuracy of the individual models is measured and compared. On the other hand, the computational complexity of the photogrammetric model generation is recorded and evaluated. These two measurement methods are explained in the following two subchapters.

4.2.3.4.1 *Geometric accuracy*

The determination of geometric accuracy is based on two types of measurements on the photogrammetric models. On the one hand, the geometric accuracy is determined by vertical measurements. On the other hand, it is estimated by horizontal measurements from the generated models. In this research project, a model's vertical geometric accuracy is defined by the mean RMSE in x- and y-direction of the GCPs from the model. The horizontal geometric accuracy is determined by the mean RMSE in z-direction of the models GCPs. The RMSE is a method which is used in regression analysis to measure the "goodness of fit" (Barber, 1988). In this case, the RMSE helps to assess how good or accurate a geometric accuracy of a model is compared to other generated models. In general, the RMSE value is defined as 'the standard deviation of the residuals about the regression line' (Barber, 1988). It is calculated using the formula:

$$RMSE\ (x) = \sqrt{\frac{\sum_{i=1}^{n}(x(d) - x(m))^2}{n}}.$$

In this case, $\sum_{i=1}^{n}(x(d) - x(m))^2$ is the sum of squared differences of the measured x-, y- and z-error values of the GCPs. "n" is the number of ground control points reference in a model. Thus, the calculated RMSE (x) value is the mean RMSE of the x, y and z error values of the individual models. These mean RMSE values are recorded and displayed in Table 4. These values can be used to examine differences between the 11 photogrammetric models and to evaluate the tradeoff for model generation based on the known geometric accuracy. The analysis of the measured values shown in Table 4 are described in chapter 4.2.3.5 Quantitative Comparison and Assessment of .

4.2.3.4.2 *Computational complexity*

In addition, to determining the geometric accuracy, the computational complexity of the photogrammetric models is also measured. The computation complexity of a photogrammetric model is identified by measuring the runtime of the individual processing steps and the total

computing time of its data modeling workflow. Thus, the computation time of the image matching, dense cloud-, DSM- and orthomosaic generation processes of each photogrammetric model workflow is recorded. Furthermore, these values are summarized for each models to obtain the total runtime of their calculation. The measured runtime values are listed in Table 5. The measurement and analysis of the computing time of processes can be advantageous to determine a favorable tradeoff between the computation complexity and the geometric accuracy of 3D models. This is of particular interest because some 3D scene reconstruction steps such as dense point cloud generation can be very computation intensive.

4.2.3.5 Quantitative Comparison and Assessment of Nadir and Oblique View Imagery

This is the final part of this implementation phase and it deals with the quantitative comparison of nadir and oblique view imagery. The comparison is based on different camera combinations and the generated results from the 11 photogrammetric models. The selected camera combinations for the 11 models are shown in column 2 of Table 4, Table 5 and Table 6 respectively. The quantitative comparison is performed with:

- visual comparisons of phenological features of vines in the 3D point clouds
- an analysis of tradeoff between geometric accuracy and computational complexity
- a comparison of local height differences between the DSMs

For these comparisons, the results of model 3 are used as a reference model, as they are generated from images from all pentacam cameras. The comparison of the results of model 1 and model 3 is of particular interest, since nadir cameras are widely used in remote sensing procedures and this comparison can provide information about advantages and disadvantages of the application of oblique cameras.

First, the comparison of nadir and oblique image data is performed by means of a visual examination with the created 3D point clouds. This analysis is executed to determine how accurately the structure of individual vines is represented in the dense point clouds of the different models. For this purpose, the point clouds are prepared in such a way that they show the same location of the vineyard. Four 3D point clouds are displayed in Table 3. These illustrate dense point clouds created from the nadir images (Figure 45), all images (Figure 46), right oblique images (Figure 47), and front oblique images (Figure 48). The 3D point clouds of the other models are shown in Appendix B: 3D point clouds showing reconstructed vines. It can be seen that fine structures of vines, such as their stems, are not reconstructed at all in the 3D point cloud of model 11 and only partially in model 1. In the dense point clouds of models 3 and 10, however, these are quite well recognizable. The overall structure of the plants are also well represented in the models 3 and 10 and therefore individual vine plants can

be be visually best distinguished from each other in these models. Thus, it seems that the application of oblique view cameras, which look at the plants at an oblique angle from the side, or a combination of these with nadir cameras are best suited for reconstructing plant structures or investigating their phenological stages.

Table 3: 3D point clouds of various models to compare reconstructed vines

Figure 45: 3D point cloud of model 1 showing reconstructed vines

Figure 46: 3D point cloud of model 3 showing reconstructed vines

Figure 47: 3D point cloud of model 10 showing reconstructed vines

Figure 48: 3D point cloud of model 11 showing reconstructed vines

Another procedure for the quantitative comparison of nadir and oblique images is performed with the geometric accuracy and computation complexity measurements. The measured geometric accuracies of the 11 models are visualized in Table 4. The vertical geometric accuracies listed in column 3 are defined by the mean RMSE values in x- and y-direction of the GCPs of the respective model. Column 4 shows the horizontal geometric accuracies, which are determined based on the average RMSE in z-direction of the GCPs. The measured processing time of the 3D modelling procedures are illustrated in Table 5.

The geometric accuracy measurements displayed in Table 4 show that models using only one camera have the best accuracy. However, model 7, for which the sidewards facing oblique cameras are used, has an equally good geometric accuracy as the single camera models. Model 8, which is also based on two oblique cameras, has a significantly less accurate geometric accuracy than Model 7, which suggests that in this research project, using the front and aft oblique cameras leads to higher geometric inaccuracies. A similar pattern can be observed in the horizontal geometric accuracy when comparing models using three cameras. Models 5 and 9, which use the front and aft oblique cameras, have a higher horizontal geometric error than models which use only one or none of these cameras. A comparison of models 1 and 3 shows that the model 3 in which all cameras are utilized has a significantly higher geometric inaccuracy than model 1, which is only based on the Nadir camera. However, overall it can be concluded that the geometric accuracy of all models is good, since the mean RMSE values of all models are in the few centimeter or even sub-centimeter range.

Table 4: Validation of the horizontal and vertical geometric accuracy of the 11 models

Model Number	Used Cameras	GCPs Mean RMSE (V)	GCPs Mean RMSE (H)
1	N	0.402cm	0.881cm
2	F + A + S + P	1.663cm	2.254cm
3	N + F + A + S + P	3.380cm	2.213cm
4	N + S + P	1.852cm	1.214cm
5	N + F + A	0.709cm	2.726cm
6	N + F + S	2.296cm	1.190cm
7	S + P	0.623cm	0.868cm
8	F + A	1.605cm	3.431cm
9	F + A + S	0.958cm	2.601cm
10	S	0.388cm	0.825cm
11	F	0.259cm	0.800cm

An analysis of the computational complexity measurements displayed in Table 5 also reveals certain patterns. On the one hand, the total computing time required by one-camera models 1, 10 and 11 is much less than those of the other models and the total computing time rapidly increases with the number of applied camera. A direct comparison between the one-camera models indicates that there are hardly any differences in the computational complexity of models based on only nadir or oblique view imagery. Furthermore, an analysis of the computational complexity of the 11 models shows that using front and aft oblique images leads to a higher total computation time. This can be observed when comparing the computational complexity of the three-camera models 5 and 9 with the models 4 and 6 and the two-camera models 8 and 7. When examining the computation time of the individual calculation steps, however, it becomes apparent that these large differences in processing time mainly occur in the dense point cloud generation. In the other processing steps, the computation time of the models that use the front and aft oblique cameras is shorter than the computation time of those which do no utilize these two cameras.

Table 5: Recorded computation time of the processing steps of the 11 models

Model Number	Used Cameras	Image Matching	Building Dense Cloud	Building DSM	Building Orthomosaic	Total Computation time
1	N	36.33min	192.19min	11.49min	20.19min	260.2min
2	F + A + S + P	242.0min	4622.06min	19.5min	60.14min	4943.7min
3	N + F + A + S + P	335.36min	8114.0min	21.19min	70.0min	8540.55min
4	N + S + P	166.36min	1695.31min	25.47min	46.44min	1933.58min
5	N + F + A	156.18min	2231.18min	20.37min	43.44min	2451.17min
6	N + F + S	164.07min	1779.25min	22.08min	48.0min	2013.4min
7	S + P	91.28min	760.1min	16.13min	38.24min	905.75min
8	F + A	84.11min	987.5min	14.52min	36.5min	1122.63min
9	F + A + S	164.14min	2344.39min	20.42min	53.29min	2582.24min
10	S	33.1min	192.11min	13.24min	22.04min	260.49min
11	F	33.02min	192.27min	11.45min	22.36min	259.1min

Furthermore, the generated DSMs of the 11 models are applied for the quantitative comparison of nadir and oblique view imagery. These are used to investigate local height differences between the DSMs of the individual models. For this purpose, the DSM of model 3, which is based on images from all cameras, is utilized as a reference model. The tool “Raster Calculator” from the software ArcGIS is executed to subtract the other DSMs from it to create height difference datasets containing information about the local height differences. Then histograms of the height difference distribution

are then generated with those information. Figure 49 displays such a histogram generated with ArcGIS. This histogram shows the distribution of calculated height difference values between the DSMs of model 1 and model 3. The other histograms of the height difference models are illustrated in Appendix C: Histograms of the DSM comparisons. The dotted lines shown in the histograms represent the onefold, twofold and threefold standard deviations. The dashed line in the middle is the visualized mean value of the datasets. An approximate Gaussian normal distribution of the height difference values can be observed in all histograms.

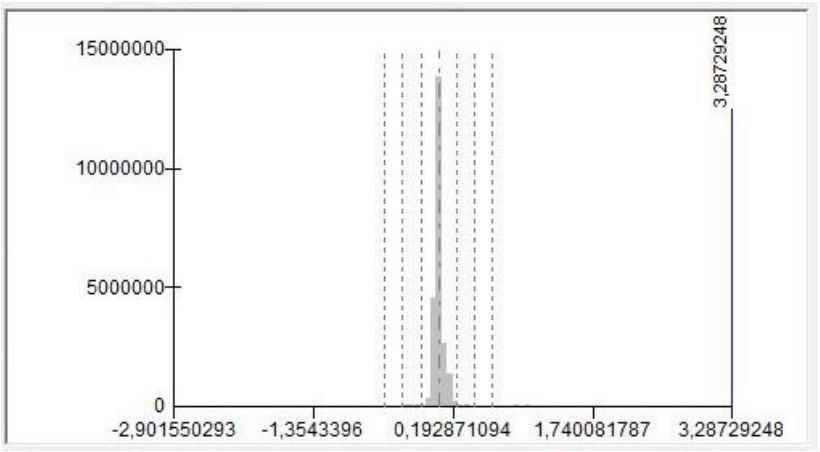

Figure 49: Histogram showing height difference distribution between model 1 and model 3

When creating histograms in ArcGIS, basic statistics such as the minimum or maximum are also calculated. These statistics of the height difference models are shown in Table 6. They are analyzed for specific patterns and utilized for the quantitative comparison of nadir and oblique view images. No height difference model could be created for model 4 because the generated DSM of the model could not be loaded into the software. For model 3 there is also no height difference information because it is applied as reference model.

Regarding the calculated minimum and maximum height differences, it can be seen that model 2 is a strong outlier. There are locations where the generated DSM of model 3 is up to 10m lower and up to 5m higher than the DSM of reference model 3. These large height deviations can be attributed to errors in the DSM calculation of model 2, as shown in Figure 50. Furthermore, the minimum height difference values reveal that the models 1, 5 and 6 which utilize the nadir camera have a slightly lower minimum height difference than the others. With the exception of model 2, the calculated maximum height differences of the models are within the same value range.

The mean height differences illustrated in the column "Mean Height Difference" in Table 6 range from sub-centimeters to a few centimeters. This suggests that the height differences of the generated DSMs are generally very small. The largest average height difference occurs between model 3 and model 7 and amounts to an average height difference of about 5cm. A pattern similar to

the maximum can be observed in the standard deviation of the height differences. They range from 15cm to 22cm and thus differ by only a few centimeters.

Table 6: Statistics of the calculated DSM height differences

Model Number	Used Cameras	Cell Count	Minimum Height Difference	Maximum Height Difference	Mean Height Difference	Standard Deviation
1	N	23.937.137	-2,902	3,287	0,0339	0,199
2	F + A + S + P	23.937.420	-10,130	5,039	-0,0040	0,194
3	N + F + A + S + P	-	-	-	-	-
4	N + S + P	-	-	-	-	-
5	N + F + A	23.936.213	-2,959	3,249	0,0109	0,173
6	N + F + S	23.936.986	-2,730	3,273	0,0201	0,148
7	S + P	23.937.493	-3,239	3,274	0,0498	0,220
8	F + A	23.937.455	-3,054	3,317	0,0255	0,184
9	F + A + S	23.937.436	-3,254	3,262	0,0157	0,168
10	S	23.936.947	-3,242	3,272	0,0302	0,221
11	F	23.937.516	-3,285	3,271	0,0072	0,200

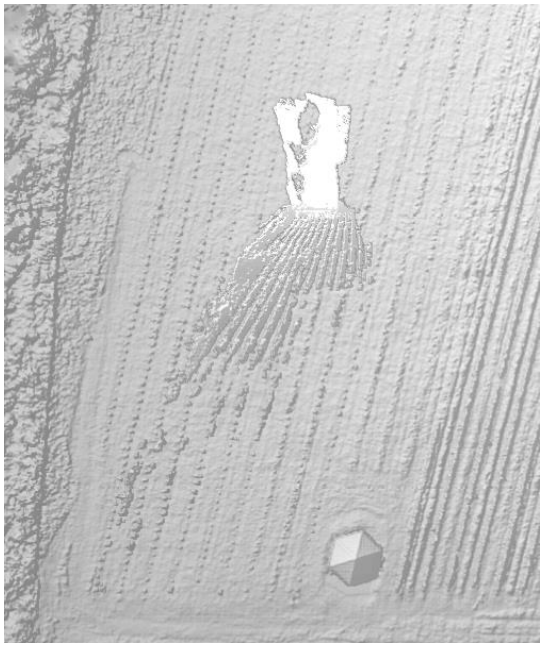

Figure 50: Error in the processed DSM of Model 2

4.2.4 3D Modelling of and Change Detection of Phenology of Vine

The third and final phase of the implementation process is dedicated to the 3D modelling of phenological stages of vines. Therefor, iterative sensor based in-field measurements with an UAS are performed to record multiple aerial image datasets which contain information about the vines in various phenological stages. The images datasets are used as input data for an iterative data modelling procedure to generate dense point clouds, DSMs and phenological 3D models of vines. The reconstructed 3D models of vine result in a multi-temporal phenological 3D model of vine. Such a model is used, among other things, for the comparison of 3D models of the vine plants to evaluate plant growth. In the following sections, the data acquisition process, the 3D modelling of phenology of vine from the captured aerial image data and a change detection of phenology of vine is explained in detail.

4.2.4.1 Data Acquisition of Low-Altitude Airborne Image Datasets

This chapter is concerned with the description of the data acquisition process that is performed to generate several low-altitude airborne image datasets containing information on various phenological phases of the vines in the vineyard. The data acquisition process is a sensor-based in-field measurement, in which an UAS consisting of an UAV and a multi-camera system is applied. The flight plan and corresponding details of the previously performed flight mission described in chapter 4.2.3.1 Data Acquisition are also retained for this data collection procedure, since the image data obtained delivered satisfactory results and only small adaptations might be necessary. Therefore, the Leica Hexacopter UAV and the novel in-house constructed pentacam with the five Sony ILCE-QX1 cameras are also used for this data recording process. However, since models of the vines in different phenological stages are to be created, it is necessary to carry out several further flight missions in different months. Thus, flight missions with this UAS setup are carried out in the months February, May, June, July and August. The generated low-altitude airborne image datasets contain information about different phenological stages of the vines in the study area. Furthermore, the ground reference dataset with the 19 GCPs from the previous implementation phase will continue to be used. In the next step, the recorded low-altitude image datasets are used as input data for data modelling and the ground reference data are utilized to georeference and scale of these models.

4.2.4.2 3D Modelling of Phenology of Vine

This phase of the research project is an extensive data modelling process which deals with the development of phenological 3D models of vine. Based on the collected low-altitude aerial image

datasets, a data modelling workflow is iteratively executed to generate dense point clouds and DSMs of the study area and to reconstruct multiple 3D models of vines from a small test area in the vineyard.

The iteratively applied 3D scene reconstruction is uniformly performed with each aerial dataset to ensure comparable results. This process and the chosen settings corresponds for the most parts to the data modeling procedure of the previous implementation process, as describe in chapter 4.2.3.3 Data Modelling. First, the input image data is selected and prepared for the subsequent data modeling. The next step deals with image matching and determining the initial camera positions and orientation parameters. Then, the ground reference data is used to georeference and scale the model. In the fourth step, an optimization process is applied to improve the camera parameters. Finally, a dense point cloud and a DSM of the entire vineyard as well as a phenological 3D model of vine of a small test area in the vineyard are generated by multiple execution of SFM-MVS techniques. The software Agisoft Metashape Professional 1.5.2 is used again for data modelling (Agisoft, 2019 b).

4.2.4.2.1 *Selection and Preparation of Input Data*

This section describes how the input data from the respective low-altitude airborne image datasets are selected and how the chosen data is prepared for data modeling in Agisoft Metashape Pro. For each performance of the data modelling workflow it is necessary to create two image data selections from the respective aerial image datasets, since on the one hand models such as a dense cloud and DSM of the entire vineyard and on the other hand phenological 3D models of vine from a small test area are to be generated. These image data selection procedures are intended to ensure uniformity in the data modelling workflows.

For the creation of the dense clouds and DSMs of the entire vineyard, care is taken that only aerial images of the actual flight strips are used. Therefore, when selecting the images for modelling the dense clouds and DSMs, no images of the take-off and landing phases of the UAV are taken into account. It is also taken into account that all five images of a trigger event are always present in the selected image data. If an image of a trigger event is not used, the other images of the same trigger event are not considered either.

For the reconstruction of the phenological 3D models of vine, a specific image data selection is also carried out. Since a 3D model of the entire vineyard would be very resource-intensive and very computational complex, a small test area in the vineyard is selected for the creation of those 3D models. Thus, also only images from an airborne image dataset which cover this test area, are selected as input data. The selection of these images is based on the actual ground which is covered by an image also called “footprint”. An open-source python script is used to determine the footprints

of the images (GitHub, 2019). It must be noted that this script is intended for use with Agisoft Metashape Pro only. First an image matching process is applied in Agisoft Metashape Pro, so that the camera positions and orientation parameters of the images are calculated. Then the Python script is executed, which uses the calculated aligned image and camera parameters to create the footprints of the images as quadrangular polygon shapes. These are exported as shapefiles and imported into a GIS for visualization and selection of the input images. In this research project ArcGIS is used for this purpose (Esri, 2019). Next, the tool "Select by Location" from ArcGIS is utilized to select those footprint polygons that intersect with a polygon representing the test area. Based on the footprint polygons selected by the program, the corresponding images of a low-altitude airborne image dataset are selected for reconstruction of the phenological 3D model.
In further data preparation, the images of the two image selections are imported into two chunks in Agisoft Metashape Pro. In addition, the coordinating system best adapted to the study area is also chosen in the program. Therefor, the coordinate system MGI / Austria GK Central (EPSG: 31255) is selected. The following data modelling processes are then executed on the chunks to create models of the vineyard such as a dense cloud and DSM in one chunk and the phenological 3D model of vine on the other.

4.2.4.2.2 *Image Matching*

In the next step, an image matching process is performed on the two previously created chunks. Image matching is usually one of the first steps of 3D scene reconstruction and plays an important role in solving problems in computer vision. Furthermore, it is a necessity in order to be able to perform processes such as bundle adjustment or the creation of a 3D model (Zhang, Xiong and Hao, 2011). In an image matching approach, SFM-MVS techniques are executed to calculate the image overlap parameters and the relative rotation angle between neighboring images and to extract feature points from matched images to create a coarse point cloud. For this purpose, the tool "Align Photos" of the software Agisoft Metashape Pro is applied (Agisoft Metashape User Manual, 2019). When selecting the settings in the tool window, the highest quality level is selected for accuracy and the default parameters are maintained for the other options. Then the image matching process is performed on the two prepared chunks that contain the imported image data. Figure 51 shows an image illustrating these selected parameters for the image matching.

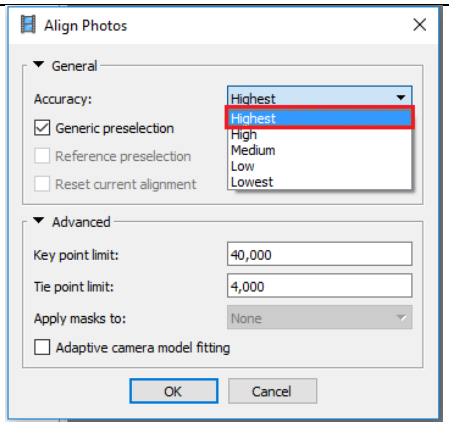

Figure 51: Selected settings for image matching

A matching process is performed first in an image matching process. In this matching step, two images are compared with each other and each feature in one image is compared with all features located within a Euclidean radius between feature vectors around that feature in the other image. Then, the feature points are extracted from the images to create a first point cloud. A refinement algorithm is applied to refine the point cloud in such a way that it only includes feature points showing the "strongest interest value" (Zhang, Xiong and Hao, 2011). The result is a sparse point cloud consisting of thousands or even millions of tie points from the overlapping images (Zhang et al., 2016). Two generated sparse clouds are visualized in Table 7. The sparse point cloud of Figure 52 represents the whole vineyard. Figure 53 shows the created sparse cloud of the small test area.

Table 7: Images of generated sparse clouds

Figure 52: Sparse cloud depicting the entire vineyard

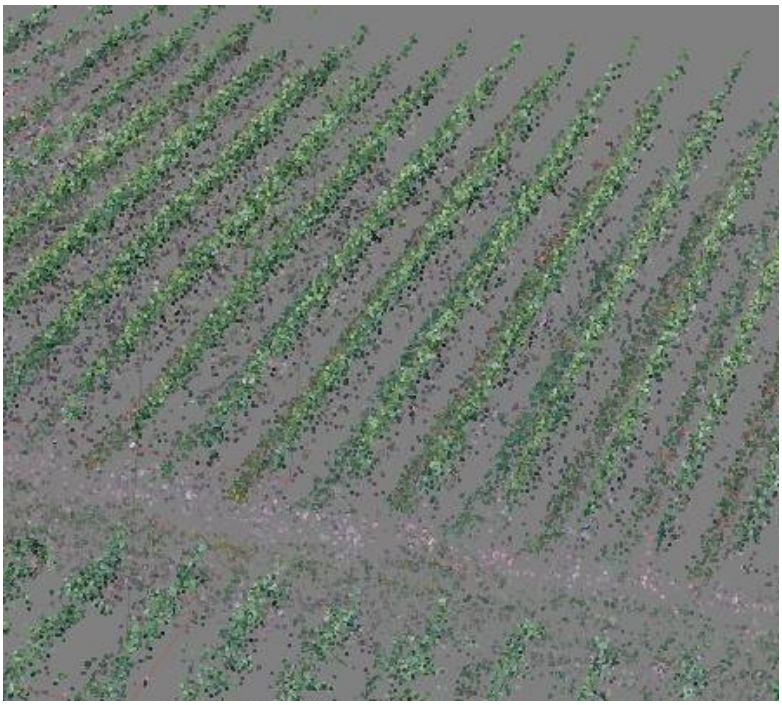

Figure 53: Generated sparse cloud of the small test area

4.2.4.2.3 *Integration of Ground Reference Data*

This chapter is concerned with the integration of the recorded ground reference data for georeferencing and scaling the point cloud and the images. The created point clouds often require a subsequent georeferencing and scaling step using GCPs. It is a necessary process as the point clouds created by SFM-MVS techniques in image matching are aspatial. Thus, it has no “absolute geographic position or scale”. One possibility to georeference and scale a point cloud and corresponding matched images is to add ground control points with known coordinates to the matched images (Morgenroth and Gomez, 2014). For this purpose, the coordinates of the GCPs recorded with the total station, which are available in the form of a .csv file, are imported into Metashape Pro. Therefor, the option "Import CSV" is utilized (Agisoft Metashape User Manual, 2019). A graphical representation of the import process of the GCP coordinates is shown in Figure 54.

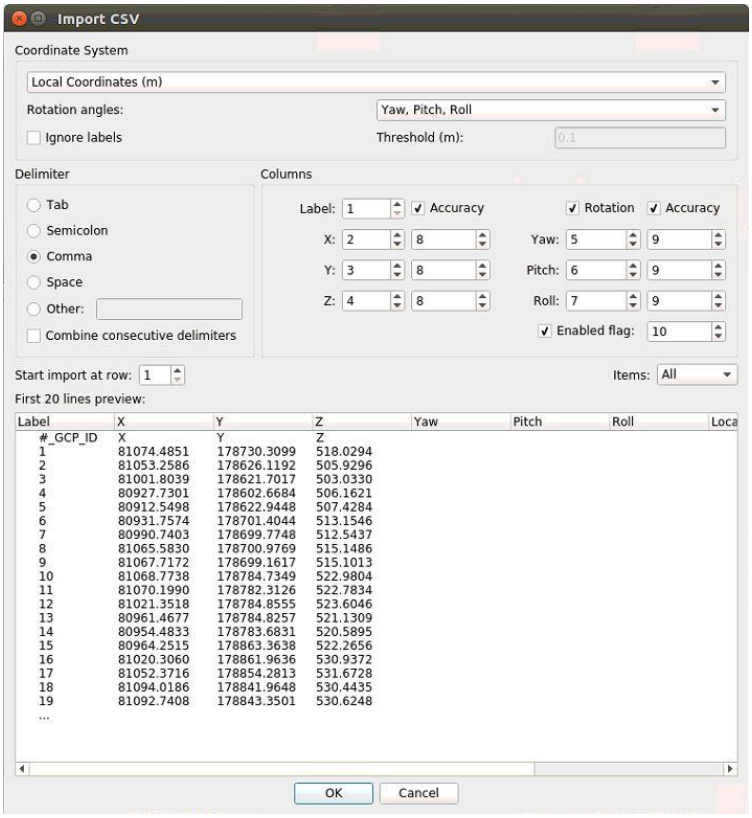

Figure 54: Importing the recorded coordinates of the GCPs

If the data was imported successfully, it is displayed as a table in the reference pane of the program. Markers can now be used to reference the positions of the examined GCPs in the aligned images. To do this, an image with a known location of a GCP must be opened. Then the marker of the respective GCP is placed on the image. Such a procedure is visualized in figures of Table 8. Figure 55 illustrates the process of placing a marker on a visible GCP in an aligned image. Figure 56 displays a marker which was places on GCP 2.

Table 8: Process of placing a marker on a visible location of a GCP

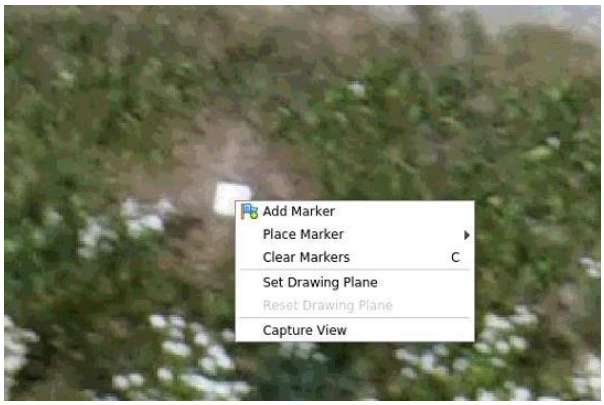

Figure 55: Placing a marker on a GCP

Figure 56: Marker placed on a ground control point visible in an image

As soon as a marker is placed on a position of a GCP in an image, a process is started in the background to automatically detect and mark other positions in images where the respective GCP is visible. This accelerates the georeferencing process considerably. If markers for the corresponding GCPs have been placed on the images, the positions of the GCPs in the point cloud are displayed. Figure 57 shows a sparse cloud with the referenced 19 GCPs of the vineyard. The yellow GCPs are used as control points and the red GCPs as check points for further data modelling steps.

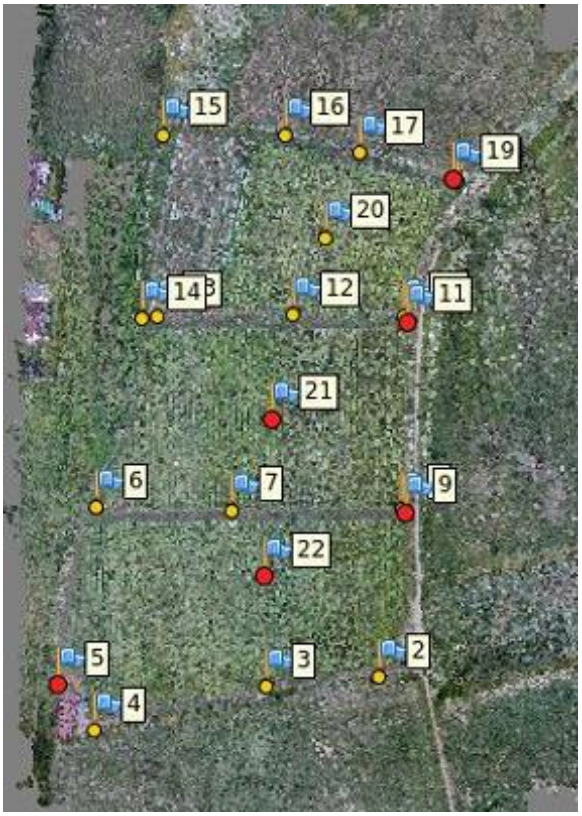

Figure 57: Visualized positions of the referenced GCPs in the point cloud

4.2.4.2.4 *Optimization of Camera Position and Orientation Parameters*

Due to possible incorrect calculations of the camera parameters or the changes of the interior and lens distortion parameters of the digital cameras over time (Zhang, Xiong and Hao, 2011), it is necessary to perform an optimization process. Thus, the "Optimize Cameras" option of Metashape Pro is applied. The default settings used are visualized in Figure 58. When the tool is started, an optimization process in form of a bundle adjustment procedure is carried out (Agisoft Metashape User Manual, 2019).

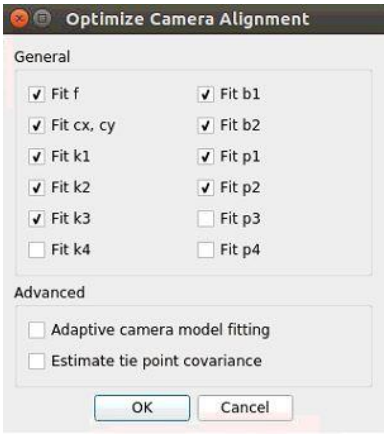

Figure 58: Default settings of the executed optimization process

Bundle adjustment is an iterative procedure in which the orientation and position parameters (Mouragnon et al., 2006) of the cameras are adjusted and refined. In this process, the estimated camera parameters and overlap values of the aligned images are used to determine the original position and coordinates of the camera stations and to refine the coordinates of the tie points. The resulting optimized camera parameters can also have an effect on the position and error values of the GCPs. Such a change of GCPs values due to an optimization process is visualized in the images of Table 9. Figure 59 displays the values of the 19 GCPs before optimization of a model. Figure 60 shows the changed parameter values of the ground control points after performing an optimization process. The blue colored rows in the two figures represent the seven GCPs which are used as checkpoints. As illustrated in the two figures in Table 9, most of the estimated position and error values of the GCPs generally improve significantly. However, the values of the GCPs can also deteriorate. This can be seen, for example, in the average error (m) values of the checkpoints in Figure 59 and Figure 60 highlighted by the red rectangles.

Table 9: GCP parameters before and after the optimization process

Markers	Easting (m)	Northing (m)	Altitude (m)	Accuracy (m	Error (m)	Projections	Error (pix)
2	81053.258600	178626.1192...	505.929600	0.005000	0.007221	89	1.067
3	81001.803900	178621.7017...	503.033000	0.005000	0.005172	98	1.069
4	80927.730100	178602.6684...	506.162100	0.005000	0.194898	21	0.716
5	80912.549800	178622.9448...	507.428400	0.005000	0.228415	11	0.407
6	80931.757400	178701.4044...	513.154600	0.005000	0.083630	15	0.450
7	80990.740300	178699.7748...	512.543700	0.005000	0.068611	83	1.164
8	81065.583000	178700.9769...	515.148600	0.005000	0.019321	64	1.013
9	81067.717200	178699.1617...	515.101300	0.005000	0.024174	62	0.860
10	81068.773800	178784.7349...	522.980400	0.005000	0.148674	58	0.843
11	81070.199000	178782.3126...	522.783400	0.005000	0.111676	62	0.745
12	81021.351800	178784.8555...	523.604600	0.005000	0.234115	64	1.107
13	80961.467700	178784.8257...	521.130900	0.005000	0.272408	38	1.303
15	80964.251500	178863.3638...	522.265600	0.005000	0.612063	19	1.094
16	81020.306000	178861.9636...	530.937200	0.005000	0.537253	44	1.108
17	81052.371600	178854.2813...	531.672800	0.005000	0.403613	42	1.193
18	81094.018600	178841.9648...	530.443500	0.005000	0.220541	35	1.019
19	81092.740800	178843.3501...	530.624800	0.005000	0.200023	39	0.957
21	81010.432400	178740.0880...	518.040300	0.005000	0.155045	41	0.820
22	81003.852500	178670.8475...	508.845500	0.005000	0.037229	74	1.361
Total Error							
Control points					0.296525		1.072
Check points					0.147165		0.973

Figure 59: GCP values before the optimization process

Markers	Easting (m)	Northing (m)	Altitude (m)	Accuracy (m	Error (m)	Projections	Error (pix)
2	81053.258600	178626.1192...	505.929600	0.005000	0.058744	89	0.292
3	81001.803900	178621.7017...	503.033000	0.005000	0.023852	98	0.346
4	80927.730100	178602.6684...	506.162100	0.005000	0.242605	21	0.290
5	80912.549800	178622.9448...	507.428400	0.005000	0.296711	11	0.188
6	80931.757400	178701.4044...	513.154600	0.005000	0.240126	15	0.219
7	80990.740300	178699.7748...	512.543700	0.005000	0.049154	83	0.334
8	81065.583000	178700.9769...	515.148600	0.005000	0.015150	64	0.314
9	81067.717200	178699.1617...	515.101300	0.005000	0.033875	62	0.312
10	81068.773800	178784.7349...	522.980400	0.005000	0.014243	58	0.357
11	81070.199000	178782.3126...	522.783400	0.005000	0.042606	62	0.277
12	81021.351800	178784.8555...	523.604600	0.005000	0.009062	64	0.285
13	80961.467700	178784.8257...	521.130900	0.005000	0.051927	38	0.349
15	80964.251500	178863.3638...	522.265600	0.005000	0.054051	19	0.267
16	81020.306000	178861.9636...	530.937200	0.005000	0.057128	44	0.394
17	81052.371600	178854.2813...	531.672800	0.005000	0.019272	42	0.450
18	81094.018600	178841.9648...	530.443500	0.005000	0.057679	35	0.322
19	81092.740800	178843.3501...	530.624800	0.005000	0.085820	39	0.314
21	81010.432400	178740.0880...	518.040300	0.005000	0.007015	41	0.197
22	81003.852500	178670.8475...	508.845500	0.005000	0.023667	74	0.301
Total Error							
Control points					0.040393		0.331
Check points					0.175435		0.292

Figure 60: GCP values after the optimization process

Before further processing steps are begin, the bounding box is checked and adjusted if necessary (Agisoft Metashape User Manual, 2019). This is advisable because in the following model calculation steps, such as dense cloud generation, only elements within the boundary are considered. Therefore, the tools "Move Region", "Resize Region" and "Rotate Region" shown in Figure 61 are used to adjust the bounding box. Following, the bounding box in one chunk is adjusted in such a way to contain the entire sparse point cloud of the vineyard. In another chunk, the bounding box is modified to include only the small test area for 3D modeling.

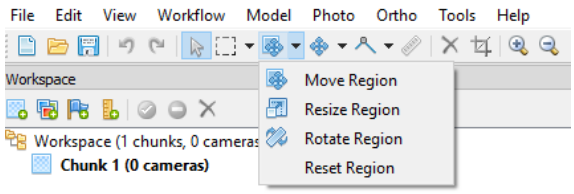

Figure 61: Location of the bounding box adjustment tools in Metashape Pro

4.2.4.2.5 *Implementation of Phenological 3D Models of Vine*

This section describes the creation of the dense point cloud and the DSM of the entire vineyard and the generation of the phenological 3D model of vine of a small test area in the vineyard. It is a three-stage process in which SFM-MVS techniques are used to create the above-mentioned models. First, it is necessary to generate the dense point cloud, since the DSM and the 3D model of vine are calculated based on the dense point cloud. The dense point cloud is created with the help of tie point information contained in the sparse point cloud (Zhang et al., 2016). The SFM-MVS methods applied use dense image matching and forward intersection (Zhang, Xiong and Hao, 2011) to calculate the dense point cloud. Therefore, the tool “Build Dense Cloud” of Agisoft Metashape Pro is executed

(Agisoft Metashape User Manual, 2019). For the dense cloud creation of the entire vineyard, the settings "High" for quality and "Mild" for depth filtering are selected. Then, the settings "Ultra-High" and "Mild" are chosen for the small test area. All other options of the tool window are retained as default settings. The pictures in Table 10 illustrate the dense point clouds calculated from the sparse clouds shown in Table 7. Figure 52 displays the dense cloud generated from sparse points of the entire vineyard and Figure 63 shows a dense point cloud of the small test area in the vineyard. It reveals that the structure of individual vines can roughly be recognized in the dense point cloud.

Table 10: Generated dense clouds of the vineyard and the small test area

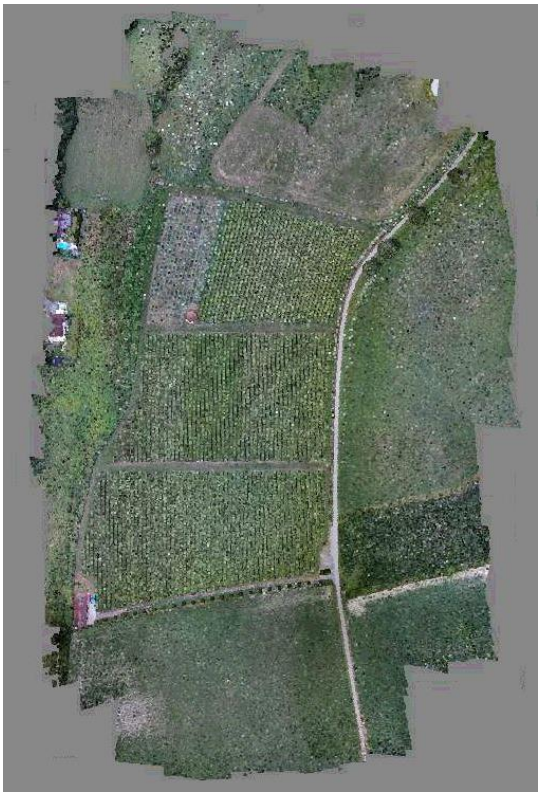

Figure 62: Generated dense cloud depicting the whole vineyard

Figure 63: Close-up view on a dense point cloud of the vines in the test area

Now SFM-MVS techniques are used to generate the DSM for the entire vineyard and to reconstruct a phenological 3D model of vine of the test area. First, a model containing height values of the vineyard is created in form of a digital surface model. Therefore, the tool "Build DEM" of the software Agisoft Metashape Pro is used. Before the tool is started, the "source data" option displayed in the tool window is set to "Dense cloud". This ensures that the DSM is generated on basis of the dense cloud (Agisoft Metashape User Manual, 2019). For all other options the default settings are used. Figure 64 shows a digital surface model of the vineyard, which was calculated based on a dense point cloud. The image of the DSM was created in Agisoft Metashape Pro and also shows the referenced GCPs of the vineyard as well as two scales.

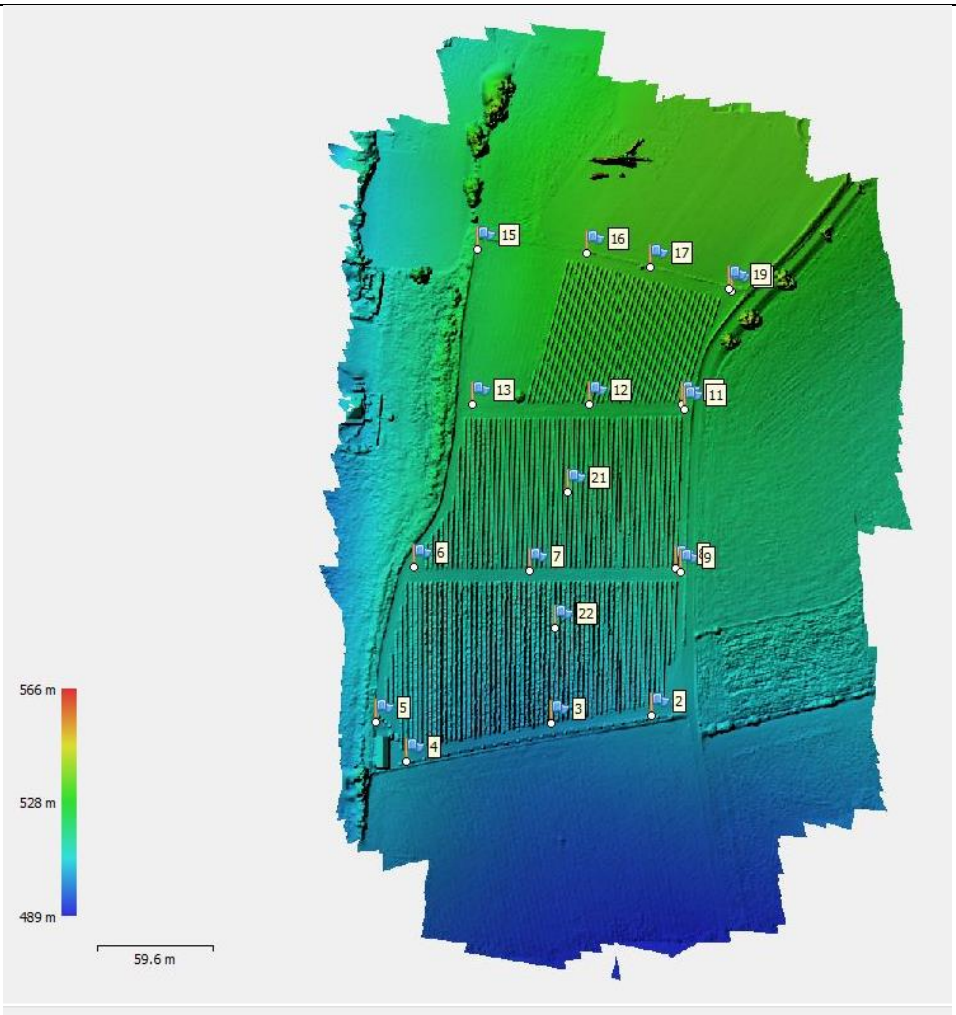

Figure 64: DSM of the vineyard "Vinum Virunum"

In the last implementation step a phenological 3D model of vine for the small test area is created. For this purpose, the tool "Build Mesh" is executed. First, the dense cloud is chosen as source data. Then, "Arbitrary" is selected as surface type, since this option is recommended for modeling closed objects (Agisoft Metashape User Manual, 2019) such as building or plants with grown leaves. For the depth map quality and face count option, the highest possible parameters are selected to ensure the construction of most accurate 3D model possible. After executing the process, a 3D model of the objects shown in the dense point cloud is created. In this case, a phenological 3D model of vine is reconstructed. Such a generated model is illustrated in Figure 65. Figure 65 shows the vegetative condition of the vines at the beginning of July. During this time of the season, the vines are usually in the fruit set stage, where the diameter of the grapes is between 1.6 and 3.2mm and the grapes are therefore too small to be seen in this 3D model. However, the structure of the individual vine plants and their vegetative state can be observed in the 3D model.

As mentioned at the beginning of chapter 4.2.4 3D Modelling of and Change Detection of Phenology of Vine, the applied 3D modelling workflow is an iterative process. Thus it is performed several times with airborne images from datasets of different months to obtain dense point clouds, DSMs and 3D models showing the vineyard and vines in their different phenological stages. The same settings are used for each of these processing steps to guarantee comparable results.

Figure 65: Image of a created phenological 3D model of vine

4.2.4.3 Change Detection of Phenology of Vine

In the next step, the previously generated DSMs of the vineyard are used to determine changes in the phenology of the vine plants in the study area. Therefor, the program ArcGIS (Esri, 2019) is utilized to compare these models to identify vegetative changes.
A model created with the ArcGIS ModelBuilder is applied to compare DSMs showing the vineyard during different phenological stages of vine and to analyze local height differences between them. Figure 66 shows the structure of the constructed DSM comparison model. The dark blue ellipses display the input data. The yellow rectangles represent the tools which are used to process the data and the processed output data is highlighted as green ellipses. First, the tool „Extract by Mask" is executed to adjust the two input DSMs in such a way that only the vineyard or a part of it is represented in the output. For this purpose, masks with the shape of the vineyard or its blocks is utilized to cut the DSMs. It assures that only actual parts of the vineyard are compared in the final step of the model.

Since the generated DSMs are raster with varying cell sizes, a further data preparation step must be performed. To be able to combine two or more raster datasets, the cells of those raster must have the same cell size. Since the cell size of the original DSMs varies between 1.6cm and 3.7cm, a uniform cell size of 4cm was defined. This uniform cell size is recorded in the light blue ellipse in the model and reference in the two "Resample" tools. Then, by executing those, two DSMs with a cell size of 4cm are created.

Finally, the tool “Raster Calculator” is applied to compare two DSMs and to create a height difference model. Through the expression „"%dsm_2_resampled%" - "%dsm_1_resampled%"“, which is stated in the tool, the older dataset (DSM 1 Resampled) is subtracted from the younger dataset (DSM 2 Resampled). This guarantees that height increases over the past time period are expressed in positive values and height losses in negative values in the calculated difference model. The symbol combination „"%“ is needed to reference the input files to-be-used by the tool.

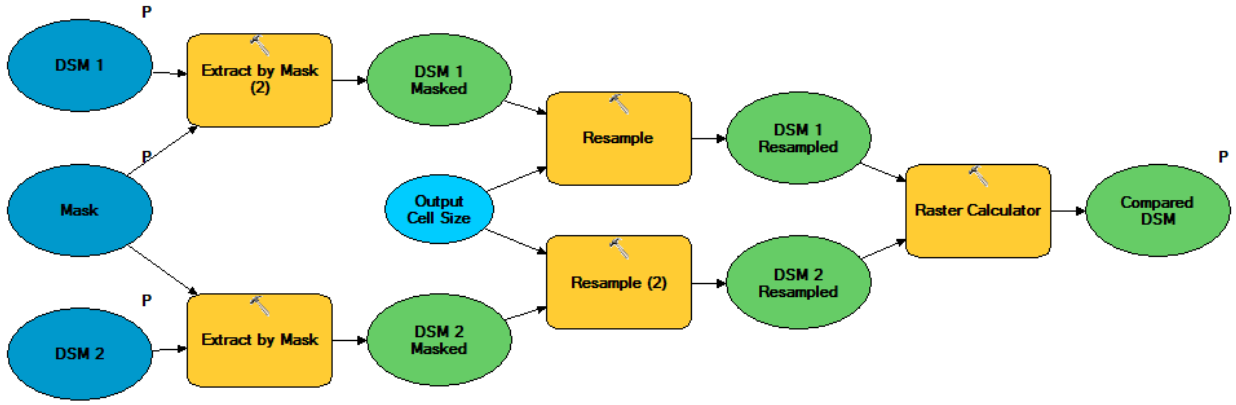

Figure 66: Tools of the applied model to compare DSMs

A close up view on a height difference model of the vineyard is illustrated in Figure 67. It displays the first block of the vineyard and the differences in altitude between February and June. Locations with a reddish color show an increase in altitude and places with a bluish color indicate a loss in height. A maximum height increase of 1.831m and a maximum decrease of 1.782m were calculated for this area. The growth of the vine plants is reflected in the positive height difference displayed as reddish color in the vine rows.

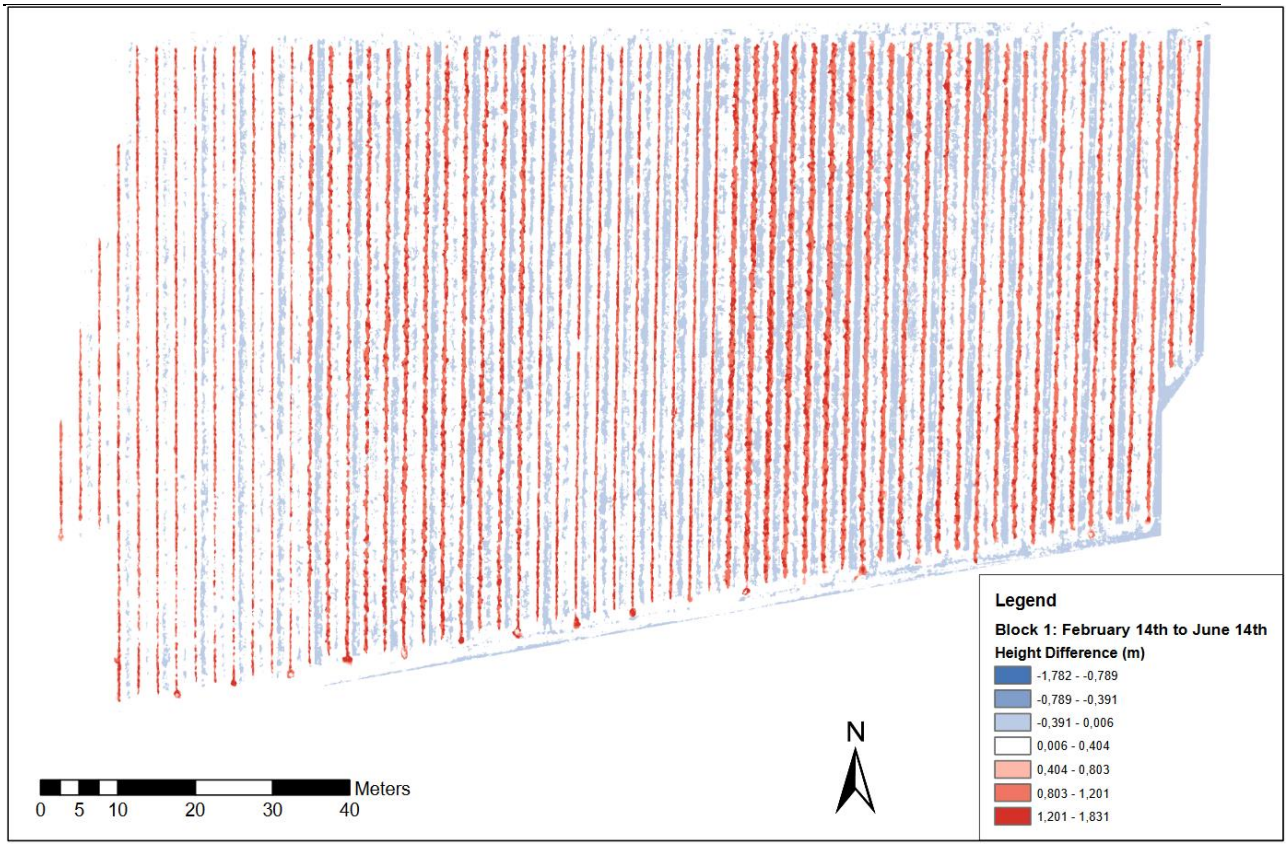

Figure 67: Height differences between February and June in block 1 of the vineyard

4.3 Results

In this section, the three implementation phases of the research project and the generated results are summarized and explained. The laboratory study focused on modelling of 3D grape models under laboratory conditions and the derivation of parameters to estimate yield based on close range photogrammetric methods. Therefor, a special setup was constructed to be able to record high-resolution images of commercially available green and red grapes from multiple angles and directions. Images of the experiment setup are displayed in Figure 13 and Figure 14. In addition, the individual grapes were also manually counted and weighed and their length and width measured and recorded. On basis of these parameters, the volume of the individual grapes and statistical values such as mean and variance were determined. The two captured close-range multi-view image datasets of the green and red grapes have been used in a data modeling process to reconstruct high-precision 3D models of the grapes. The resulting 3D models are illustrated in Figure 25 and Figure 26. In the next step, the 3D models were used to determine parameters to estimate yield. Consequently, parameters such as length, width, weight and volume of the digitally reconstructed grapes were calculated. To validate the yield parameters of the digital grapes, these were compared with the manually measured values in a table. These measurements are visualized in Table 2.

The first implementation procedure of the field study deals with the quantitative comparison of nadir and oblique images. The necessary image dataset was recorded in a data acquisition process using a UAS consisting of a UAV and a novel in-house constructed pentacam. Based on the pentacam, 11 models were determined which represent different combinations of the five pentacam cameras. Then a dense point cloud, a DSM and an orthomosaic were created for each model based on the acquired low-altitude aerial image dataset. Close-up views of the dense point clouds of the 11 models are illustrated in Table 3 and Table 12. Furthermore, the geometric accuracy, computational complexity and height differences between the models were determined and recorded in tables. The geometric accuracy is shown in Table 4, the computational complexity in Table 5 and statistics of the height differences in Table 6. These measurements and a visual analysis of the dense point clouds were used to compare nadir with oblique images and to determine specific patterns.

The final implementation process deals with the creation of the multi-temporal phenological 3D model of vine and the detection of changes in phenology of vine. For the data acquisition the UAS consisting of a hexacopter and the pentacam was used again. However, for this procedure several flight missions were executed in different months. Thus, several low-altitude aerial image datasets could be recorded, which show the vines of the vineyard in different phenological stages. Then, dense point clouds and DSMs of the vineyard were generated in an iterative data modelling process using the aerial image datasets. However, since the reconstruction of high-resolution 3D models is a very resource-intensive process, a small test area in the vineyard was selected for the creation of the phenological 3D models of vine. Several dense point clouds were also generated for this test area. The dense point clouds of the test area can be seen in Figures 68-71. These depict the individual vines of the test area in the months of February (Figure 68), June (Figure 69), July (Figure 70) and August (Figure 71). The representation of the vines in their dormant form throughout winter is displayed in Figure 68. In this dense point cloud it can also be seen that some fine structures such as stems of vines and posts were only partially reconstructed. Furthermore, in these images, the growth of the vine plants can already be observed. Especially from June to July a strong growth of the vines can be seen in the dense clouds. A comparison of Figure 70 and Figure 71 shows a decrease in plant height and leaf volume. This can be attributed to the pruning of branches from the vines by the employees in the vineyard.

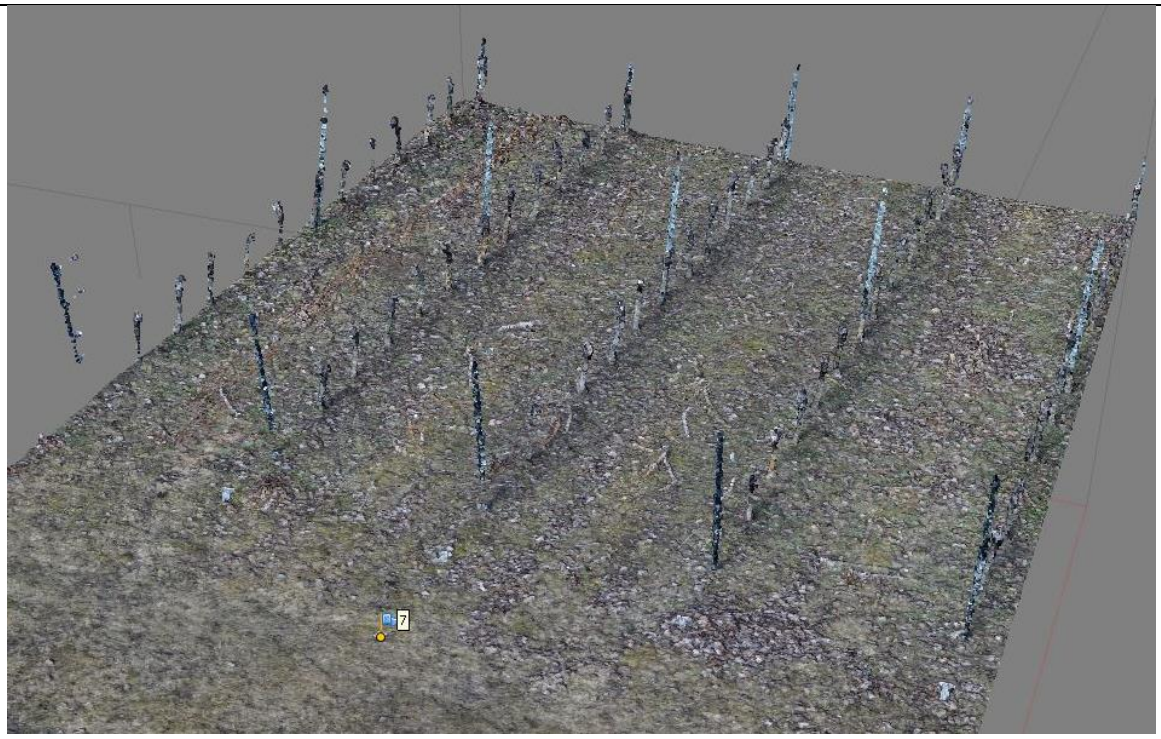

Figure 68: Dense cloud showing vines in February

Figure 69: Dense cloud showing vines in June

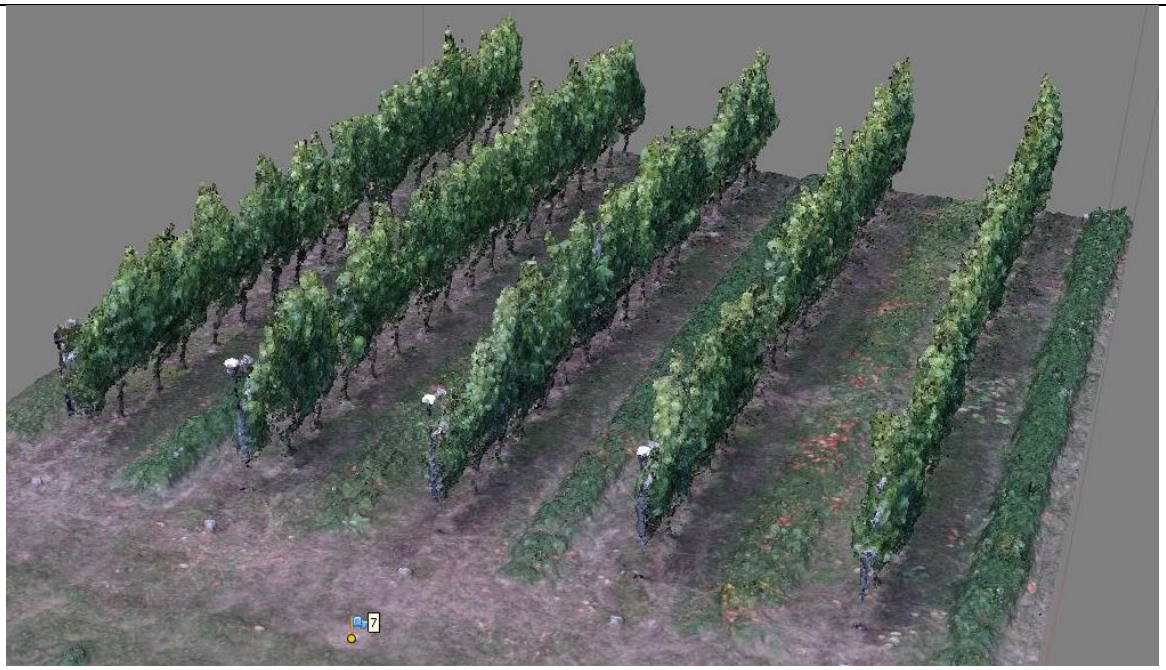

Figure 70: Dense cloud showing vines in July

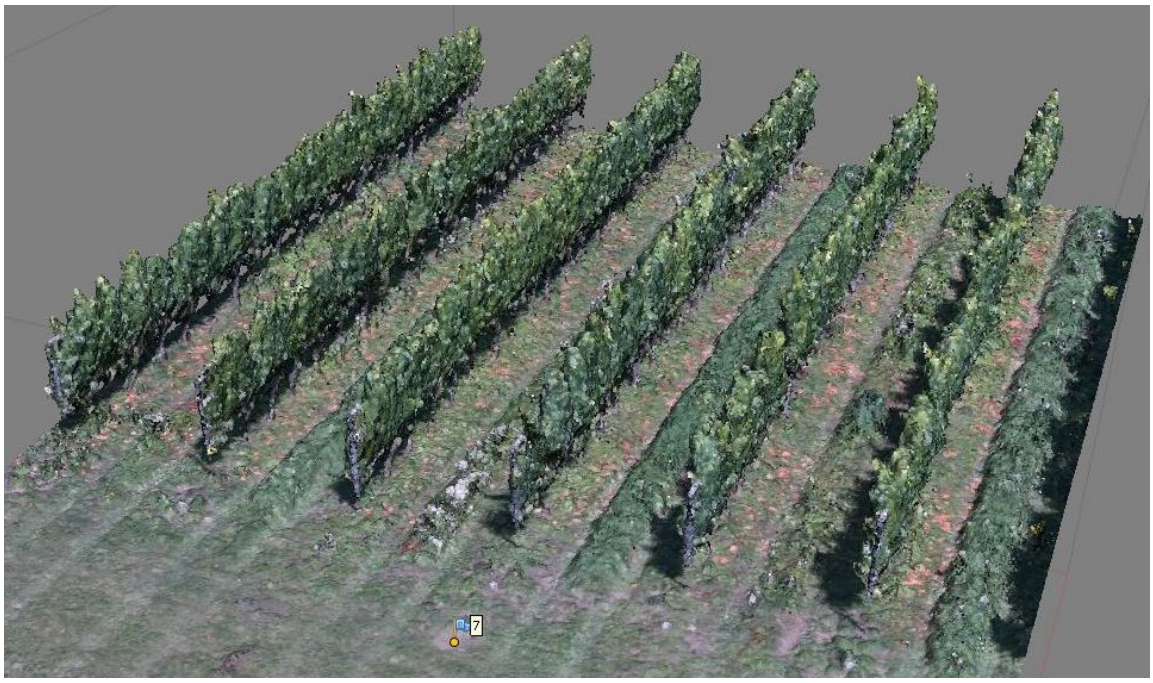

Figure 71: Dense cloud showing vines in August

In a further data modeling step, 3D models were generated and textured from the dense point clouds illustrated in figures 68 to 71. These phenological 3D models of vine are shown in the figures 72 to 75. Figure 72 displays a 3D model of the test area in February, Figure 73 the vines in June, Figure 74 a 3D model of the plants in July and finally Figure 75 the vines in August. In the majority of these images it can be observed that large parts of the visible structure of the vines are also preserved in the 3D models. In addition, individual plants can also be distinguished from each other

in the 3D models visualized in the figures 73, 74 and 75. However, it can also be seen that fine structures of objects, such as stems of vines or posts, are partly or completely lost in the 3D models. This is particularly serious in Figure 72. In the illustrated 3D model, which represents vines in February, hardly any structures of the plants could be correctly reconstructed.

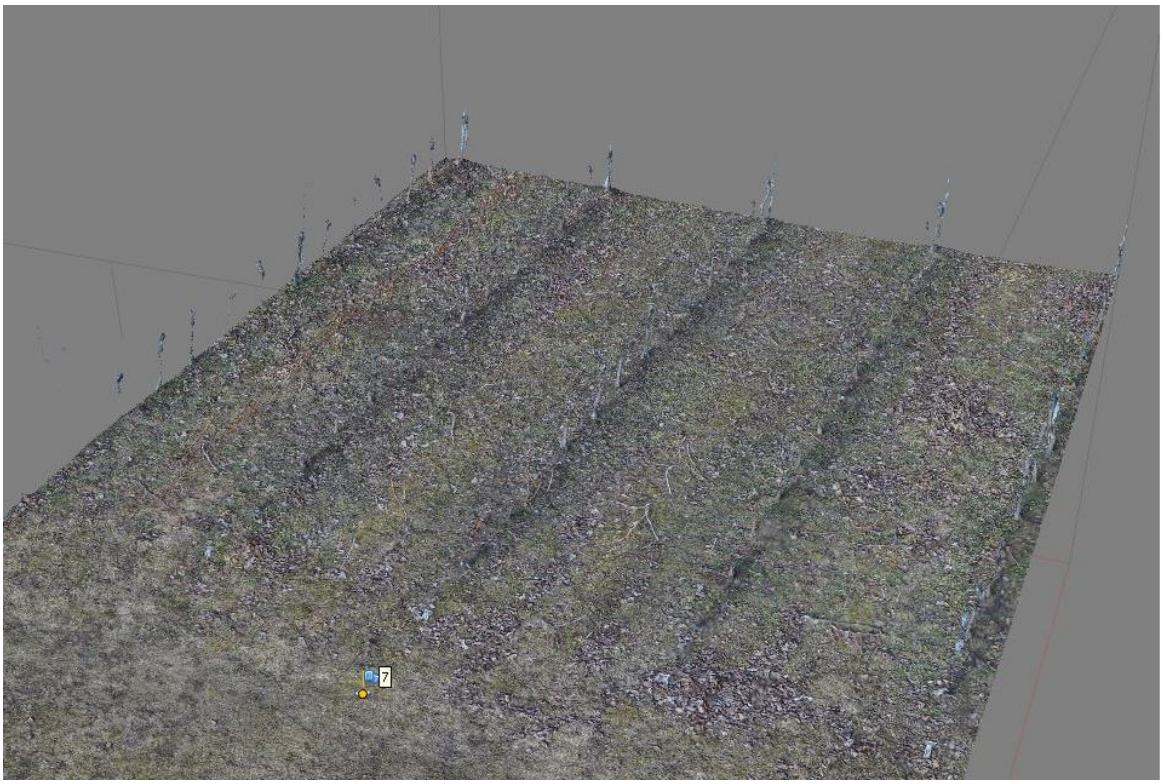

Figure 72: Phenological 3D Model showing vines in February

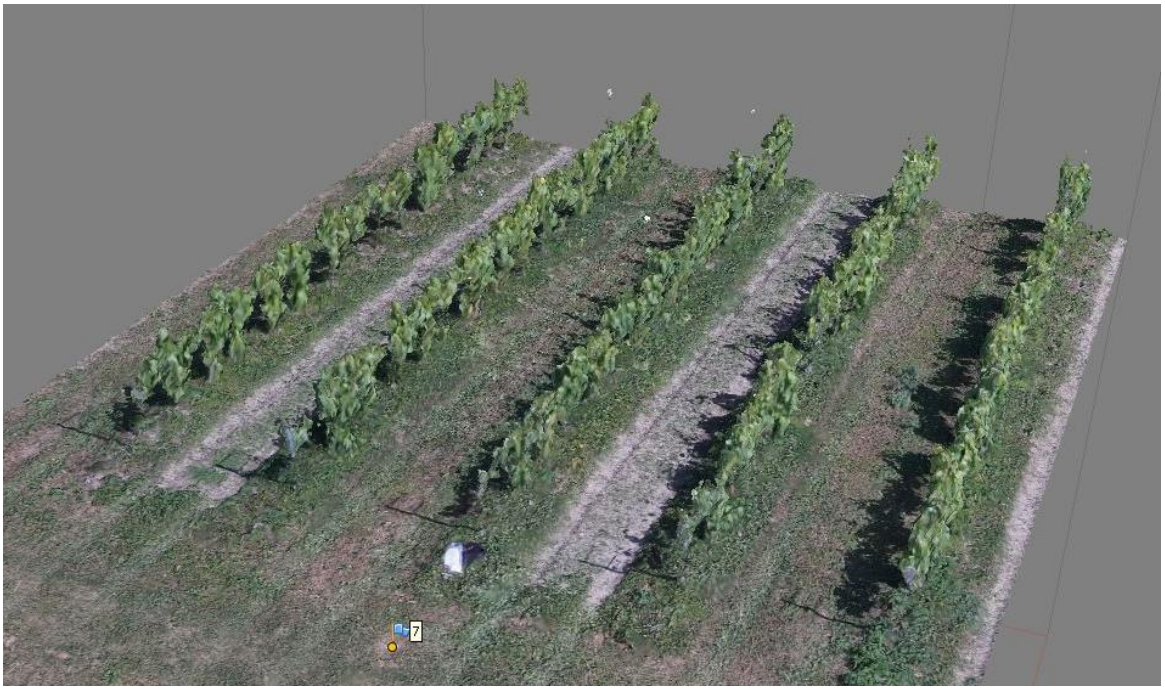

Figure 73: Phenological 3D Model showing vines in June

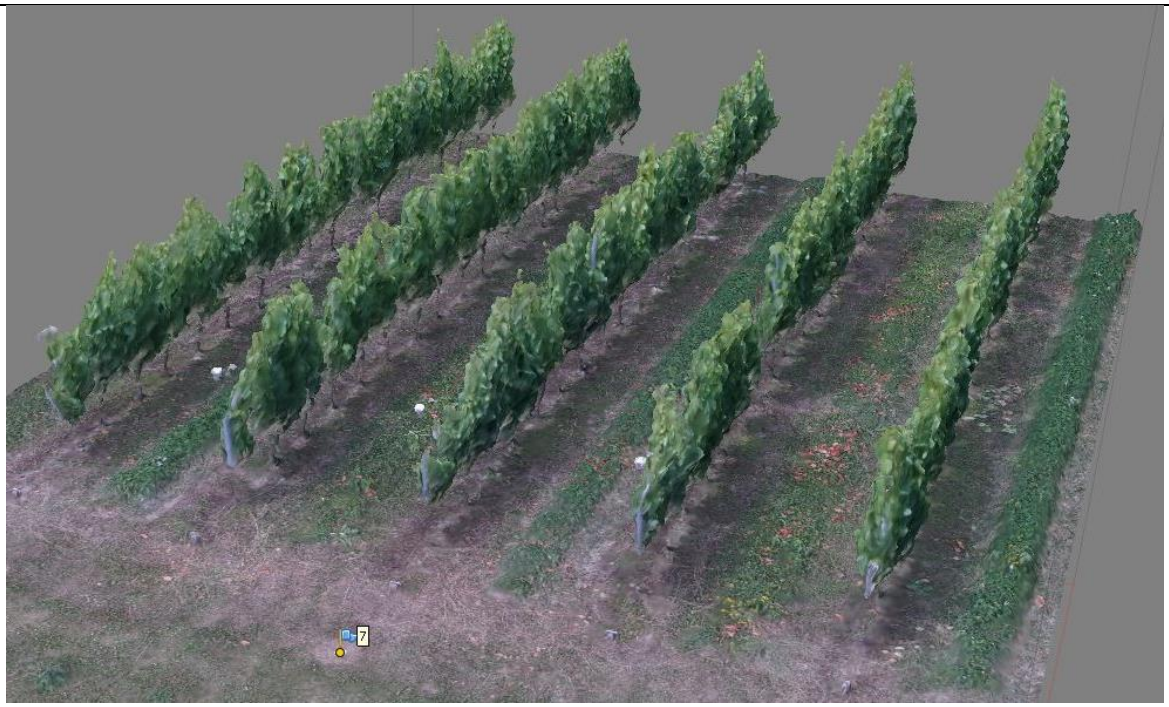

Figure 74: Phenological 3D Model showing vines in July

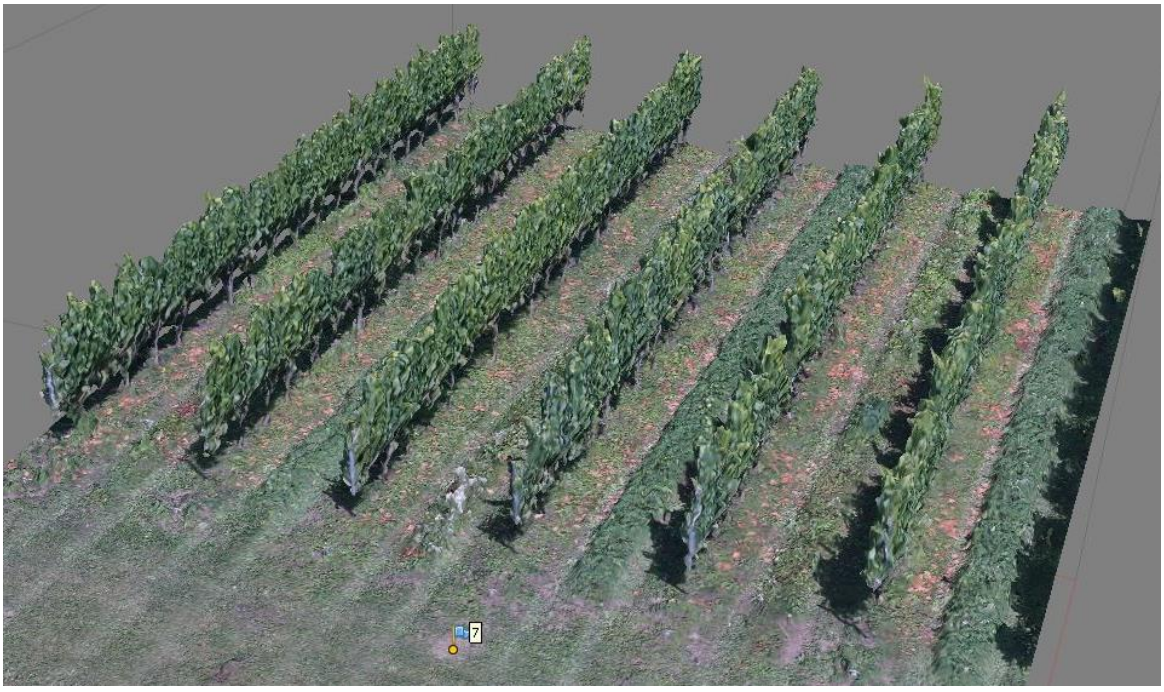

Figure 75: Phenological 3D Model showing vines in August

The generated DSMs of the vineyard are compared using the ArcGIS model illustrated in Figure 66 to generate height difference models. Such a difference model of two DSMs shows local height differences that occurred between the recordings of the aerial images which the DSMs are based on. Local height differences in the areas of the vine rows can be an indication of phenological changes of vines in vineyard. Three generated height difference models are visualized in Figure 67, Figure 76 and Figure 77. Figure 67 displays the height differences that occurred in the first block of the vineyard between February and June. Figure 76 and Figure 77 illustrate the height differences in the first block between the months June - July (Figure 76) and July - August (Figure 77). A reddish color in these images indicates an increase in altitude and a bluish color represents a height decrease. White color depicts little or no altitude difference. In the height difference models of Figure 67 and Figure 76, the vine rows show places with partly strong red colors, which indicates a strong growth of the vines from February to June and June to July. In the height difference model representing the months July to August a height loss, visualized as bluish color, can be seen in some areas of the vine rows. This can be attributed to the pruning of branches from the vines.

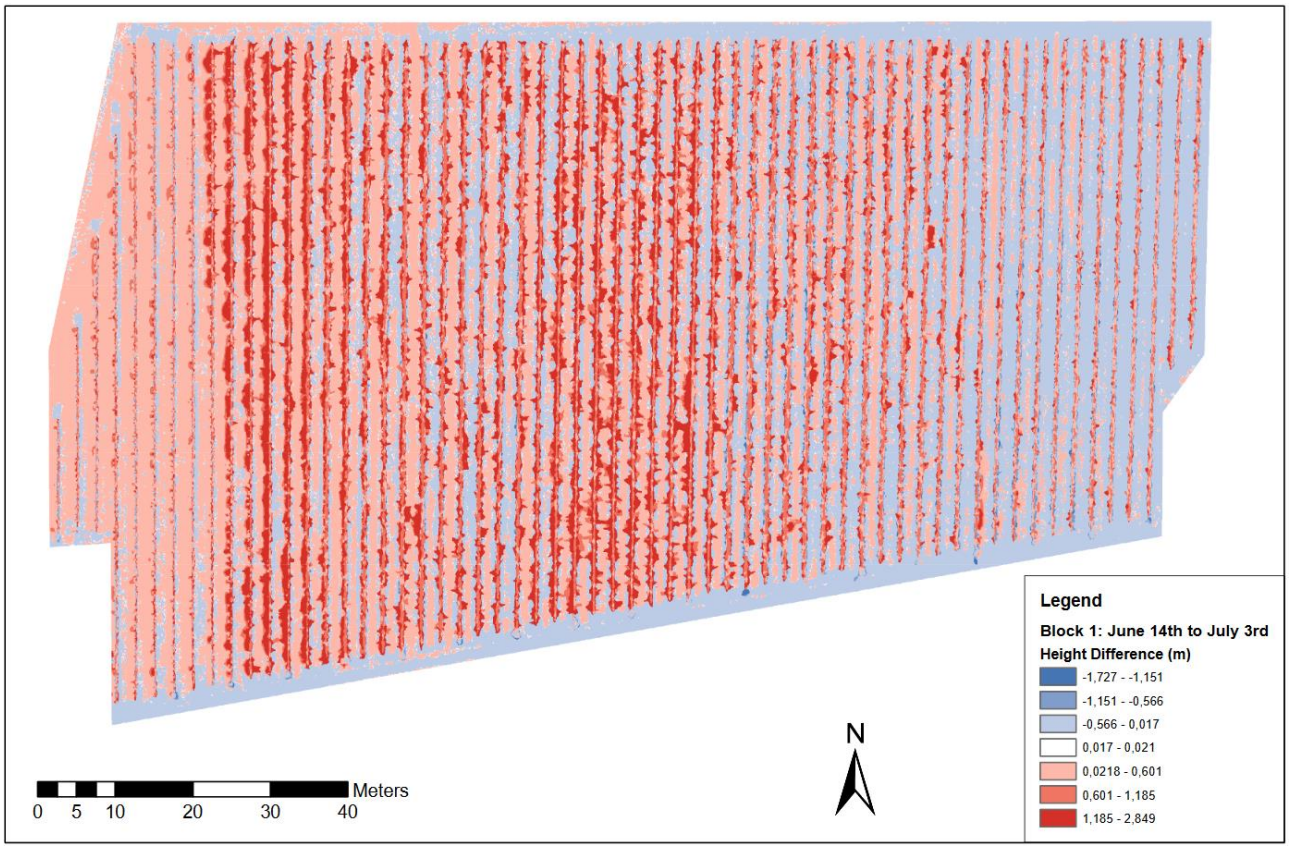

Figure 76: Height differences between June and July in block 1 of the vineyard

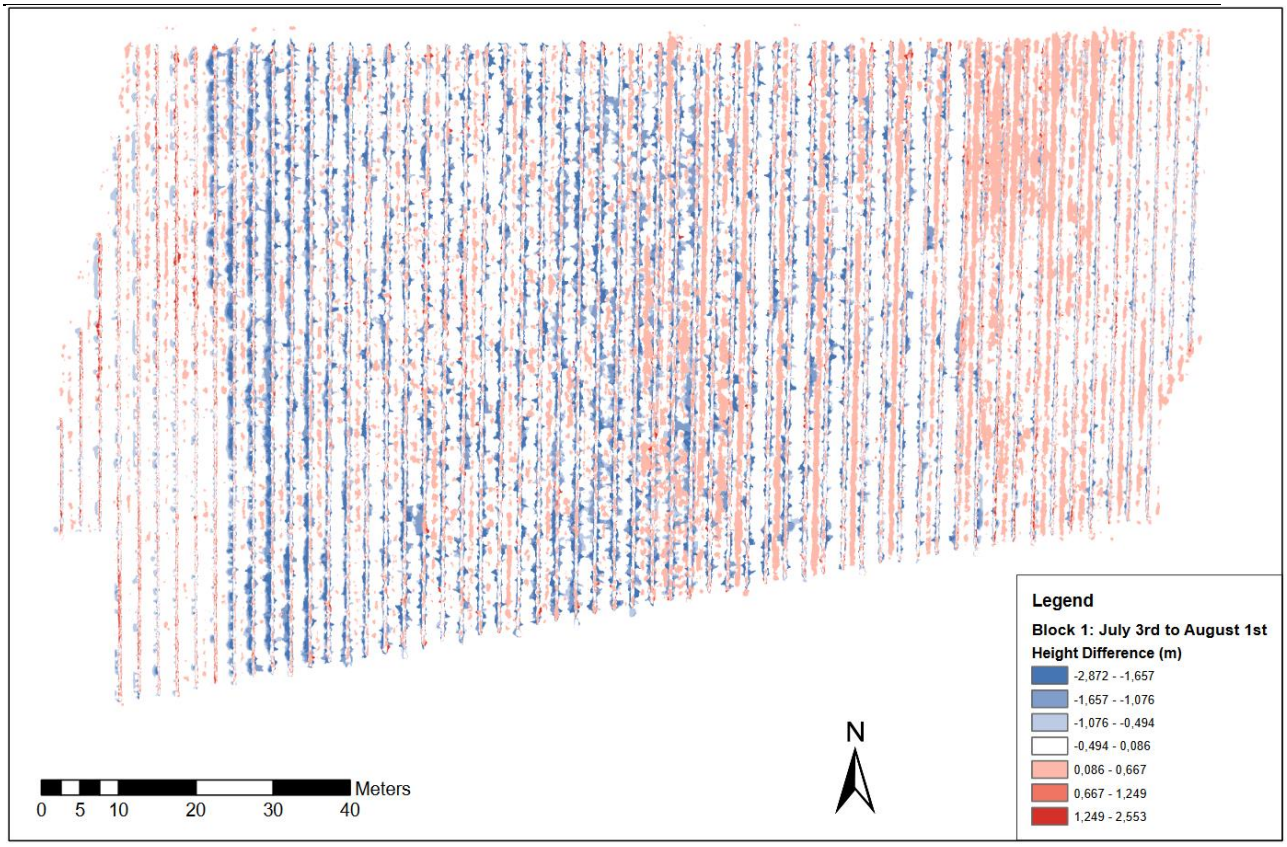

Figure 77: Height differences between July and August in block 1 of the vineyard

Furthermore, to compare the high-precision 3D models of individual bunches generated in the laboratory study, a similar approach was executed in the field study. Therefore, a close-range photogrammetric data acquisition process was performed in the vineyard to obtain a multi-view image dataset of an individual vine. Subsequently, a 3D modelling process similar to that of the laboratory study was carried out with the image data of the single vine to reconstruct a 3D model of it. The resulting dense point cloud of this reconstruction process is visualized in Figure 78. This dense point cloud shows not only the vine in high detail, but also the individual grapes. Such a 3D point cloud could be used to determine phenological parameters such as length, width and volume of the individual grapes. These parameters could then be used to estimate the yield of the plant. However, this analysis of the 3D point cloud of the vine was no longer possible within the framework of the research project due to time constraints.

Figure 78: Reconstructed 3D model of a single vine in the vineyard

5. Evaluation

In this chapter, the generated results and the gained knowledge are critically reflected. The phenological 3D models of vine created in this research project show that it is possible to digitally represent the phenological stages of vines to a certain extent with a multiscale photogrammetric approach. The vegetative state of individual plants can be roughly estimated in the 3D models based on the structure of their canopy and their size. For example, it can be identified that the vines illustrated in the 3D model of Figure 68 are in their dormant form during winter because there is no greenish plant material present. The 3D point cloud displayed in Figure 70 shows a very advanced growth of the individual vines during July. However, due to the resolution of the 3D models, it is not possible to perform a more detailed analysis of the phenological stages of individual plants. For this, the 3D models would have to have such a high resolution that for example single stems or bunches of plants can be seen.

The laboratory study has shown that it is possible to on the hand, create 3D models of individual parts of vines with a correspondingly high image resolution and on the other hand, to derive phenological parameter from them. Furthermore, the measured phenological parameters could be used to estimate yield-relevant parameters such as the volume of an entire bunch. In a further process in the field study, a similar high-resolution 3D model of a vine plant, shown in Figure 78, was created. In this model stems as well as single grapes of the grapevine can be seen. Thus, such a 3D model could be used to determine phenological parameters of vines and to estimate the yield of the particular plant.

In the course of the research project, phenological changes in the vineyard over a certain period of time, such as the growth of individual plants, were also investigated. In a visual comparison of the individual models of the multi-temporal phenological 3D model of vine, a strong plant growth from February to June and June to July could be determined. This vegetative change was also investigated with height difference models, which show local height differences that occurred between the flight missions. In the generated height difference models, strong plant growth, represented by red color, can also be observed between the months February to June (Figure 67) and June to July (Figure 76). However, the height differences models of Figure 67 and Figure 76, also reveal an area-wide low height-loss, visualized as bright bluish areas. In the difference model of Figure 77, partly strong height decreases can be seen in the vine row areas. The area-wide loss of altitude can be attributed to mowing work and the strong height decline in the vine rows to the so-called “pruning”. During pruning, employees remove excess stems, twigs, leaves and even bunches from the vines, thus resulting in smaller vines. This shows that both 3D models and surface models of the vineyard can be used to investigate phenological changes in the vines over a certain period of time.

In addition, the phenological 3D models of vine have shown that the reconstruction of fine structures such as stems of vine plants or posts is sometimes only partially possible or not possible at all. An example can be seen in the 3D model illustrated in Figure 72. Only very few stems of the vines, which are visible in the dense point cloud in Figure 68, could be correctly reconstructed in the 3D model. This suggests that an image resolution of less than 1cm is necessary for high-resolution 3D modelling of such fine structures of vines.

Furthermore, a comparison of nadir and oblique view imagery was performed based on a visual examination of 3D point clouds and a statistical analysis of the geometric accuracy, computational complexity and height differences of several models consisting of different combinations of nadir and oblique cameras. Observations from this comparison are:

- In 3D point clouds of the models which use either the sideward facing oblique cameras or all pentacam cameras, the structures of the vine plants are best reconstructed.
- The best geometric accuracies could be achieved with the single camera models and the model that only uses the sideward facing oblique cameras.
- Using the forward and backward facing oblique cameras in a model results in worse horizontal geometric accuracy than of those models that do not apply them.
- A comparison of the total computing time of the one-, two-, three-, four- and five-camera models reveals that the computational complexity at least doubles with the number of cameras used.
- If both the forward and backward facing cameras are used, the total computing time of a model is significantly higher. However, these large differences in computational complexity occur mainly during the creation of the dense point cloud.

6. Conclusion

The main goal of this research project was the development of a multi-temporal phenological 3D model of vine using multiscale photogrammetric approaches. With regard to achieve the project's goal, an extensive literature review was first successfully executed. On the one hand, information on the individual key phenological stages of vine could be obtained. From these data a matrix of the characteristics of the individual phenological stages of vine was created. Such a table can be applied to determine the current vegetative stage of a vine plant. On the other hand, a state-of-the-art analysis was carried out in the literature review to obtain information on traditional and new technologies and methods used to measure phenological parameters in vineyards and to determine and predict the yield. Based on the findings of the literature review, the requirements and to be applied technologies and processes for the development of a multi-temporal 3D model of the key phenological stages of vine were defined. Subsequently, a conceptual workflow for the creation of a multi-temporal phenological 3D model of vine was successfully designed using the information acquired in the requirement analysis and literature review. As part of the implementation process, an iterative procedure was performed to create 3D models of grapes in a laboratory study and to develop a multi-temporal phenological 3D model of vine in the field study. The image data of commercially available grapes for the laboratory study was recorded in a close-range photogrammetric data acquisition process. Furthermore, multiscale photogrammetric methods were applied to acquire ground reference data and low-altitude aerial images of the vineyard. These data were then be used in a multi-step automated 3D scene reconstruction process to on the one hand successfully create 3D models of individual bunches and on the other hand a multi-temporal phenological 3D model of vine. The validation of the created 3D models was carried out by means of a multi-step validation procedure. Phenological parameters and statistical values were recorded from the 3D grape models of the laboratory study using digital and manual measurement methods. Then, these digital and manual measured parameters were compared with each other to validate the reconstructed 3D grape models. In order to validate the multi-temporal phenological 3D models of vine and to detect phenological changes of vine plants, a visual comparison was conducted with the created phenological 3D models and height difference models were created, showing local height differences between these 3D models. Furthermore, a quantitative comparison of nadir and oblique view imagery was performed. For this comparison 11 models representing different combinations of pentacam cameras were designed. Then the aerial image data of the vineyard was used as input data to create 3D models and several statistical values for each of the 11 models. These were then subjected to visual comparison and statistical analysis to determine the effects of the nadir and oblique images.

7. Future Work

This chapter deals with possible improvements and extensions of the executed research project. The flight missions to record the aerial image data were performed at an altitude of 70m. However, in the resulting phenological 3D models, no precise analysis of the phenological stages of vine could be performed, as the resolution of the reconstructed vines is too coarse to see parts such as single bunches. Thus the question arises whether higher resolution 3D models can be reconstructed from images of flight missions at lower altitudes such as 30m or 25m. With a very high-resolution phenological 3D model showing small elements of vines such as individual grapes, investigations could be made regarding identification and change detection of phenological stages of vines and phenological parameters could be derived in order to estimate yield.

In a further step, the effects of the flight direction on the reconstructed 3D models could be tested. In this research project the vineyard was flown parallel to the rows of vines with the UAS. Could higher resolution 3D models be created by flying over the vineyard at right angles to the vine rows? Furthermore, an analysis could be carried out to identify how the angles of oblique cameras influence the image overlap, the area covered by an image and the image resolution. Thus, in a future project it could be investigated whether there is an optimal angle of oblique cameras to record phenological characteristics of vines.

Additionally, volume calculations could be performed with the generated phenological 3D models of vine using the RANSAC shape detection tool of CloudCompare. With such a method it could be determined whether these large 3D models, which among other things represent entire rows of vines, can be used to derive yield-relevant parameters for all reconstructed vines in the 3D model.

Last but not least, it could be investigated whether the classification of individual elements of vine plants, such as leaves, stems or grapes, is possible in the generated phenological 3D models. For this the CANUPO plugin of CloudCompare could be used.

References

Agisoft (2019 a) Professional Edition. *Agisoft LLC*. [Online] Available at: https://www.agisoft.com/features/professional-edition/ [Accessed: 22 Jan. 2019].

Agisoft (2019 b) Downloads - Agisoft Metashape 1.5.3. *Agisoft LLC.* [Online] Available at: https://www.agisoft.com/downloads/installer/ [Accessed: 27 Jun. 2019].

Agisoft Metashape User Manual (2019) Agisoft Metashape User Manual: Professional Edition, Version 1.5. *Agisoft LLC.* [Online] Available at: https://www.agisoft.com/pdf/metashape-pro_1_5_en.pdf [Accessed: 29 Apr. 2019].

Ames, Z. R., Olmstead, M., Sims, C. and Darnell, R. (2016) Effect of Shoot and Cluster Thinning on Vine Performance, Fruit and Wine Quality of 'Blanc Du Bois'. *Journal of the American Pomological Society*. 70(1). pp.2-15.

Barber, G. (1988) *Elementary statistics for geographers*. New York: Guilford Press, pp.430-432.

Carmona, M. J., Cubas, P., Calonje, M. and Martínez-Zapater, J. M. (2007) Flowering transition in grapevine (Vitis vinifera L.). *Canadian Journal of Botany*. 85(8). pp.701-711.

Centinari, M. (2015) Fruit Set in Grapevines 101. *Wine & Grapes U*. [Online] Available at: https://psuwineandgrapes.wordpress.com/2015/08/07/fruit-set-in-grapevines-101/ [Accessed: 22 Nov. 2018].

Centinari, M. (2018 a) Assessing grape maturity for harvest planning. *Wine & Grapes U*. [Online] Available at: https://psuwineandgrapes.wordpress.com/2018/09/07/assessing-grape-maturity-for-harvest-planning/ [Accessed: 22 Nov. 2018].

Centinari, M. (2018 b) Grapevine Bud Break 101. *Wine & Grapes U*. [Online] Available at: https://psuwineandgrapes.wordpress.com/2018/05/14/grapevine-bud-break-101/ [Accessed: 22 Nov. 2018].

Christensen, P. L. (2000) *Raisin production manual*. Oakland: University of California, Agriculture and Natural Resources, pp.30-37.

CloudCompare (2019) CloudCompare - Open Source project. *CloudCompare*. [Online] Available at: http://www.cloudcompare.org/ [Accessed: 23 Jan. 2019].

Demarée, G. R. and Rutishauser, T. (2011) From "Periodical Observations" to "Anthochronology" and "Phenology" – the scientific debate between Adolphe Quetelet and Charles Morren on the origin of the word "Phenology". *International Journal of Biometeorology*, 55(6), pp.753-761.

Dey, D., Mummert, L. and Sukthankar, R. (2012) Classification of Plant Structures from Uncalibrated Image Sequences. *2012 IEEE Workshop on the Applications of Computer Vision (WACV).* DOI: 10.1109/WACV.2012.6163017 [Accessed: 02 Dec. 2018].

Dunn, G. M. (2010) Yield Forecasting. Fact Sheet. *Grape and Wine Research and Development Corporation.* [Online] Available at: https://www.wineaustralia.com/getmedia/5304c16d-23b3-4a6f-ad53-b3d4419cc979/201006_Yield-Forecasting.pdf [Accessed: 12 Oct. 2018].

Eisenbeiss, H. (2009) UAV photogrammetry. *ETH Zürich*. [Online] pp.2-7. DOI: 10.3929/ethz-a-005939264 [Accessed: 05 Feb. 2019].

Esri (2019) Get started with ArcMap. *Esri*. [Online] Available at: http://desktop.arcgis.com/en/arcmap/10.6/get-started/main/get-started-with-arcmap.htm [Accessed: 1 Jul. 2019].

Gillies, D. (2015) Close Range Photogrammetry. *The Photogrammetric Record*, 30(151), pp.318-322.

GitHub (2019) agisoft-llc/metashape-scripts. *GitHub Inc*. [Online] Available at: https://github.com/agisoft-llc/metashape-scripts/blob/master/src/footprints_to_shapes.py [Accessed: 6 Aug. 2019].

Goldammer, T. (2015) *The grape grower's handbook*. 2nd ed. Centreville: Apex Publishers.

Goldammer, T. (2018) *The grape grower's handbook*. 3rd ed. Centreville: Apex Publishers.

Gómez-Gutiérrez, Á., Schnabel, S., Berenguer-Sempere, F., Lavado-Contador, F. and Rubio-Delgado, J. (2014) Using 3D photo-reconstruction methods to estimate gully headcut erosion. *CATENA*, 120, pp.91-101.

Hack, H., Bleiholder, H., Weber, E., Feller, C., Hess, M., Wicke, H., Meier, U., van den Boom, T., Lancashire, P. D., Buhr, L., Klose, R. and Stauss, R. (2001) *Entwicklungsstadien mono- und dikotyler Pflanzen*. 2nd ed. Berlin: Biologische Bundesanstalt für Land und Forstwirtschaft.

Harlfinger, O., Koch, E. and Scheifinger, H. (2002) *Klimahandbuch der Österreichischen Bodenschätzung Klimatographie Teil 2*. Innsbruck: Klimareferat der Österreichischen Bodenschätzung.

Hellman, E. (2003) Grapevine Structure and Function. *Oregon Viticulture*. [Online] Available at: https://www.researchgate.net/publication/237296145_Grapevine_Structure_and_Function [Accessed: 26 Nov. 2018].

Hellman, E. (2015) Parts of the Grape Vine: Flowers and Fruit. *Texas AgriLife Extension*. [Online] Available at: https://articles.extension.org/pages/31097/parts-of-the-grape-vine:-flowers-and-fruit [Accessed: 23 Nov. 2018].

Iland, P., Dry, P., Proffitt, T. and Tyerman, S. (2011) *The grapevine: from the science to the practice of growing vines for wine*. Adelaide: Patrick Iland Wine Promotions.

James, M. R., and Robson, S. (2012) Straightforward reconstruction of 3D surfaces and topography with a camera: Accuracy and geoscience application, *Journal of Geophysical Research: Earth Surface*, 117(F3), doi:10.1029/2011JF002289.

Lee, P., Huang, J. and Lin, H. (2012) 3D model reconstruction based on multiple view image capture. *2012 International Symposium on Intelligent Signal Processing and Communications Systems*, pp.58-63. doi:10.1109/ISPACS.2012.6473453.

Leica (2018) Leica Aibot Intelligent aerial reality capture. Leica Geosystems AG. [Online] Available at: http://www.vt-engelmann.de/cms/upload/_Produkte/UA_Luftroboter/UA_HA_LA_AX20_DS.pdf [Accessed: 12 Jul. 2019].

Lodi Growers (2018) Important Structures & Features of Grapevines. *Lodi Growers*. [Online] Available at: https://www.lodigrowers.com/important-structures-features-of-grapevines/ [Accessed: 10 Dec. 2018].

Maniak, S. (2004) *Datenaustausch in geographischen Informationssystemen*. Aachen: Shaker, pp.5-14.

Merriam-Webster (2019) Definition of NADIR. *Merriam-Webster, Incorporated*. [Online] Available at: https://www.merriam-webster.com/dictionary/nadir [Accessed: 07 Feb. 2019].

Morgenroth, J. and Gomez, C. (2014) Assessment of tree structure using a 3D image analysis technique—A proof of concept. *Urban Forestry & Urban Greening*, 13(1), pp.198-203.

Mouragnon, E., Lhuillier, M., Dhome, M., Dekeyser, F. and Sayd, P. (2006) 3D Reconstruction of Complex Structures with Bundle Adjustment: an Incremental Approach. *HAL archives-ouvertes*. HAL Id: hal-00091147.

Moyer, M. M. and Komm, B. L. (2015) Vineyard Yield Estimation. Technical Report EM086E. *Washington State University Extension.*

Murtiyoso, A., Remondino, F., Rupnik, E., Nex, F. and Grussenmeyer, P. (2014) Oblique Aerial Photography Tool for Building Inspection and Damage Assessment. *ISPRS - International Archives of the Photogrammetry, Remote Sensing and Spatial Information Sciences*, XL-1, pp.309-313.

Nuske, S., Achar, S., Gupta, K., Narasimhan, S. and Singh, S. (2011) Visual Yield Estimation in Vineyards: Experiments with Different Varietals and Calibration Procedures. Technical Report CMU-RI-TR-11-39. *Carnegie Mellon University.* [Online] Available at: https://www.researchgate.net/publication/221066368_Yield_estimation_in_vineyards_by_visual_grape_detection [Accessed: 16 Oct. 2018].

Nuske, S., Wilshusen, K., Achar, S., Yoder, L., Narasimhan, S. and Singh, S. (2014) Automated Visual Yield Estimation in Vineyards. *Journal of Field Robotics*, 31(5), pp.837-860.

Odneal, M. (2018) What's happening in the field?. *Missouri State University*. [Online] Available at: https://blogs.missouristate.edu/fruitexperimentstation/2016/06/20/grape-phenology-and-gdd-accumulation-147/9_arandel062016/ [Accessed: 20 Nov. 2018].

Philpot, W. D. and Philipson, W. R. (2012) *Remote Sensing Fundamentals: Photogrammetry*. 10th ed. Ithaca: Cornell University. [Online] Available at: http://ceeserver.cee.cornell.edu/wdp2/cee6100/6100_monograph/mono_07_F12_photogrammetry.pdf [Accessed: 30 Apr. 2019].

Poupin, M. J., Matus, J. T., Leiva-Ampuero, A. and Arce-Johnson, P. (2011) The Flowering Process and its Control in Plants: Gene Expression and Hormone Interaction. 1st ed. Kerala: Research Signpost, pp.173-197.

Purdue University (2018) Photogrammetry. *Purdue University*. [Online] Available at: https://engineering.purdue.edu/~asm215/topics/phtogrmt.html [Accessed: 07 Feb. 2019].

Remondino, F. and Gerke M. (2015) Oblique Aerial Imagery – A Review. *Wichmann/VDE Verlag*. p.75. [Online] Available at: http://www.ifp.uni-stuttgart.de/publications/phowo15/090Remondino.pdf [Accessed: 07 Feb. 2019]

Rose, J., Kicherer, A., Wieland, M., Klingbeil, L., Töpfer, R. and Kuhlmann, H. (2016) Towards Automated Large-Scale 3D Phenotyping of Vineyards under Field Conditions. *Sensors*, 16(12).

Rossi, P., Mancini, F., Dubbini, M., Mazzone, F. and Capra, A. (2017) Combining nadir and oblique UAV imagery to reconstruct quarry topography: methodology and feasibility analysis. *European Journal of Remote Sensing*, 50(1), pp.211-221.

Schenk, T. (2005) Introduction to Photogrammetry. *Ohio State University, Department of Civil and Environmental Engineering and Geodetic Science*. [Online] Available at: http://www.mat.uc.pt/~gil/downloads/IntroPhoto.pdf [Accessed: 07 Feb. 2019].

Smith, M. and Centinari, M. (2017) Early season grapevine canopy management, Part I: Shoot thinning. *Wine & Grapes U*. [Online] Available at: https://psuwineandgrapes.wordpress.com/2017/05/19/early-season-grapevine-canopy-management-part-i-shoot-thinning/ [Accessed: 22 Nov. 2018].

Sony (2018) Sony α7R III 35 mm full-frame camera with autofocus. *Sony India*. [Online] Available at: https://www.sony.co.in/electronics/interchangeable-lens-cameras/ilce-7rm3/specifications [Accessed: 30 Jul. 2019].

Sony (2019) Sony ILCE-QX1 Lens-Style Camera with 20.1MP Sensor - Full Specifications & Features. *Sony Europe B.V*. [Online] Available at: https://www.sony.co.uk/electronics/interchangeable-lens-cameras/ilce-qx1-body-kit/specifications [Accessed: 25 Jun. 2019].

Stafne, E. and Martinson, T. (2012) Stages of Grape Berry Development. *eXtension*. [Online] Available at: https://articles.extension.org/pages/31096/stages-of-grape-berry-development [Accessed: 23 Nov. 2018].

Tello, J. and Ibáñez, J. (2014) Evaluation of indexes for the quantitative and objective estimation of grapevine bunch compactness. *Vitis*, 53(1), pp.9-16.

USGS National UAS Project Office (2017) Unmanned Aircraft Systems Data Post-Processing Structure-from-Motion Photogrammetry. *USGS*. [Online] Available at: https://rmgsc.cr.usgs.gov/outgoing/UAS/workshop_data/2017_UAS_Federal_Users_Workshop/Lab%201%20UAS%20DSLR%20sfm%20Workshop%202017/PhotoScan%20Processing%20Procedures%20DSLR%20Mar%202017.pdf [Accessed: 15. Apr. 2019].

Vacca, G., Dessì, A. and Sacco, A. (2017) The Use of Nadir and Oblique UAV Images for Building Knowledge. *ISPRS International Journal of Geo-Information*, 6(12), p.393.

Vincent, C., Isaacs, R., Bostanian, N. J. and Lasnier, J. (2012) Principles of Arthropod Pest Management in Vineyards. *Arthropod Management in Vineyards*. pp.1-16. [Online] DOI: 10.1007/978-94-007-4032-7_1 [Accessed: 02 Dec. 2018].

Westover, F. (2018) Grapevine Phenology Revisited. *Wines & Vines*. [Online] Available at: https://www.winesandvines.com/features/article/196082/Grapevine-Phenology-Revisited [Accessed: 11 Oct. 2018].

Wine Folly (2016) Lifecycle of a Wine Grapevine. *Wine Folly*. [Online] Available at: https://winefolly.com/review/lifecycle-of-a-wine-grapevine/ [Accessed: 20 Nov. 2018].

Wine Institute (2019) World Wine Production by Country. *Wine Institute*. [Online] Available at: https://www.wineinstitute.org/files/World_Wine_Production_by_Country_2015.pdf [Accessed: 06 Feb. 2019].

Wolf, P. R., Dewitt, B. A. and Wilkinson, B. E. (2014) *Elements of Photogrammetry with Applications in GIS*. 4th ed. McGraw-Hill Global Education Holdings, LLC.

Zhang, Y., Xiong, J., and Hao, L. (2011) Photogrammetric processing of low-altitude images acquired by unpiloted aerial vehicles. *Photogrammetric Record*, 26(134), 190-211. doi:10.1111/j.1477-9730.2011.00641.x.

Zhang, S., Lippitt, C. D., Bogus, S., Loerch, A., and Sturm, J. (2016) The accuracy of aerial triangulation products automatically generated from hyper-spatial resolution digital aerial photography. *Remote Sensing Letters*, 7(2), 160-169.

Appendix A: Phenological Characteristics Matrix

Nbr.	E-L stage Number	Phenological Stage Name	Image	Appearance/Growth Duration	Phenological Characteristic	Characteristic Reference
1	E-L 4	Bud burst	 *Figure 79: Bud Burst (Vincent et al., 2012)*	Early April - End April (Hellman, 2003)	Appearance of green tissue through the bud scales; Leaf tips are visible; 0.6 – 1 mm;	(Centinari, 2018 b) (Westover, 2018)
2	E-L 12	Shoots 10 cm	 *Figure 80: Shoots 10 cm (Vincent et al., 2012)*	End of April – Early June	Inflorescence is clear, 5 leaves are separated, Shoots are about 10 cm long;	(Westover, 2018)
3	E-L 19	Flowering begins	 *Figure 81: Flowering Begins (Vincent et al., 2012)*	Early June – Mid June, 6 to 8 weeks after bud burst (Goldammer, 2018)	Flowering beginning on the uppermost shoots; About 16 leaves separated, First flower caps loosening;	(Goldammer, 2018) (Westover, 2018)
4	E-L 23	Flowering	 *Figure 82: Grapevine Flowering (Vincent et al., 2012)*	Mid June – Early July (Hellman, 2003); Lasts 1 to 3 weeks (Goldammer, 2018)(Hellman, 2015)	50% to 2/3 of flower caps are off; 17-20 leaves separated; Flower size = 4 – 5 mm;	(Hellman, 2015) (Westover, 2018) (Lodi Growers, 2018)

5	E-L 27	Setting/Fruit set	 *Figure 83: Grapevine Setting (Vincent et al., 2012)*	Early July – Mid/End July, Immediately follows after end of flowering (Goldammer, 2015); Lasts between 3 and 4 weeks (Christensen, 2000) (Hellman, 2003)	Berry diameter is between 1.6 and 3.2mm; Berries are firm, Dark green in color; Young berry enlarging (>2 mm diameter), Bunch at right angles to stem;	(Christensen, 2000) (Goldammer, 2015) (Westover, 2018)
6	E-L 31	Berry pea-size/Lag phase	 *Figure 84: Berries at pea-size (Vincent et al., 2012)*	End July – Mid August; Lasts between 2 and 3 weeks (Christensen, 2000)	Color of the berries starts to change; Berries reduce chlorophyll content, causing color change to a lighter green; Berries at pea size (7 mm diameter), Bunches hanging down;	(Goldammer, 2015) (Hellman, 2003) (Westover, 2018)
7	E-L 35	Véraison	 *Figure 85: Véraison (Vincent et al., 2012)*	Mid August – Early September (Hellman, 2003)	Berry doubles in size (~14 mm diameter); Development of characteristics colors yellow-gold/pink/red (véraison), Uneven color change within and among clusters, Berries begin to soften; Berries begin to color and enlarge;	(Stafne and Martinson, 2012) (Goldammer, 2015) (Westover, 2018)
8	E-L 38	Harvest	 *Figure 86: Harvest-ripe berries (Vincent et al., 2012)*	Mid September – Early November (Hellman, 2003)	Berries are fully ripe, Ripeness is determined by sugar content, acidity, pH-value, color and flavor; “Fruit ripeness” and “fruit quality” do not have absolute values but are defined subjectively; Berries are harvest-ripe; Bunch length: min = 10.3 cm, max = 31 cm, average = 17.4 cm Bunch width: min = 7 cm, max = 17.6 cm, average = 10.88 cm	(Goldammer, 2015) (Hellman, 2003) (Westover, 2018) (Tello and Ibáñez, 2014)

Table 11: Phenological characteristics matrix

Table 12: Images of 3D points clouds form the 11 models

Appendix B: 3D point clouds showing reconstructed vines

The following images show 3D point clouds which illustrate reconstructed vine plants. The point clouds were generated on basis of different combinations of the pentacam cameras.

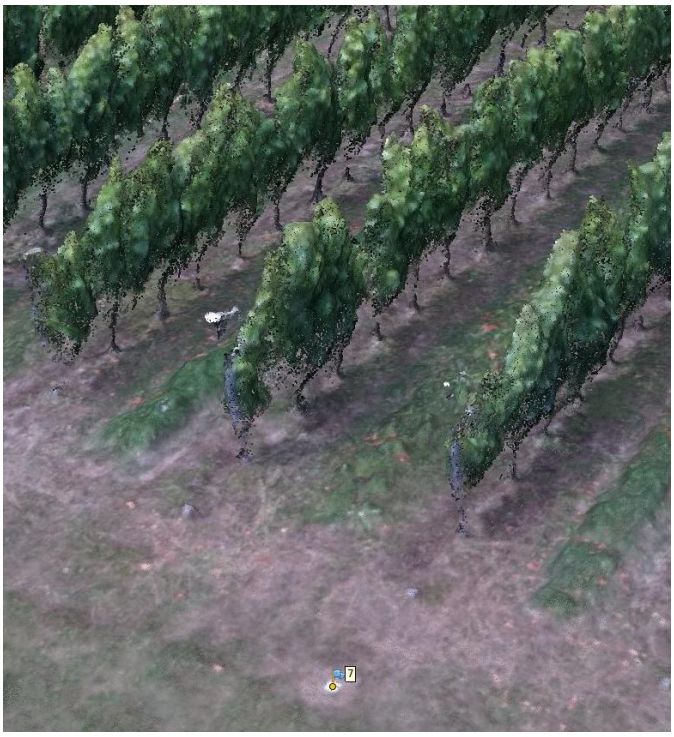

Figure 87: 3D point cloud of model 2 showing reconstructed vines

Figure 88: 3D point cloud of model 4 showing reconstructed vines

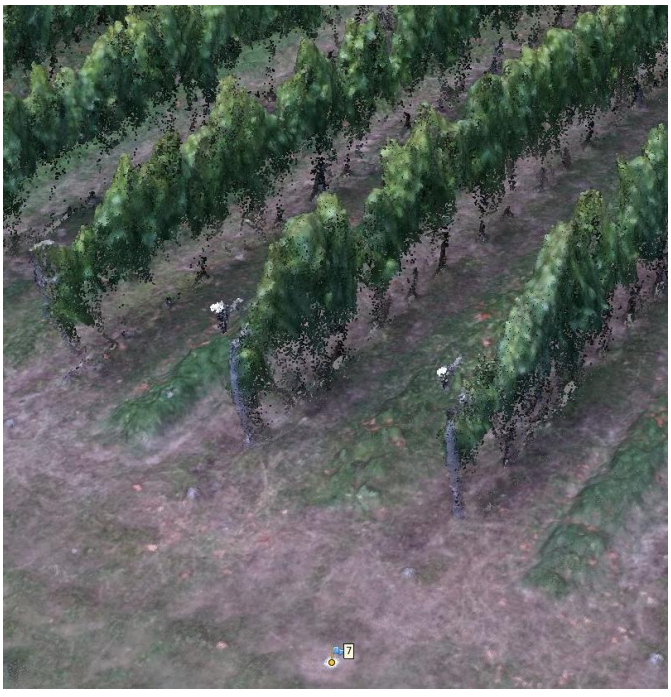

Figure 89: 3D point cloud of model 5 showing reconstructed vines

Figure 90: 3D point cloud of model 6 showing reconstructed vines

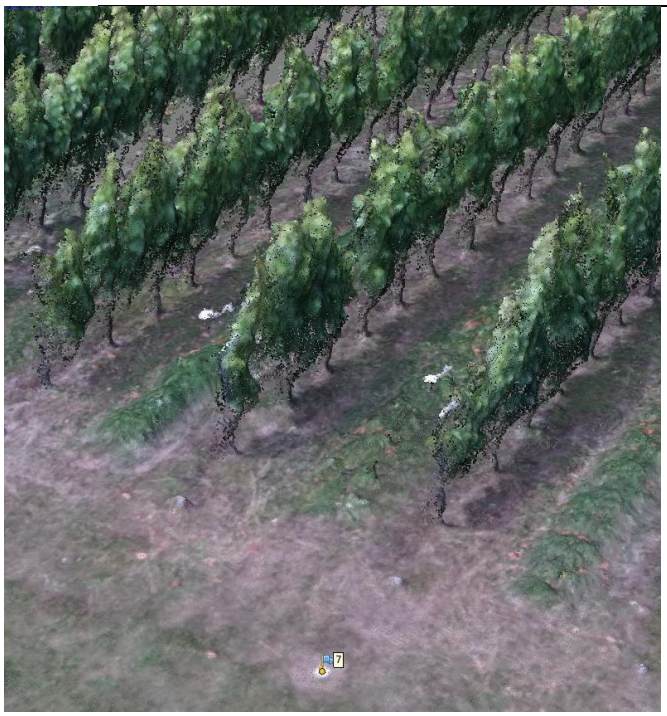

Figure 91: 3D point cloud of model 7 showing reconstructed vines

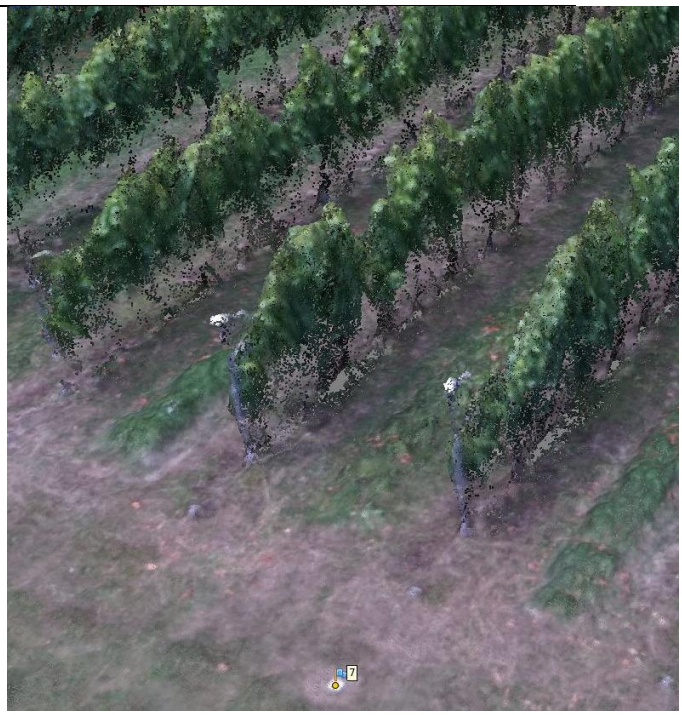

Figure 92: 3D point cloud of model 8 showing reconstructed vines

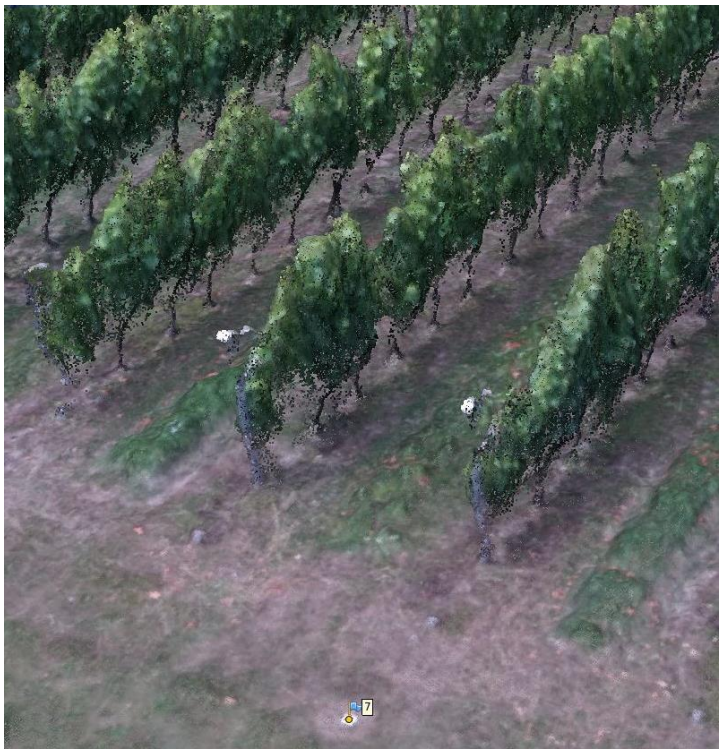

Figure 93: 3D point cloud of model 9 showing reconstructed vines

Table 13: Histograms of height difference distributions between DSMs

Appendix C: Histograms of the DSM comparisons

The histograms illustrate height difference distributions based on calculated height differences between the DSMs of the 11 models. The DSM of model 3 was used as reference model for the height difference calculations.

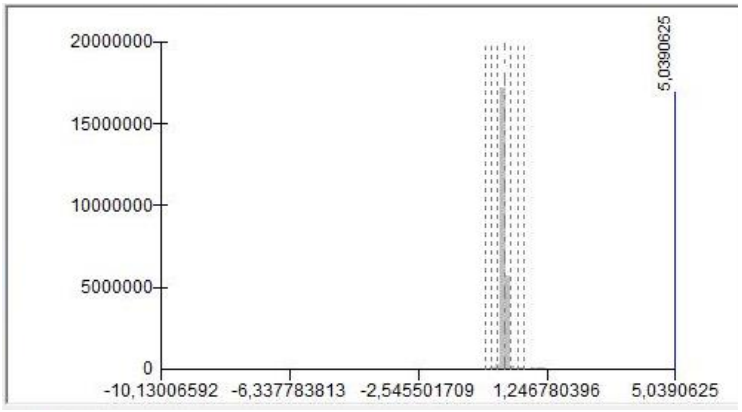

Figure 94: Histogram showing height difference distribution between model 2 and model 3

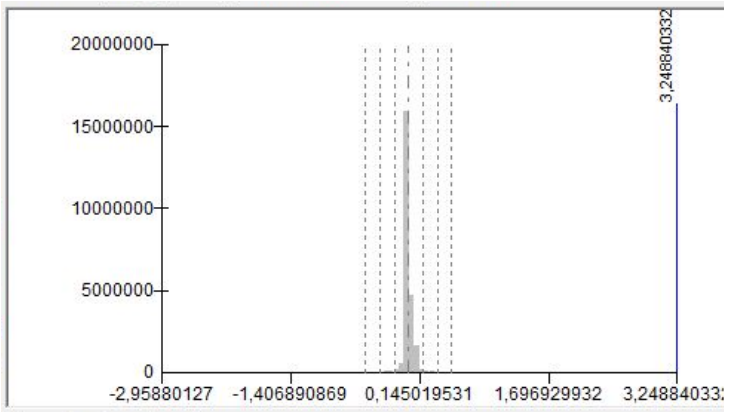

Figure 95:Histogram showing height difference distribution between model 5 and model 3

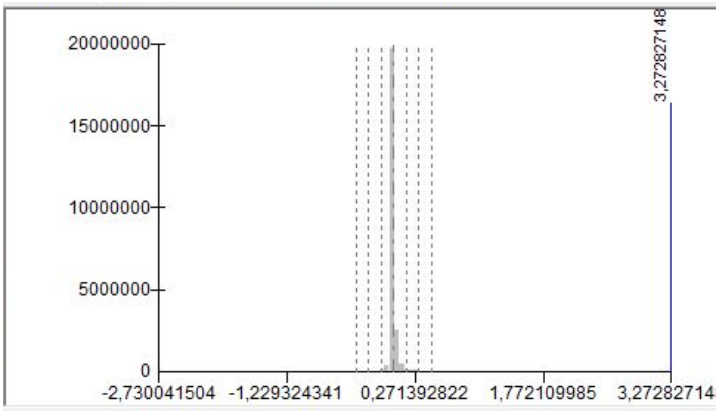

Figure 96: Histogram showing height difference distribution between model 6 and model 3

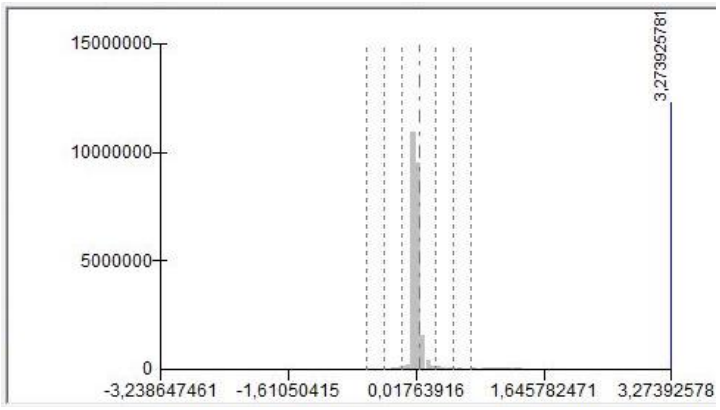

Figure 97: Histogram showing height difference distribution between model 7 and model 3

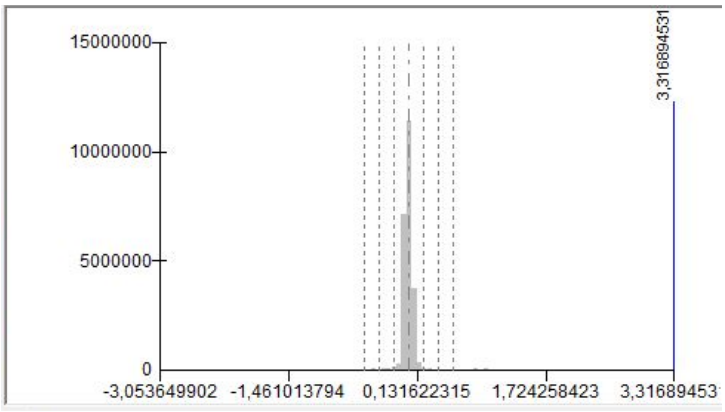

Figure 98: Histogram showing height difference distribution between model 8 and model 3

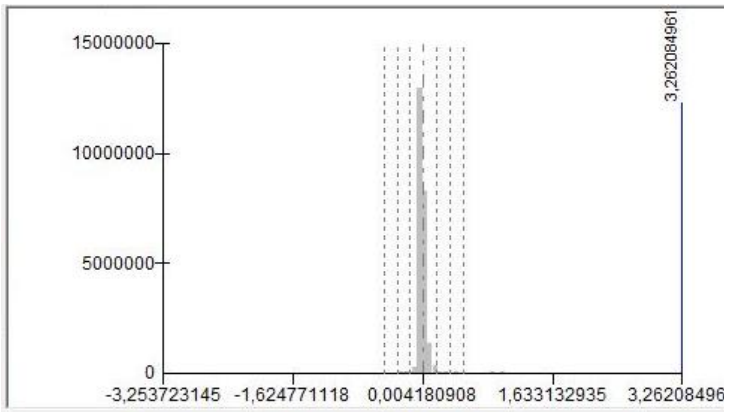

Figure 99: Histogram showing height difference distribution between model 9 and model 3

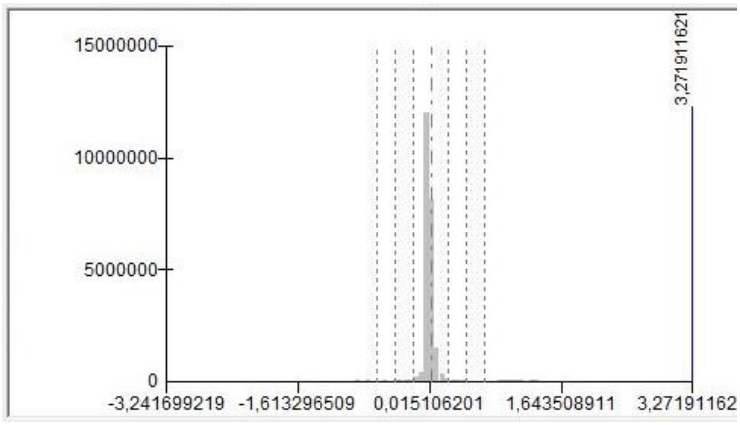

Figure 100: Histogram showing height difference distribution between model 10 and model 3

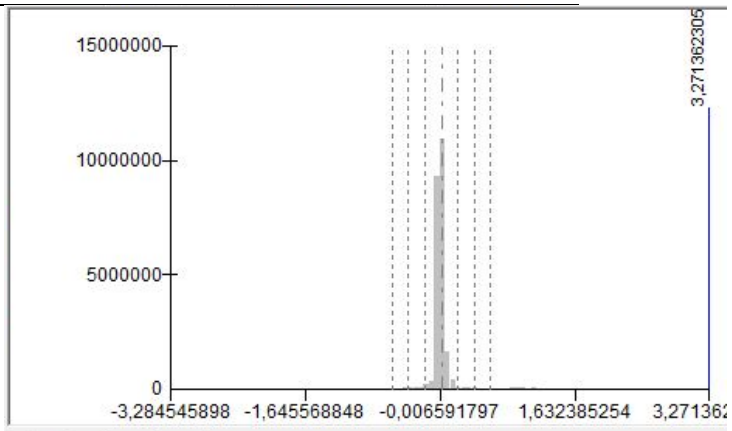

Figure 101: Histogram showing height difference distribution between model 11 and model 3